Spring 2015

An integrated system of vapor-compression chiller and absorption heat pump: Experiment, modeling, and energy and economic evaluation

Yi-Shu Kung
Purdue University

Graduate School Form 30
(Revised 08/14)

PURDUE UNIVERSITY
GRADUATE SCHOOL
Thesis/Dissertation Acceptance

This is to certify that the thesis/dissertation prepared

By Yi-Shu Kung

Entitled
AN INTEGRATED SYSTEM OF VAPOR-COMPRESSION CHILLER AND ABSORPTION HEAT PUMP: EXPERIMENT, MODELING, AND ENERGY AND ECONOMIC EVALUATION

For the degree of Doctor of Philosophy

Is approved by the final examining committee:

Ming Qu

Eckhard Groll

W. Travis Horton

Srinivas Peeta

To the best of my knowledge and as understood by the student in the Thesis/Dissertation Agreement, Publication Delay, and Certification/Disclaimer (Graduate School Form 32), this thesis/dissertation adheres to the provisions of Purdue University's "Policy on Integrity in Research" and the use of copyrighted material.

Ming Qu

Approved by Major Professor(s): _____

_____

Approved by: Dulcy M. Abraham 04/27/2015

Head of the Department Graduate Program Date

AN INTEGRATED SYSTEM OF VAPOR-COMPRESSION CHILLER AND ABSORPTION HEAT PUMP: EXPERIMENT, MODELING, AND ENERGY AND ECONOMIC EVALUATION

A Dissertation

Submitted to the Faculty

of

Purdue University

by

Yi-Shu Kung

In Partial Fulfillment of the

Requirements for the Degree

of

Doctor of Philosophy

May 2015

Purdue University

West Lafayette, Indiana

For my parents and lovely wife

ACKNOWLEDGEMENTS

In my homeland, we describe that learning is like a journey of sailing. I was glad to board on the famous ship named Purdue in 2010 and began my adventure on the academic ocean. How lucky I am to have so many people assist me to finish the journey.

Thanks Prof. Ming Qu who has led me toward to the right directions. She is stringent and serious, just like any other advisors, when we are dealing with the researches. However, she is also kind and caring which is not always found in every advisor. I really appreciate her guidance in the past five years. Thanks Steve Peng who supports our project and is always willing to help. His points of view from the industry can point out the insufficiency and inspire the new ideas. Thanks Prof. Eckhard Groll, Prof. Travis Horton, and Prof. Srinivas Peeta for their treasured advice. It is my honor to have them as my committee and I really learn a lot from them. I would also like to thank all of my friends here especially the members in our research team, the colleagues in our group, and the folks from Taiwan. I cannot image how terrible my life will be without you.

Finally, I want to thank my parents and lovely wife. I can have the courage to explore the world because of the fully and unquestionable support from my parents. And I shared everything with my wife, Shu-Yen Chen, no matter sorrow or happiness. Let us keep holding our hangs tightly till the end.

Yi-Shu Kung

4/26/2015 @ West Lafayette, IN

TABLE OF CONTENTS

Page

Page

Page

LIST OF TABLES

Table Page

Table Page

LIST OF FIGURES

Figure Page

Figure Page

ABSTRACT

Kung, Yi-Shu. Ph.D., Purdue University, May 2015. An Integrated System of Vapor-compression Chiller and Absorption Heat Pump: Experiment, Modeling, and Energy and Economic Evaluation. Major Professor: Ming Qu.

Buildings currently consume 41% of the primary energy in the United States. Among the 41% primary energy, approximate 50% are used for building heating, cooling, and water heating. Improving the efficiencies of the devices for building heating and cooling has potentials to reducing the energy consumptions. This research aims to find one solution for building energy efficiency through investigating an Integrated System of an Integrated Compression-Absorption Subcooling System (ICASS) Based upon the principle of subcooling effect, the ICASS can improve the efficiency of the cooling device but also achieve additional useful heating sources potentially used for space heating and domestic hot water. The ICASS utilizes thermal energy as a part of power inputs to reduce the dependency of electricity so that it can reduce the peak power demand. Due to the improved system efficiency and the availability of heating source, the ICASS could also improve the cost effectiveness of the system.

The objectives of this research include:

Objective 1) To develop the thermodynamic and heat transfer models of the ICASS for system design and performance. Objective 2) To test the performances of a test bed for data analysis and model validation. The data collected from the test bed will also

contribute the fields of vapor-compression refrigeration system (VCRS) and absorption heat pump (AHP).Objective 3) To conduct different analyses of the ICASS based on the validated models. Objective 4) To evaluate the energy and economic benefits and to discover the commercial potentials of the ICASS.

In order to predict the potential improvements of the ICASS, an integration of a VC and a single-effect lithium bromide AHP was modeled in the Engineering Equation Solver (EES) as a case study according to the engineering fundamentals and scientific principles. A test bed was constructed following the design models of ICASS. The test bed is located in the Herrick Labs at Purdue University, West Lafayette, IN. The VCRS, AHP, and ICASS were tested at different operation conditions and the system performances were recorded. Experimental data collected was also used to develop, adjust, and validate the models of VCRS, AHP, and ICASS.

The validated models of VCRS, AHP, and ICASS were extended for system sensitivity analyses and overall system performance prediction when ICASS is used to various applications. The sensitivity analyses were able to identify the key parameters, which most influence the system performance. Since the ICASS utilizes both electricity and thermal energy as the energy inputs, exergy analysis was conducted to calculate the exergy efficiency and determine the irreversibilites of the system to address the potentials of the improvements. To compare the performance of ICASS with other equivalent systems, the separated systems of VCRS, absorption chiller, AHP, and water heater were used to identify the benefits due to the ICASS. The results showed that ICASS consumed the less energy by providing same heating and cooling than the equivalent systems. Finally, building energy simulations were carried out to evaluate the economic

performance of the ICASS when it is applied to the full service restaurant. The simulation results indicated that the applications with high cooling demands and high electricity price are favorable for ICASS. Additionally, more hot water can be generated by the ICASS if the cooling demands are higher.

CHAPTER 1. INTRODUCTION

1.1 Background

In the United States, buildings account for 41% and 35% of the primary energy consumptions and greenhouse gas emissions, respectively. Among the 41% primary energy, approximate 50% are used for building heating, cooling and water heating (DOE, 2011). Accordingly, reducing the energy consumed by the equipment for building heating and cooling can be one of the most effective ways to saving energy, as well as reducing greenhouse gas emissions.

1.2 Motivation

Vapor-compression refrigeration system (VCRS) has been widely used for decades to provide cooling in buildings. The VCRS has dominated the market because its energy source, the electricity, is cheap and easy to get generally. However, with the increasing of power demands, the price of electricity has increased over the past years. For example, the average retail price of electricity for commercial usage has increased from 7.43 to 10.29 ¢/kWh in the U.S. from 2000 to 2013 (EIA, 2014). Except the rate of electricity, power outage happens due to the increasing demand of electricity, especially during the on-peak period. Therefore, the technologies for improving energy efficiency are highly needed aiming to reducing power demands. Those technologies can not only reduce the

operational cost but also reduce the chances of power outage for both consumers and utility companies.

Improving the efficiency of VCRS is one of the technologies needed to reduce the electricity consumption. Coefficient of performance (COP), the ratio of the cooling output and the power input, is typically used as the indicator to evaluate the efficiency of VCRS. The higher the COP of VCRS, the less power input for the same cooling goal. Many researchers have investigated approaches to improve the COP of VCRS. Combining multiple refrigeration cycles is one of the approaches. For instance, a dedicated mechanical-subcooling system (DMSS) combines two VCRS cycles. In a DMSS, the evaporator of the smaller VCRS is also served as the subcooler, a heat exchanger between condenser and the expansion valve of the main VCRS to further cool the refrigerant out of the condenser. The overall COP of DMSS is improved because of the subcooling effect. As another example, the cascade refrigeration system combines two or more cycles for operating at the condition of large temperature difference with an improved efficiency (Moran, 2010). In a cascade system, the evaporator of the upper VCRS cycle is also the condenser of the lower VCRS cycle. For the different operation temperatures, the upper and lower cycles can utilize different refrigerants to reach the highest overall COP.

Another way to reduce the electricity consumption of VCRS is replacing electricity by alternative energy such as thermal energy or others. For instance, the absorption chillers (AC) utilize thermal energy from natural gas, waste heat, or solar as driven power and consume only a little electricity to produce cooling power. However, the COP of an AC is lower than the COP of VCRS. For a single-effect AC, the COP is around 0.8 (Herold et

al., 1996). Additionally, unlike the electricity, the price of natural gas has been decreasing over the past years (EIA, 2014). Under such circumstances, the operation cost of natural gas driven AC with a higher efficiency, such as the double-effect absorption chiller with COP around 1.2 (Herold et al., 1996), may compete with the VCRS. Therefore, introducing AC to VCRS could be a promising idea to lowering the dependency of electricity and further reducing the peak power demand.

Some researchers thus tried to integrate the two approaches together: shifting a part of VCRS's cooling duties from electricity to thermal energy through the combination of multiple refrigeration cycles. The compression-absorption cascade system was proposed to use the AC as the upper cycle of the cascade system. Similarly, a system proposed uses an AC to replace the smaller VCRS in the DMSS. Both systems reduce the dependency of the electricity. Moreover, if the AC of the integrated systems utilizes free thermal energy such as waste heat or solar energy as driven power, the COP improvement can be significant.

Up to date, all the studies focus on how to improve the cooling performance of the equipment. However, if the AC in the integrated system can be replaced by an absorption heat pump (AHP), the integrated system can also provide useful hot water additional to cooling at the same time.

This research aims to investigate an Integrated Compression-Absorption Subcooling System (ICASS) for improving energy efficiency and cost effectiveness. The ICASS combines a VCRS and an AHP through a subcooler. The VCRS in the ICASS produces cooling power, a part of which is shifted to the AHP via the subcooler. The AHP in the ICASS, driven by thermal energy, can provide not only chilled water but also the hot

water at the range of 50 - 60℃, which can be used as domestic hot water or heating water with additional heat inputs. Compared to the previous studies, the ICASS can not only improve the cooling performance but also provide useful hot source. The ICASS has great potentials on the market of the cooling and heating equipment used for both new and retrofit buildings due to its higher efficiency and less dependency to electricity.

1.3 Objectives

The objectives of this research include:

Objective 1: To develop the thermodynamics and heat transfer models of the ICASS for system design and performance evaluation.

Objective 2: To construct a test bed of the ICASS for data analysis and model validation. The data collected from the test bed will also contribute the fields of the VCRS and the AHP.

Objective 3: To conduct both energy and exergy analysis of the ICASS to understand the influences of key parameters.

Objective 4: To evaluate the energy and economic benefits and discover the commercial potentials of the ICASS.

1.4 Organization

In the first chapter, the background, motivation, and objectives of this research have been introduced. Literatures related to the VCRS, absorption refrigeration system (ARS), and the integrations of the two systems are reviewed in the next chapter. These literatures include the integration of different refrigeration cycles, the technology of ARS, the

experiments and models of VCRS and ARS, the exergy analysis of the refrigeration system, and the building energy simulation. The research approach is illustrated in Chapter 3.

In Chapter 4, the test bed and experiments are introduced and discussed. The major components of the test bed including the vapor-compression chiller (VC), the AHP, the heating/cooling load simulator, and the DAQ system are described. Tests of the AHP, the VC, and the ICASS are presented in different sections. These sections contain the test programs, the experimental results, and the discussions.

The development and validation of the energy models are provided in Chapter 5. The models of the AHP, the VC, and the ICASS are presented in different sections. These sections include the assumptions, variables, equations, and inputs of the components and systems as well as the validations of the models.

Model-based analysis is presented in Chapter 6. The influences of candidate parameters on system performance were analyzed by the energy and exergy studies based on the models of the VC, AHP, and ICASS addressed in Chapter 5. The key parameters were identified via the sensitivity analysis.

In Chapter 7, the energy and economic benefits of the ICASS are discussed. The ICASS were compared with different separated systems to evaluate the savings. The last chapter is the conclusion. The key findings and the contributions of this research are presented. Some future research suggestions are described in this chapter.

The last two parts of the dissertation are the references and the appendices. The citations used can be found in the reference. Some detailed information beyond the core of the thesis is presented in the appendices.

CHAPTER 2. THE PROPOSED SYSTEM AND RESEARCH APPROACH

2.1 Introduction to the proposed system

This research aims to find one solution for building energy efficiency through investigating an Integrated Compression-Absorption Subcooling System (ICASS). Based upon the principle of subcooling effect, the ICASS can improve the efficiency of the cooling device but also achieve additional useful heating sources potentially used for space heating and domestic hot water. The ICASS utilizes thermal energy as a part of power inputs to reduce the dependency of electricity so that it can reduce the peak power demand. Due to the improved system efficiency and the availability of heating source, the ICASS could also improve the cost effectiveness of the system.

Figure 2.1, the schematic system diagram for the ICASS, depicts the system configuration and design. The ICASS is composed of one VCRS and an AHP. For instance, the VCRS can be rooftop unit used for space cooling or the low temperature refrigeration system. The AHP can be single- or double-effect absorption heat pump using lithium bromide or ammonia water solution as the working fluid. The schematic diagram here only focuses on the integration of an air-cooled VC and a single-effect AHP to illustrate the working principles. In the ICASS, as the schematic diagram shows, the VC is integrated with the AHP by an additional heat exchanger called subcooler. The VC is driven by electricity consists of four major components connected in series: a

compressor, a condenser, an evaporator, and an expansion valve. Work is required to drive the compressor to circulate the refrigeration in the VC. The AHP driven by thermal energy uses the combination of desorber and absorber to replace the function of compressor in the VC. The strong mixture solution of the absorbent and the refrigerant absorbs refrigerant at lower temperature and pressure in the absorber and become dilute. The dilute mixture solution is heated at high temperature and pressure in the desorber by the external heat added. The refrigerant is boiled off from the dilute mixture solution in the desorber and goes into the condenser. In both the VC and AHP, the refrigerants absorb heat at the evaporator and reject heat in the condenser.

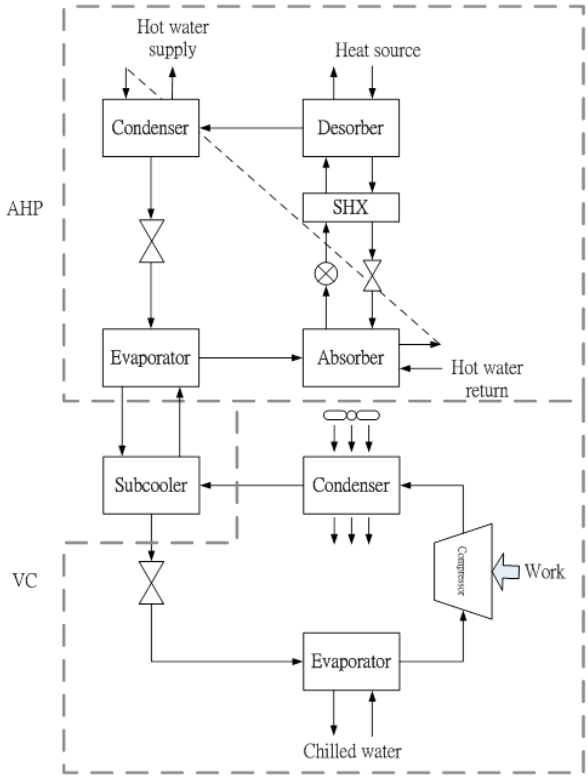

Figure 2.1 Schematic diagram of the ICASS

The VC in the ICASS severs as the cooling power producer while the AHP is used for providing hot water. The chilled water produced by the AHP is used as the cold stream to subcool the refrigerant exiting the condenser of the VC through the subcooler. The subcooler is installed between the condenser and the expansion valve of the VC. The subcooled refrigerant entering the evaporator with a lower quality can absorb more heat and produce more chilled water. Therefore, comparing to the VC alone, the ICASS can achieve the same cooling capacity by using less electricity.

The ICASS is able to provide not only cooling but also heating for buildings at the same time. The hot water return can be heated by the absorber and the condenser to around $50-60℃$, which can be directly used as domestic hot water or for heating with additional energy added.

2.2 Research approach

The research approach of this study is shown in Figure 2.2. First of all, a test bed of the ICASS was designed and constructed. The VC and AHP were tested individually and together as the ICASS according to the designed test programs. Thermodynamics and heat transfer models of the VC, AHP, and ICASS were developed based on the test bed. Experimental data such as water return temperatures and flow rates were used as inputs of the models. The modeling and calculated results such as the water supply temperatures and heating and cooling capacities were compared with the experimental data. The models were adjusted until the modeling results made good agreements with the experimental data. These validated models were used for the following studies.

The model-based energy and exergy analysis was the extension of the thermal and heat transfer models. The influences on system performance from the candidate parameters were analyzed via the validated models. Key parameters were then identified by conducting the sensitivity analysis.

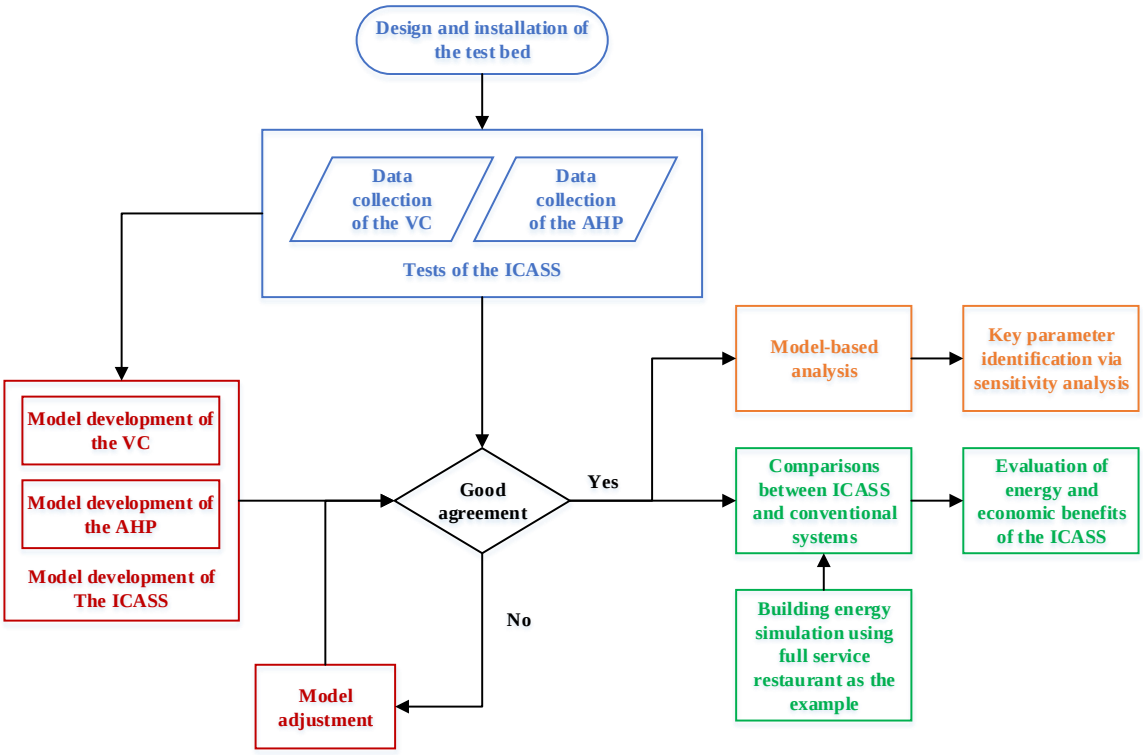

Figure 2.2 Flow chart of the research approach

The validated models were also used to evaluate the energy and economic benefits of the ICASS. The energy and economic savings of the ICASS was predicted and compared with other different systems. Finally, full service restaurant was selected as the example to conduct the building energy simulation. The most suitable locations and building types for applying the ICASS were discussed through the building energy simulation.

CHAPTER 3. LITERATURE REVIEW

This chapter is the literature review for this research. The reviews focused on the researches which are related to this study. The researches include the integration of different refrigeration cycles, the technology of ARS, the experiments and models of VCRS and ARS, the exergy analysis of the refrigeration system, and the building energy simulation.

3.1 Integration of different refrigeration cycles

In this section, the integrated systems which include two or more refrigeration cycles are reviewed. The refrigeration cycles here include vapor-compression or absorption refrigeration cycles.

3.1.1 Cascade refrigeration system

For a VCRS, the electricity consumption will be large and the COP will be very low if the system is operated at the condition of significantly large temperature and pressure difference. One of the solutions to solve this issue is staging the cycle through integrating two or more cycles. These kinds of systems are so called cascade refrigeration systems (Moran, 2010). Figure 3.1 shows the schematic diagram of the cascade refrigeration system. Take a two-stage cascade VCRS as an example, two refrigeration cycles are

integrated through a heat exchanger. The heat exchanger serves respectively as the condenser of the lower temperature cycles and the evaporator of the higher temperature cycle at the same time. The heat rejected by the lower temperature cycle at the condenser is thus the same as the heat absorbed by the higher temperature cycle at the evaporator. The two integrated cycles can use different but the most suitable refrigerants for the operation temperatures. The cascade refrigeration system can reduce the power consumption and increase the COP comparing to the system with only one refrigeration cycle.

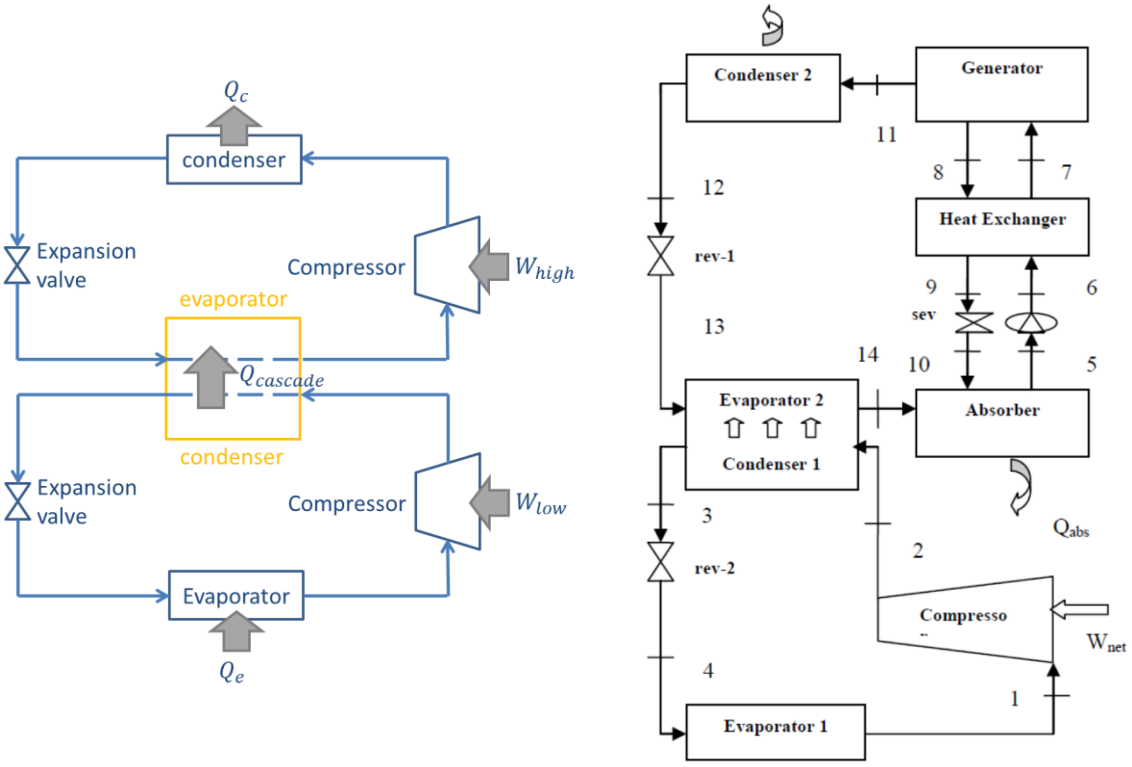

(a) vapor-compression cascade system

(b) compression-absorption cascade system (Cimsit and Ozturk, 2012)

Figure 3.1 The cascade refrigeration system

In order to reduce the dependency of the electricity, many researchers used the ARS to replace one of the VCRS in a cascade refrigeration system. For the compression-

absorption cascade system, Tarique and Siddiqui (1999) conducted performance and economic analyses for the comparison of the combined absorption/compression cycle using NH_3–NaSCN solution and the compression cycle with pure ammonia. The results showed the capital and operation costs of the compressors in the NH_3–NaSCN were significantly reduced. Kairouani and Nehdi (2006) investigated the compression-absorption cascade system which used ammonia–water solution for the absorption cycle and R717, R22, and R134a for the compression cycle respectively. The results showed the COP was improved by 37–54% of the integrated system comparing with the conventional single-stage cycle at the same operation conditions. Cimsit and Ozturk (2012) studied the compression-absorption cascade system used LiBr–H_2O and NH_3–H_2O solutions for the absorption cycle and R134a, R-410A and NH_3 for the compression cycle respectively. It was found that electricity consumption in the cascade refrigeration cycle was 48–51% lower than the conventional vapor-compression refrigeration cycle at the same operation conditions.

3.1.2 Dedicated mechanical-subcooling system

Many studies investigated different methods to improve the efficiency of the VCRS (Minh et al., 2006). Among them, DMSS, as one of the approaches, combines two VCRSs to improve the overall efficiency. Figure 3.2 shows the schematic diagram of the DMSS. For example, a main VCRS and another VCRS with a smaller capacity integrated together via a sub-cooler. The sub-cooler is actually the evaporator of the smaller VCRS and is located between the condenser and the expansion valve of the main VCRS. The refrigerant of the smaller VCRS is the coolant of the refrigerant of the main chiller. These

two refrigerants exchange heat in the sub-cooler. The refrigerant of the main VCRS exiting the sub-cooler has been subcooled to lower temperature; it thus has lower quality exiting the expansion valve. This refrigerant with lower quality can absorb more heat in the evaporator. Meanwhile, the condensing temperature of the main VCRS decreases so the electricity consumption decreases and the COP increases. Couvillion et al. (1988), based on their modeling work, concluded that the improvements of COP and the system capacity due to the DMSS were 80% and 170%, respectively. Thornton et al. (1994) investigated the optimal evaporating temperature of the smaller VCRS to maximize the COP of the overall system. However, the improved COP of the DMSS was limited by the smallest COP of the two VCRSs. Khan and Zubair (2000) drew similar conclusions based on the modeling results. There exists an optimal evaporation temperature of the subcooling cycle which maximizes the overall COP. Additionally, this optimal temperature is affected by the size of the sub-cooler. Qureshi and Zubair (2012) investigated different refrigerant combinations for the application of DMSS. R134a and R717 were used in the main cycle and R134a, R410A, and R407C used in the subcooling cycle respectively. The results showed the case of using R134a in both cycles had the best performances. Qureshi et al. (2013) conducted an experiment of the DMSS which used R22 and R12 in the main and subcooling cycles respectively. The results showed the second-law efficiency of the system increased by an average of 21%. Furthermore, the results indicated the improvement was inversely influenced by the variation of ambient temperature. The experimental results proved that DMSS can be used for increasing both the cooling capacity and the efficiency. Following the same idea as the compression-absorption cascade system, some studies focused on the integration of VCRS and ARS

for the DMSS. Hwang (2004) carried a model based study on an integrated system, which combines a micro-turbine and an absorption chiller with a main VCRS. The micro-turbine used natural gas as the fuel to generate power. The exhaust gas emitted from the micro-turbine was used as the thermal source to drive an absorption chiller. The chilled water produced by the absorption chiller was used to subcool the refrigerant exiting the condenser of the main VCRS powered by electricity. The VCRS was mainly used to provide space cooling. According to their modeling results, it is predicated that the COP was improved from 1.43 - 3.70 to 1.78 - 3.84. The annual energy consumption reduced 12% and the simple payback period was 7 years.

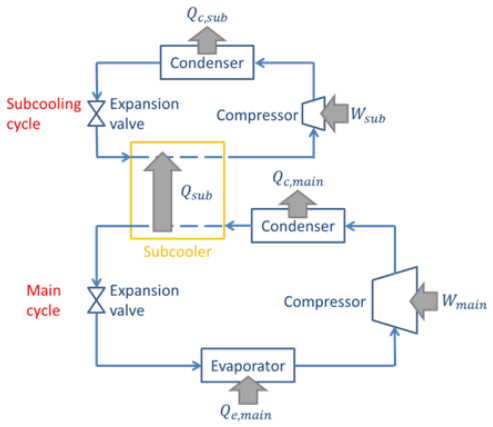

Figure 3.2 Schematic diagram of the DMSS

Another similar system was installed in San Antonio, Texas. According to the final report submitted to Oak Ridge National Laboratory (2005), the system combined an 18 tons absorption chiller with the original refrigeration system. Although the report indicated that the system was not cost effective because of the high parasitic electricity consumption and relatively high natural gas price at that time, the annual savings due to the subcooling effect was still reported at $4,400.

3.2 The technology of the absorption refrigeration system

The development of ARS can be traced back to the 1700's. A vessel with water was placed within an evacuated container with sulfuric acid. Ice could thus be produced by the evaporation of water (Gosney, 1982; Herold and Radermacher, 1989) Ferdinand Carre introduced a prototype in 1859 which used ammonia water solution as working fluid to make ice and store food. It was seen as the basic design in the early age of the refrigeration development (Srikhirin et al., 2001). A system which used lithium bromide water solution as the working fluid was introduced later in the 1950's for industrial applications. A few years later, a double-effect absorption system was introduced (Srikhirin et al., 2001). The major difference between the VCRS and the ARS is, the ARS uses the combination of desorber (or generator) and absorber to replace the function of compressor in the VCRS. Therefore, the ARS utilizes thermal energy instead of electricity as driven power.

Another difference between VCRS and the ABS is the working fluid. Most VCRS uses chlorofluorocarbon (CFC) refrigerant as working fluid. However, CFCs may cause the depletion of the ozone layer. Unlike the VCRS, ARS uses eco-friendly mixture such as lithium bromide or ammonia water solution as working fluid. Although there are hundreds of availabilities for working fluid used in the ABS (Marcriss, 1988), lithium bromide and ammonia water solutions are the two most common choices. Both mixtures meet the requirements of working fluid for the ABS but also have some shortages. For the lithium bromide water solution, it has high safety, high volatility ratio, high affinity, high stability and high latent heat. However, it is corrosive to some materials. Also, it is possible for solid formation. Water turns into ice at 0°C so the lithium bromide water

solution cannot be used for low temperature refrigeration. Furthermore, lithium bromide crystallizes at moderate concentrations. When the absorber is air-cooled, these concentrations tend to be reached. Therefore, ARS with lithium bromide water solution is usually limited to the water cooled type (Mansoori and Patel, 1979; Horuz, 1998).

For the ammonia water solution, it is chemical stable and non-corrosive. Also, it has high affinity and high latent heat. It can be used for all kinds of applications, especially in large capacity industrial applications requiring low temperatures for process cooling. Nevertheless, ammonia is toxic and has strong odor. Additionally, water is reasonably volatile so the ammonia vapor leaving the desorber usually contains certain amount of water vapor. In order to further purify the ammonia vapor, additional device such as rectifier must be installed to remove the water vapor from the mixture leaving the desorber (Mansoori and Patel, 1979; Horuz, 1998). The cycle of the ammonia solution system is thus more complex; the design and simulation will be more difficult as well.

3.3 Tests of the refrigeration systems

In AHRI standard 550/590 (IP) or 551/591 (SI) (2013), it defines the test conditions of a vapor-compression chiller to rate its performance at full and part load conditions. For example, the water flow rate of the cooling water should be at the range of 0.018 – 0.0108 L/s-kW at full load condition. This value is held but the temperature of the cooling water entering the condenser should change from 30℃ to 24.5℃ at 75% of full load condition. Similar standard is defined in the AHRI standard 560 (2000) for the absorption chiller. The AHRI standards are the references for the manufacturers to test their machines and published the performance data. However, researchers are more

interested in the influences of the controlled or environmental parameters. Horuz and Callander (2004) investigated the performance of a commercially available air-cooled absorption chiller. The gas-fired chiller used ammonia water solution as the working fluid. The rated cooling capacity is 10 kW. The unit was extensively modified to allow pressures, temperatures, and flow rates to be measured. Yin (2006) conducted experiments of a double-effect absorption chiller using lithium bromide water solution as the working fluid. Five different parameters were tested. Only the tested parameter changed and the other parameters remained the same at the design values. The calculated cooling capacity and the COP were the performance indicators to compare the influences of the tested parameter. Rossa and Bazzo (2009) conducted both experiment and modeling of a small cogeneration system which included a 5 ton absorption chiller connected by a thermosyphon heat exchanger to a 28 kW natural gas microturbine. The results showed the consistency of the proposed model and a good performance of the cogeneration system, however, detailed comparisons between the modeling and experimental results were not found. Jawahar and Saravanan (2011) investigated on the performance of an air-cooled modified generator absorber heat exchange (GAX) absorption cooling system. The system is designed for a cooling capacity of 10.5 kW using ammonia water solution as the working fluid. The results indicated that, when the temperatures of the generator and evaporator were 120℃ and 2℃, respectively, the system has the highest cooling capacity of about 9.5 kW with a fuel and total COP of 0.61 and 0.57, respectively.

3.4 Models of the refrigeration systems

The models of VCRS and ARS are basically the combination of the models for its components. The most components for the refrigeration systems are the heat exchangers. The other components are related to the pressure changes such as the compressor, the solution pump, and the expansion devices. The models of the components and systems will be discussed in this section.

3.4.1 Modeling of the vapor-compression refrigeration system

A VCRS model primarily includes a compressor, a condenser, an evaporator, and an expansion device. For the compressor models, Zhao et al. (2009) categorized them into three groups which are 1) map-based model, 2) efficiency-based model, and 3) detailed model. The detailed model needs the most information about the compressor and has the highest accuracy. Rasmussen and Jakobsen (2000) also categorized the compressor models based on the detail level of knowledge needed to develop the model. Models that require the lowest level of knowledge are called "Black-box" models and models that require the highest level of knowledge are called "White-box" models. From black to white, these models are 1) model with statistical correlations based on system performance variables, 2) model with statistical correlations based on compressor performance variables, 3) process-oriented models, 4) phenomena-oriented models, 5) construction-oriented models, and 6) distributed models. Again, models with more information are more accurate. However, for the system level modeling, the map-based model or efficiency-based model are typically used for its relative accuracy and

simplicity. For example, polynomial equation from AHRI stand 540 (2004) can be used for describing the compressor performances on system level modeling.

The condenser and evaporator of the VCRS are essentially heat exchangers. Heat exchanger models can be largely classified into four categories: 1) lumped parameter model, 2) zone model or moving boundary model, 3) distributed parameter model or finite volume model, and 4) tube-by-tube model (Qiao et al., 2010). Heat exchanger models with more information has higher accuracy as same as the compressor model. For the system level modeling, the lumped parameter model can be used for its relative accuracy and simplicity. Two methods usually used for the heat exchanger modeling are the log mean temperature difference (LMTD) method and effectiveness-NTU (ε-NTU) method (Incropera, 2011). Both methods are easy to use, however, using LMTD method requires more given parameters while ε-NTU method only needs the inlet conditions of the fluids.

The two groups of the models for expansion devices are: 1) correlation-based model and 2) distributed parameter model (Qiao et al., 2010). However, these two models are both used for detail modeling of the expansion devices. In the system level modeling, isenthalpic process is usually assumed for the expansion device.

3.4.2 Modeling of the absorption refrigeration system

The working fluid of the ARS is the mixture of absorbent and refrigerant rather than pure refrigerant. Additionally, the ARS usually has many internal heat exchanges which make the models complicated. Herold et al. (1996) used lumped parameter model for all the absorption cycles in their book. These models were developed in the EES. Gordon and

Ng (1995) used the approach based on the first and second laws of thermodynamics to simulate an absorption chiller. Grossman and Zaltash (2000) proposed an absorption system simulation software called ABSIM, which allows users to add and assemble the components together to finish an absorption cycle. The ARS using lithium bromide and ammonia water solutions were successfully modeled in the ABSIM. Additionally, it provides many examples for users to choose. Darwish et al. (2008) used a commercial program called Aspen Plus to simulate an air-cooled ammonia/water absorption chiller. Aspen Plus is an advanced flow sheet simulator that has extensive databases available for the physical–chemical properties (Aspen Plus, 2004). The simulation results were similar to the results from Lazzarin et al. (1996). May et al. (2010) developed a modular simulation program of the absorption heat pumps, refrigerators and air conditioners in MATHEMATICA. This program was used to simulate the ARS using either lithium bromide or ammonia water solution as working fluid. The results showed favorable agreements with the experimental measurements.

3.5 Exergy analysis of the refrigeration system

In most of the studies, the models developed and the analyses were based on the energy method, also known as the first-law analysis. However, exergy analysis, also known as second-law analysis, gives more details about how well the energy input is used by the system. The definition of exergy is: the maximum useful work that can be achieved for a system by reducing the system losses in environmental conditions. Exergy reduction is due to the friction and other irreversibilities. The reduction in the exergy content of

energy will decrease the efficiency of the system. The exergy losses should thus be minimized for increasing the system efficiency (Moran. 2010).

For the exergy analysis of VCRS, Yumrutas et al. (2002) investigated the effects of the evaporating and condensing temperatures on the irreversibilities, COP, and exergy efficiency of a VCRS. It was found that the evaporating and condensing temperatures strongly affected the irreversibilities in the evaporator and condenser, the COP, and the exergy efficiency. However, they had only little effects on the irreversibilities in the compressor and the expansion valve. Ahamed et al. (2011) reviewed many studies which performed exergy analysis of the VCRS. It was found that exergy efficiency depend on evaporating temperature, condensing temperature, subcooling, compressor pressure and environmental temperature. Furthermore, different refrigerants will also affect the exergy efficiency.

Similarly, the irreversibility of each component, the COP, and the exergy efficiency of the ARS were analyzed and discussed on different design and operation conditions. The studies can be categorized into two groups: Ataer and Gogus (1990), Sozen et al. (2002), and Ezzine et al. (2004) conducted exergy analysis of the ARS which utilizes ammonia water solution as the working fluid while Talbia and Agnew (2000), Lee and Sherif (2001), and Sencan et al. (2005) have performed the exergy analysis of the ARS with lithium bromide water solution as working fluid. In these studies, the calculations of heating and cooling exergy efficiency, the selection of proper control volume, and the determinations of component temperatures were emphasized and reviewed.

The exergy analysis of the ICASS should be similar to the compression–absorption cascade system. Colorado and Velazquez (2013) investigated the compression–

absorption cascade system with different combinations of refrigerants and working fluids. The irreversibility of each component, the COP, and exergy efficiency were analyzed and discussed. It was found that the R134a–LiBr/H_2O system had the highest COP. Cimsit and Ozturk (2014) performed energy and exergy analysis of the compression-absorption cascade system. Also, different combinations of refrigerants and working fluids were analyzed and compared. It was found that ammonia-LiBr/H_2O cascade system had the best performance. Moreover, the results showed that the COP increased with the temperatures of generator and evaporator, while it decreased as the temperatures of condenser and absorber increased. However, the exergy efficiency decreased as the temperatures of generator, absorber and condenser increased. Jain et al. (2013 and 2015) treated the electricity and thermal energy as high grade energy and low grade energy respectively. The electricity and thermal energy consumed by the compression and absorption cycles were converted back to the primary energy. The resource COP and the exergy efficiency of the overall system were then calculated. Also, the separated COP for the compression and absorption cycles were calculated and shown as the references.

CHAPTER 4. THE TEST BED AND EXPERIMENT

4.1 Overview of the test bed

A test bed of the ICASS was designed and constructed in the Herrick Labs at Purdue University. Figure 4.1 shows the components of the test bed and the locations of the sensors. The test bed is primary composed by an electrical water-cooled chiller, a direct-fired absorption heat pump, three flat plat heat exchangers, two water circulation pumps, and the data acquisition (DAQ) system.

The test bed was designed for the tests of the VC, the AHP, and the ICASS. When the VC was tested alone (marked 1), the chilled water loop is connected between the evaporator and the steam-to-water heat exchanger (HX). The chilled water from the chiller was balanced by the hot steam in the steam-to-water HX and returned to the chiller. The steady state operations were achieved or a dynamic building cooling load was simulated by regulating the pressure of the steam. City water was used as the cooling water to remove the heat in the condenser and the heated water was directly drained out. For the tests of the AHP (marked 2), the hot water loop was connected between the condenser and the water-to-water HX. The hot water was balanced by the city water and returned to the heat pump. The steady state operations and a dynamic building heating load were applied to the heat pump by regulating the flow rate of the city water. The chilled water loop bypassed the subcooler and went through the steam-to-water HX just

like the chilled water loop of the VC. Again, hot steam was used to simulate the cooling load.

In the tests of the ICASS, the chilled water loop of the AHP was connected between the subcooler and the condenser of the AHP. The chilled water from the AHP was balanced by the refrigerant of the VC in the subcooler.

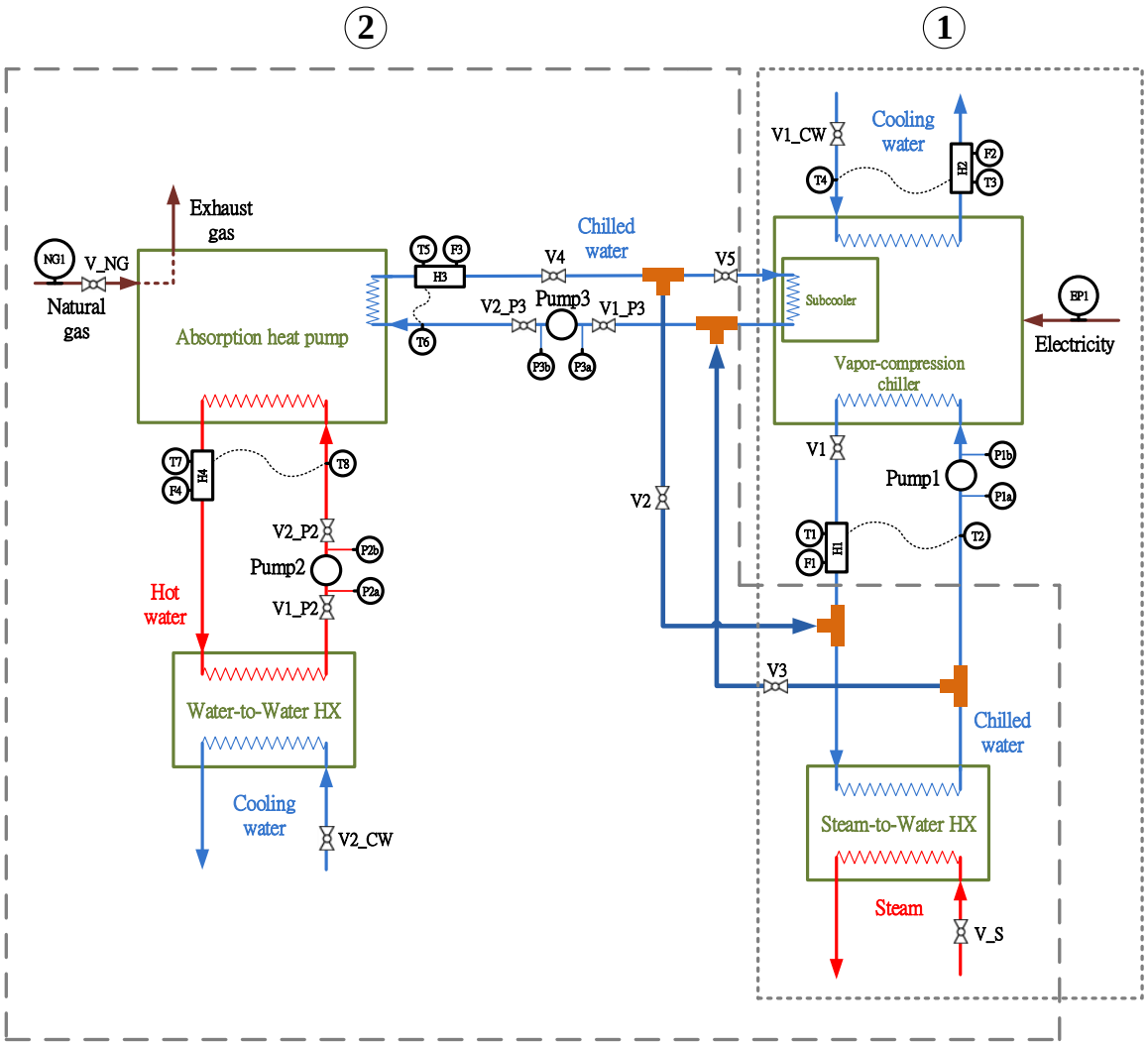

Figure 4.1 Schematic diagram of the test bed and the sensor locations

4.1.1 Vapor-compression chiller

The VC installed was manufactured by Dunham-Bush. It uses R22 as the refrigerant. According to the name plate, the cooling capacity of the chiller is 15 tons (52.8 kW). The picture of the chiller is shown as Figure 4.2.

Figure 4.2 Dunham-Bush electrical water-cooled chiller

Figure 4.3 shows the components of the VC. The VC is mainly comprised of a compressor, a condenser, a receiver, an expansion, an evaporator, and ad internal heat exchanger (IAX). Electricity is used as power to drive the compressor. The refrigerant can thus be lifted from low to high temperature and pressure through the compressor. The refrigerant with high pressure and temperature is cooled by rejecting heat to the cooling water in the condenser. The receiver is right after the condenser. It serves as a temporary storage for the liquid refrigerant and a vapor seal to keep vapor out of the liquid line to the expansion valve. The liquid refrigerant is subcooled by the refrigerant exiting the evaporator in the IHX then enters the expansion valve. The refrigerant exiting the expansion valve has lower temperature and pressure and can thus absorb heat from the chilled water in the evaporator. Again, the refrigerant exiting the evaporator is preheated

in the IHX to make it fully evaporated. The refrigerant goes back to enter the compressor and finish the working cycle. The components mentioned above are shown in Figure 4.3

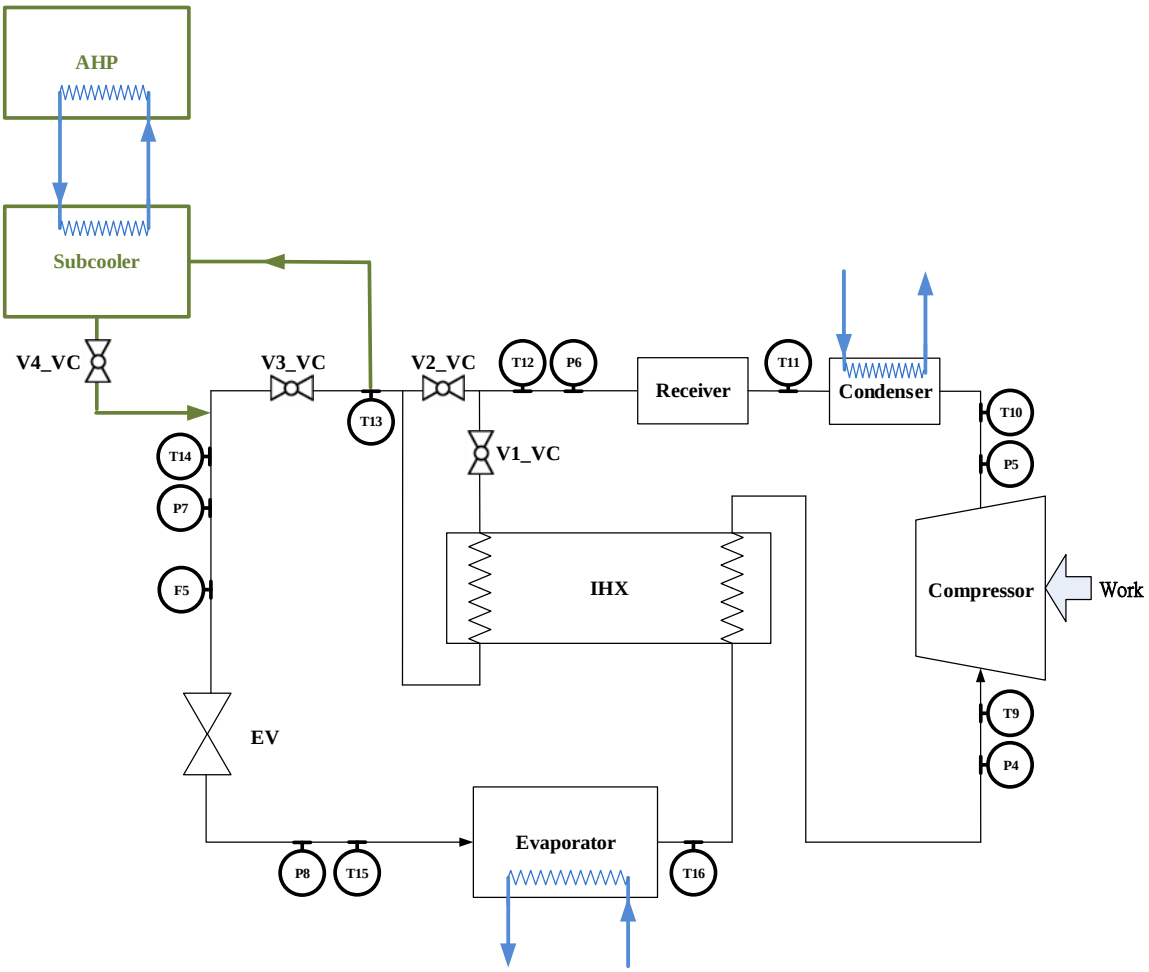

Figure 4.3 Schematic diagram of the VC and the modification

Besides, the VC was modified in order to integrate with the AHP. The refrigerant pipe line of the VC between the receiver and the expansion valve was broken and connected to the subcooler. Additional four valves (V1_VC, V2_VC, V3_VC, and V4_VC) were installed for switching the VC from independent or integrated operation mode.

4.1.2 Absorption heat pump

The AHP installed is manufactured by Robur. The AHP uses ammonia water solution as the working fluid. It is able to produce chilled and hot waters simultaneously. According to the manufacturer, the cooling and heating capacities of the AHP at the design condition are around 16.82 kW and 39.53 kW respectively. The supply/return chilled water temperatures are 7/12℃ while the supply/return hot water temperatures are 50/40℃ (Robur, 2013). The detailed specification of the heat pump is illustrated in Table 4.1; the picture of the heat pump is shown as Figure 4.4.

Table 4.1 Specification of the absorption heat pump installed
(Robur, 2013)

Parameter		Unit	Quantity
Hot water	Hot water supply temperature	℃	50
	Hot water temperature difference	℃	10
	Hot water flow rate	kg/s	0.92
	Heating capacity	kW	39.53
	Heating efficiency	%	141
Chilled water	Chilled water return temperature	℃	12
	Chilled water temperature difference	℃	5
	Chilled water flow rate	kg/s	0.78
	Cooling capacity	kW	16.82
	Cooling efficiency	%	60
Burner	Nominal heat capacity	kW	27.98
Power	Power voltage, 60 HZ, single phase	V	208-230
	Total electrical operating consumption (nominal)	kW	0.4
Physical data	Operating weight	Pounds	630.5
	Width	Inches	33.25
	Depth	Inches	25.75
	Height	Inches	50.75

The AHP is comprised of many different heat exchangers as shown in Figure 4.5. The strong ammonia water solution, which is rich in ammonia, entering the generator (desorber) is heated at high temperature and pressure by external heat added. Ammonia

vapor is boiled off from the strong ammonia water solution and goes into the rectifier; meanwhile, the weak ammonia water solution exits the desorber at the other end. Because of the high affinity, the ammonia vapor exiting the desorber will always contain some water vapor. The water vapor is cooled and condensed in the rectifier so the almost pure ammonia vapor can be obtained. The almost pure ammonia vapor enters the condenser next and the condensed water goes back to the desorber. The ammonia vapor rejects heat at the condenser then reduces its pressure and temperature by going through two expansion valves. This ammonia with lower pressure and temperature will absorb heat in the evaporator.

Figure 4.4 Robur GAHP-W heat pump

There is actually an additional heat exchanger called precooler between the condenser and the evaporator. Ammonia fluids exiting the condenser and the evaporator will exchange heat at the precooler. The ammonia vapor exiting the precooler will be absorbed in the absorber by the weak ammonia water solution from the desorber. The weak ammonia water solution also goes through an expansion valve before enters the

absorber. The ammonia vapor from the precooler and the weak ammonia water solution from the desorber will thus at the same pressure level. Since the ammonia vapor is absorbed by the weak ammonia-water solution, strong ammonia water solution is formed and exits the absorber. This strong ammonia water solution rejects heat again at the condenser and enters the pump. The ammonia water solution after the pump will go through the rectifier and absorber in series as the cold stream to absorb heats. It finally enters the desorber to finish the cycle.

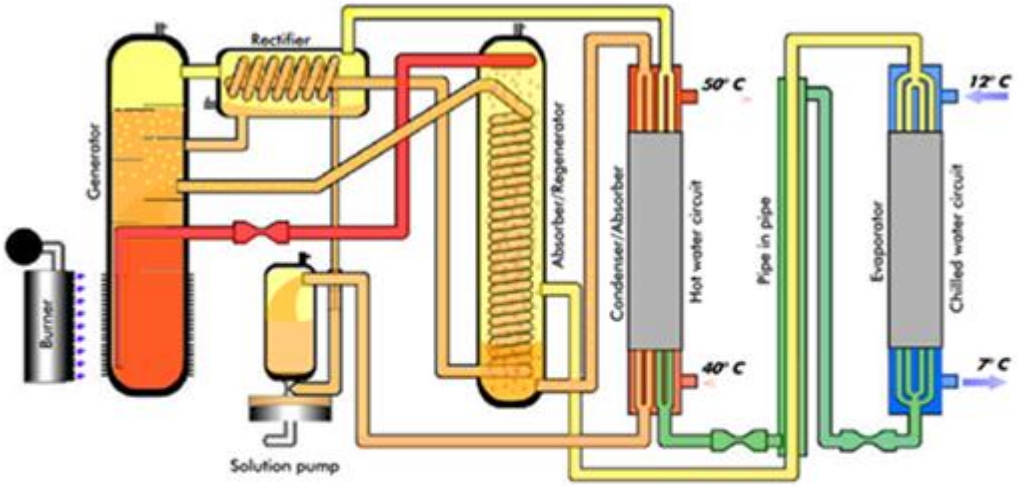

(Robur, 2013)

Figure 4.5 Operation cycle of the Robur GAHP-W heat pump (Robur, 2013)

4.1.3 Heat exchanger

The three heat exchangers installed in the test bed are the subcooler, the steam-to-water HX, and the water-to-water HX as shown in Figure 4.6(a), (b), and (c) respectively. Flat plate type of heat exchangers was selected for the three heat exchangers. For the

subcooler, it should be brazen sealed or sealed with epoxy in order to prevent leaking of the refrigerant.

(a) Subcooler

(b) Steam-to-water HX

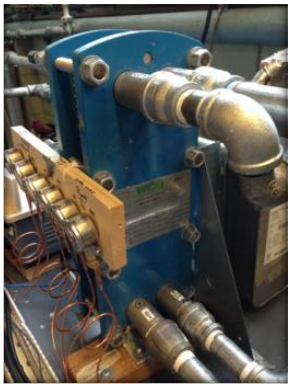

(c) Water-to-water HX

Figure 4.6 The heat exchangers installed in the test bed

4.1.4 Pump

The two water loops of the AHP need pumps which can overcome the pressure drops in the system and provide the required flow. TACO 2400-50 circulation pump, as shown in Figure 4.7, were selected for both the hot and chilled water loops of the AHP. The VC already has a pump for the chilled water loop. For the cooling water of the VC, city water is directly driven by the pressure difference.

Figure 4.7 Pumps for the water loops of the AHP

4.1.5 Data acquisition system

The DAQ system used for the test bed consists of different kinds of sensors, measurement hardware such as data logger to receive signals from the sensors, and programmable software on the computer to display and store the data. The sensors installed in the test bed were used to measure temperature, pressure, flow rate, electrical power, and natural gas consumption. T type thermocouples and pressure transducers were selected to measure the temperatures and pressures of the refrigerant in the VC; both of them were manufactured by Omega. A flow meter from Micro Motion was installed to measure the flow rates of the refrigerant in the VC. The electrical power of the VC compressor was measure by a power transducer manufactured by Ametek. A natural gas meter produced by Itron was used to measure the natural gas consumption. Finally, heat meters manufactured by Broad were installed in the water loops to measure the flow and both the supply and return temperatures.

For the DAQ measurement hardware and software, all of the sensors have analog signal outputs except the heat meters and the natural gas meter. The sensors with analog signal outputs were connected to the data logger which comprised of two modules and a chassis. The two modules and the chassis are the NI 9210, NI9103, and NI cDAQ 9178 from National Instruments. The heat meters have digital output and use RS485 as the communication protocol. Therefore, a RS485-to-USB cable was used to connected heat meters to the computer. The data logger and the RS485-to-USB cable were connected to the computer. LabVIEW, the programmable software also from National Instruments, was used to interpret the signals, display the readings, and save the data.

Additionally, some readings of the sensors could only be monitored and recorded manually. Six physical pressure gauges were installed at the inlets and outlets of the three water circulation pumps; their readings could only be recorded manually. These pressure gauges were used to monitor the pressures of the water loops. The natural gas meter is located outside of the building and far from the test bed. The reading of the natural gas meter was thus also recorded manually. The sensors and data logger are shown and listed in Figure 4.8 and Table 4.2. The locations of the sensors are illustrated in Figure 4.1 and Figure 4.3.

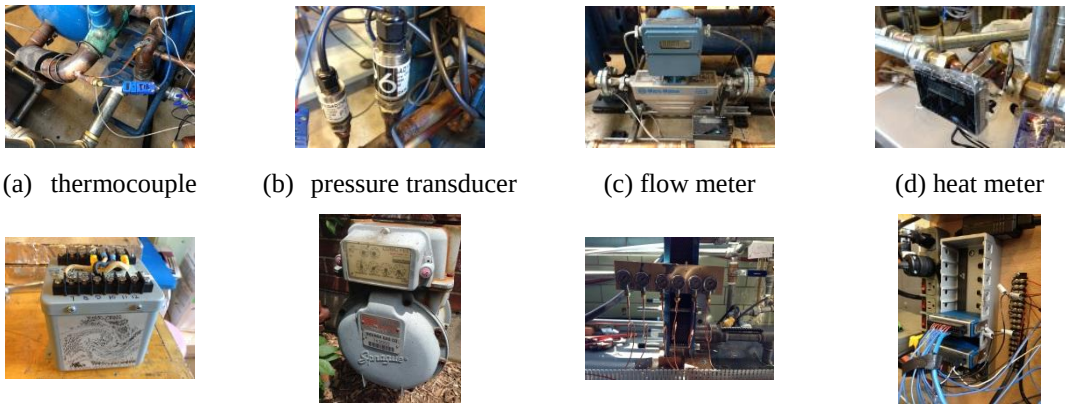

(a) thermocouple (b) pressure transducer (c) flow meter (d) heat meter

(e) power transducer (f) natural gas meter (g) pressure gauge (h) data logger

Figure 4.8 Sensors and data logger installed in the test bed

4.2 Test programs

Before the tests of the ICASS, the AHP and the VC were tested individually to understand their performances. The following sections will introduce the test programs of the AHP, the VC, and the ICASS.

Table 4.2 DAQ system of the test bed

Sensor						
	Label	Location	Medium	Measurement Range	Manufacturer accuracy	Note
Temperature	T1(H1)	VC, chilled water outlet	water	0 - 105°C	Matching precision: 0.1˚C	Digital output, RS485 protocol
	T2(H1)	VC, chilled water inlet				
	T3(H2)	VC, cooling water outlet				
	T4(H2)	VC, cooling water inlet				
	T5(H3)	AHP, chilled water outlet				
	T6(H3)	AHP, chilled water inlet				
	T7(H4)	AHP, hot water outlet				
	T8(H4)	AHP, hot water inlet				
	T9	VC, compressor inlet	Refrigerant(R22)	-250 - 350°C	±0.4%	-
	T10	VC, compressor outlet				
	T11	VC, condenser outlet				
	T12	VC, receiver outlet				
	T13	VC, subcooler inlet				
	T14	VC, subcooler outlet				
	T15	VC, expansion valve outlet				
	T16	VC, evaporator outlet				
Pressure	P1a	Pump1 inlet	Water	0 - 100 PSI	-	Physical meter
	P1b	Pump1 outlet				
	P2a	Pump2 inlet				
	P2b	Pump2 outlet				
	P3a	Pump3 inlet				
	P3b	Pump3 outlet				
	P4	VC, compressor inlet	Refrigerant(R22)	0 - 300 PSI	±0.25%	4 – 20 mA output
	P5	VC, compressor outlet				
	P6	VC, receiver outlet				
	P7	VC, expansion valve inlet				
	P8	VC, expansion valve outlet				

Table 4.2 continued

Flow rate	F1(H1)	VC chilled water loop	Water	0.2 - 20 m^3/h	Precision: Grade 2	Digital output, RS485 protocol
	F2(H2)	VC cooling water loop		0.12 - 12 m^3/h		
	F3(H3)	AHP chilled water loop		0.05 - 5 m^3/h		
	F4(H4)	AHP hot water loop		0.05 - 5 m^3/h		
	F5	VC refrigerant	Refrigerant(R22)	0 - 1360 kg/hr	±0.5%	4 – 20 mA output
	EP1	Compressor of the chiller	n/a	0 – 20 kW	±0.2%	4 – 20 mA output

Data logger	
Name	Function
NI cDAQ 9178	CompactDAQ chassis (8-slot USB) for NI 9213 and NI 9203
NI 9213	16-channel thermocouple input module
NI 9203	8-Channel +/-20 mA analog input module
USB TO RS485 ADAPTER	Receive the signal from the heat meters

4.2.1 Test program of the AHP

The AHP was first tested at the design condition. Based on the design condition, four parameters were tested which were the hot water return temperature (T_hw,r), the chilled water return temperature (T_chw,r), the hot water flow rate (FR_hw), and the chilled water flow rate (FR_chw). The tests of different hot and chilled water temperatures actually represented the tests of AHP at different heating and cooling loads respectively. The flow rates of the hot and chilled waters were the other two parameters which could be modulated. Only one tested parameter was changed and tested at one time while the other three tested parameters remained at the same as the design condition. For example, when the T_hw,r was tested, it changed from 40℃ to 30℃, but the T_chw,r, the FR_hw, and the FR_chw remained at 12℃, 0.92 kg/s, and 0.78 kg/s respectively as the same as the design condition. The design condition and the test ranges of the tested parameters are summarized in Table 4.3. The test range of the T_hw,r and T_chw,r and the minimum tested value of the FR_hw and FR_chw were referred to the manual of the AHP. The maximum tested value of the FR_hw and FR_chw were limited by the equipment.

Table 4.3 Test ranges of the parameters for the AHP

	T_hw,r [℃]	T_chw,r [℃]	FR_hw [kg/s]	FR_chw [kg/s]
Design condition	40	12	0.92	0.78
T_hw,r	30 - 50	12	0.92	0.78
T_chw,r	40	12 - 30	0.92	0.78
FR_hw	40	12	0.51 - 0.97	0.78
FR_chw	40	12	0.92	0.63 - 0.84

4.2.2 Test program of the VC

Two parameters of the VC could be controlled and tested. The two tested parameters were the cooling water flow rate (FR_cw) and the chilled water return temperature (T_chw,r). The test range of the FR_cw was 0.83 to 1.94 kg/s. The FR_cw was the only parameter which could be tested of the cooling water since the temperature of the city water remained constantly around 15℃. The test range of the T_chw,r was 11.07 – 20.19℃. Different T_chw,r could be achieved by modulating the steam pressure. Different combinations of these two parameters were tested in order to collect as much data as possible. The collected data was used to develop the correlation equations of some parameters, for example, power input as the function of condensing and evaporating pressures or temperatures.

4.2.3 Test program of the ICASS

The tests of the ICASS focused on two aspects which were 1) the steady state operation and 2) the comparison with the VC alone. The ICASS was first operated at one steady state to see its performance. The six parameters mentioned in the previous two sections, the four parameters of the AHP and the two parameters of the VC, were modulated to make the ICASS stable. Some crucial points of the ICASS were identified via the test. The next step was the comparisons between the ICASS and the VC alone. The two systems were operated at the same cooling capacity or power input. Their performances were compared to see the differences.

4.3 Test result

The test results of the AHP, the VC, and the ICASS will be discussed in the following sections. The tests were conducted in the summer of 2014 from June to September. The total hours of the tests were around 115 hours: 52, 38, and 25 hours for the AHP, the VC, and the ICASS respectively. Except understanding the performances of the systems, the test results were used for the model validations later.

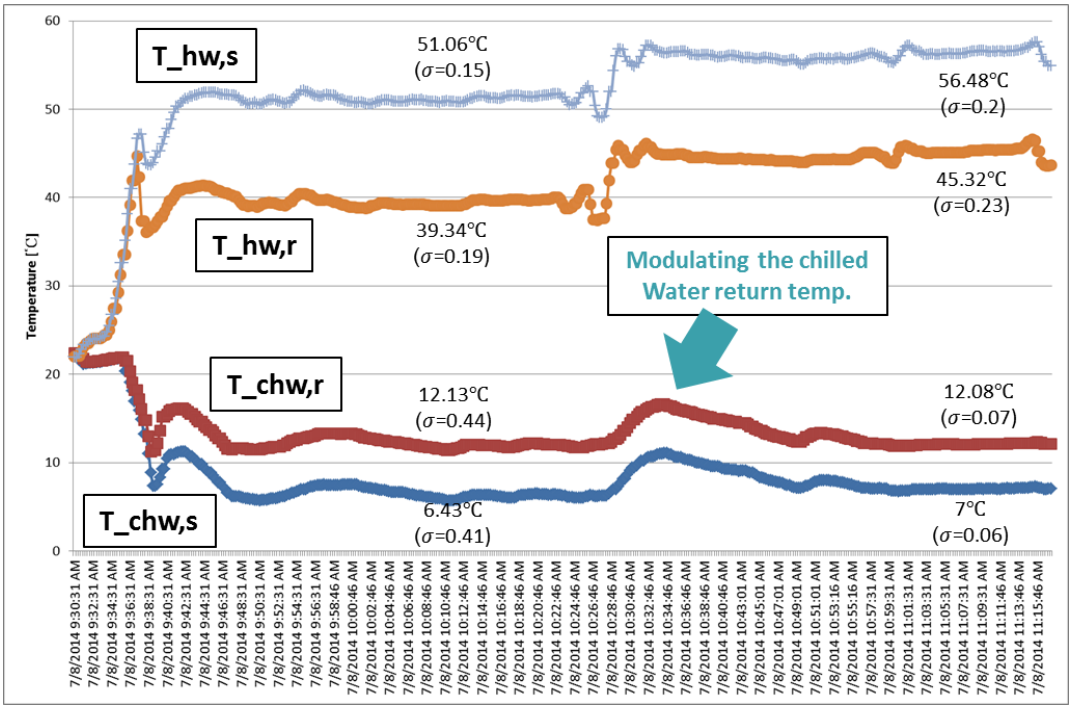

Figure 4.9 An example for the tests

Figure 4.9 shows an example for the tests. The tests were conducted on July 8, 2014 for two different T_hw,r. Data was recorded every 15 seconds. It can be observed from the diagram, when the T_hw,r was increased from 40 to 45℃, the chilled water temperatures also increased at the beginning. However, since only one parameter changed at one time, the other parameters were controlled as the designed value, the T_chw,r was thus

controlled back to around 12℃. The four water temperatures were monitored to see if the system was stable or not. The average of a parameter was calculated to represent the value of the parameter during the selected period. The process for the testes of VC and ICASS were similar as the example showed here.

4.3.1 Test result of the AHP

4.3.1.1 Test result of the AHP at design condition

The tests of the AHP at design condition were carried out twice on July 8 and August 7, 2014. The test results are listed in Table 4.4. The temperatures and flow rates of the chilled and hot waters were measured and recorded by the DAQ system. The heat input of the AHP was calculated from the readings of the natural gas meter. The temperature differences, the capacities, and the COPs were calculated from the measured values. The capacity is the product of the temperature difference, the flow rate, and the specific heat of the water. The COP is the value of the capacity over the heat input. The mean value was calculated to represent the value of the parameter during the test period. The standard deviation and the coefficient of variation were calculated to see the dispersion and used to compare with different data set.

Although the measured and calculated values on August 7 had less dispersion and were slightly larger than the values on July 8, it can be seen that the tests on these two days had similar results. Both results showed the tested heat pump has higher heating and cooling capacities than the manufacturer's data listed in Table 4.1. This may be because of the actual heat input of the tested AHP is larger than the manufacturer's data. Other test

results of the AHP at off-design conditions are described in Table 4.5. The hot water supply temperature (T_hw,s), the chilled water supply temperature (T_chw,s), the heating capacity (Q_h), and the cooling capacity (Q_c) were the indicators of the performances. The T_hw,s and T_chw,s were able to be measured and the Q_h and Q_c was calculated.

Table 4.4 The test results of AHP at design condition

Date			7/8/2014			8/7/2014		
Test period			10:00 – 10:20			14:20 – 14:59		
Parameter		Unit	Mean	σ	CV	Mean	σ	CV
Temperature	T_hw,r	℃	39.34	0.19	0.005	39.39	0.080	0.002
	T_hw,s	℃	51.06	0.15	0.003	51.49	0.082	0.002
	T_chw,r	℃	12.13	0.44	0.036	12.15	0.384	0.032
	T_chw,s	℃	6.43	0.41	0.063	6.37	0.404	0.063
Flow rate	FR_hw	kg/s	0.92	0.01	0.009	0.89	0.008	0.009
	FR_chw	kg/s	0.78	0.00	0.003	0.78	0.002	0.003
Heat input	Q_des	kW	33.04	-	-	33.04	-	-
Data analysis	dT_hw	℃	11.72	-	-	12.09	-	-
	dT_chw	℃	5.70	-	-	5.78	-	-
	Q_h	kW	44.85	-	-	45.17	-	-
	Q_c	kW	18.54	-	-	18.81	-	-
	COP_h	n/a	1.36	-	-	1.37	-	-
	COP_c	n/a	0.56	-	-	0.57	-	-

4.3.1.2 The test result of the AHP for different T_hw,r

The tests of the AHP for different T_hw,r were conducted on July 7, July 8, August 7, and August 14, 2014. The test range of the T_hw,r was 30 to 50℃. The changes of the water supply temperatures and capacities with the T_hw,r are illustrated in the charts of Table 4.5.

For the water supply temperatures, the results showed the T_hw,s increased as the T_hw,r increased, meanwhile, the T_chw,s remained at the same level. For the calculated capacities, the part-load and overload conditions will be discussed separately. When the AHP was operated at part-load condition, the capacities decreased as the T_hw,s

Table 4.5 The test results of the AHP at off-design conditions

	T_hw,r	T_chw,r	FR_hw	FR_chw	T_hw,s & T_chw,s	Q_h & Q_c
Unit	℃	℃	kg/s	kg/s	℃	kW
Design condition	40	12	0.92	0.78	45.17	18.81
T_hw,r	**30 - 50**	12	0.92	0.78	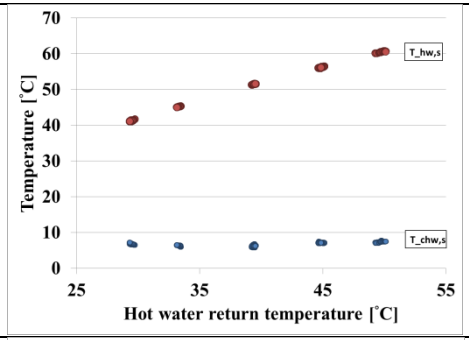	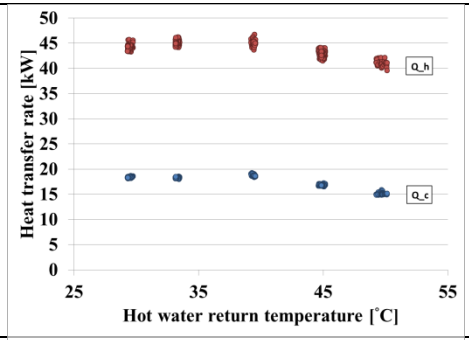
T_chw,r	40	**12 - 30**	0.92	0.78	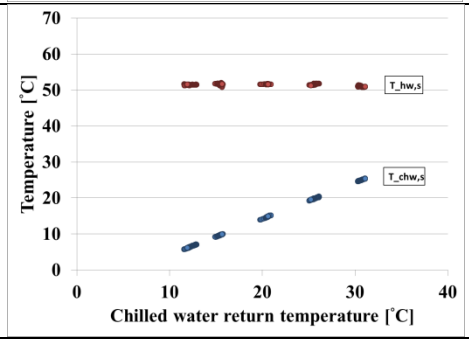	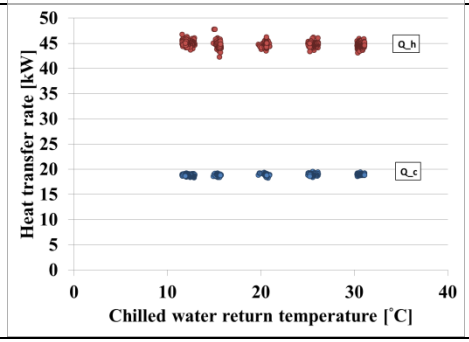

Table 4.5 continued

FR_hw	40	12	**0.51 – 0.97**	0.78	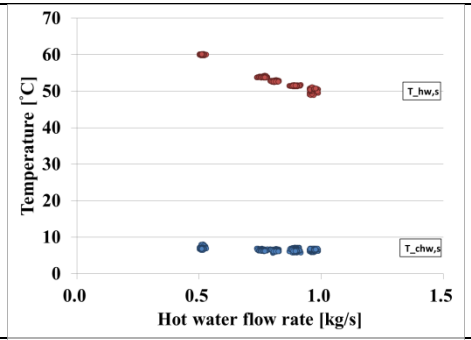	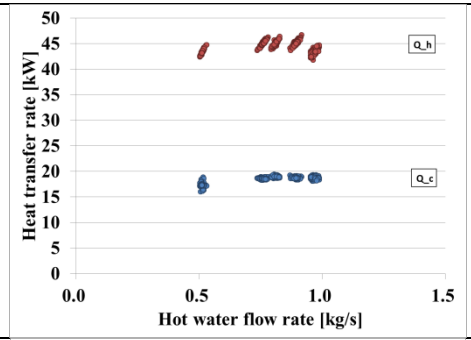
FR_chw	40	12	0.92	**0.63 – 0.84**	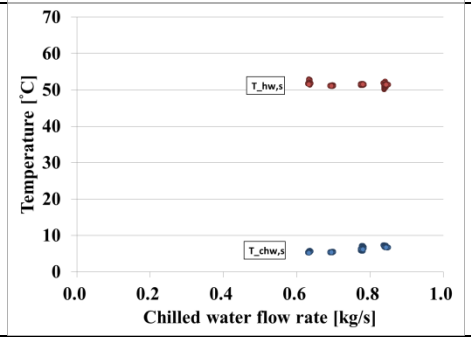	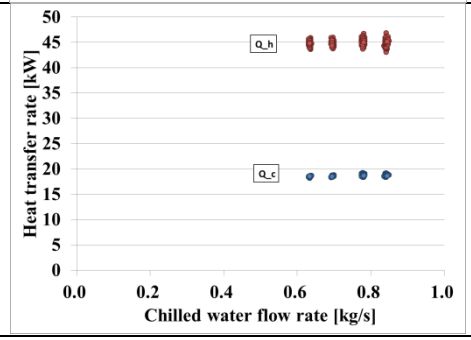

increased. However, in the overload condition, the capacities of the AHP did not increased as the T_hw,s decreased.

It can be observed from the test results that the AHP can actually only deal with small ranges of off-design conditions. When the heating load decreases, the T_hw,r increases as well as the high side pressure of the heat pump. The AHP stops to prevent the high side pressure increases further. The AHP can thus only be operated at part-load condition within certain range. For the overload condition, since the AHP only has fixed thermal input, it limits the heating power of the heat pump. Additionally, the T_hw,s is influenced by the heating load. When the heating load is high, the T_hw,s drops so the AHP cannot provide useful hot water.

4.3.1.3 The test results of the AHP for different T_chw,r

The tests of the AHP for different T_chw,r were conducted on July 9, July 10, and August 14, 2014. The test range of the T_chw,r was 12 to 30℃. Starting from the design condition, the next tested T_chw,r was 15℃. The interval of the following tests was 5℃ till 30℃. The AHP tended to stop when the T_chw,r was lower than 12℃ so the AHP was only tested at higher cooling load condition. The changes of the water supply temperatures and capacities with the T_chw,r are illustrated in the charts of Table 4.5. For the water temperatures, the results showed the T_chw,s increased as the T_chw,r increased, however, the T_hw,s remained at the same level. For the calculated capacities, it seemed the changes of the T_chw,r had no significant influences on both the heating and cooling capacities. There are two possible explanations for this phenomenon. The

first one is that the AHP is dominated by the heating demand. The second reason is also due to the fixed thermal input which limits the cooling power of the heat pump.

4.3.1.4 The test results of the AHP for different FR_hw

The tests of the AHP for different FR_hw were conducted on July 11, 2014. The test range of the T_chw,r was 0.51 to 0.97 kg/s. In this range, there were four other tested flow rates except the rated one. The changes of the water supply temperatures and capacities with the FR_hw are illustrated in the charts of Table 4.5.

For the water temperatures, the results showed the T_hw,s decreased as the FR_hw increased but the T_chw,s remained at the same level. For the calculated capacities, the FR_hw had no significant influences on both the heating and cooling capacities.

4.3.1.5 The test results of the AHP for different FR_chw

The tests of the AHP for different FR_chw were conducted on July 13 and August 7, 2014. The test range of the T_chw,r was 0.63 to 0.84 kg/s. In this range, there were three other tested flow rates except the rated one. The heat pump stopped when the FR_chw was lower than 0.63 kg/s. The changes of the water supply temperatures and capacities with the FR_chw are illustrated in the charts of Table 4.5. The T_chw,s was the only parameters affected by the FR_chw.

4.3.2 Test results of the VC

As mentioned in the previous section, the VC was tested at different combinations of FR_cw and T_chw,r. Some of the test results are shown in Table 4.6 to see the influences

of the T_cw,r and FR_cw. The chilled water supply temperature (T_chw,s), power input (W), cooling capacity (Q_e), and COP were used as the performance indicators of the VC. The first two terms were measured during the tests and the last two terms were calculated values.

4.3.2.1 The test results of the VC for different T_chw,r

It can be observed from Table 4.6, for a constant FR_cw, the T_chw,s and Q_e increased as the T_chw,r increased. However, the W and COP only slightly increased as the T_chw,r increased.

The increment of the T_chw,r represented a higher cooling load. The Q_e of the VC thus increased to meet the requirement. The flow rate of the refrigerant increased in order to produce more cooling power in the evaporator; the W hence also increased to drive the circulation of the refrigerant. The COP increased a little bit since the Q_e increased more than the W.

Although the increment of the T_chw,r could increase the COP of the VC, it also increased the T_chw,s. This implied that the VC may not be able to provide useful chilled water if the cooling load was too high.

4.3.2.2 The test results of the VC for different FR_cw

Table 4.6 shows the influences of the FR_cw. It can be seen from the charts, the increment of the FR_cw reduced the T_chw,s and W but increased the Q_e and COP respectively.

Table 4.6 The influences of T_chw,r and FR_cw for the VC

	T_chw,r [℃]	FR_cw [kg/s]	T_chw,s	Work
T_chw,r	**14.64 – 18.74**	1.27	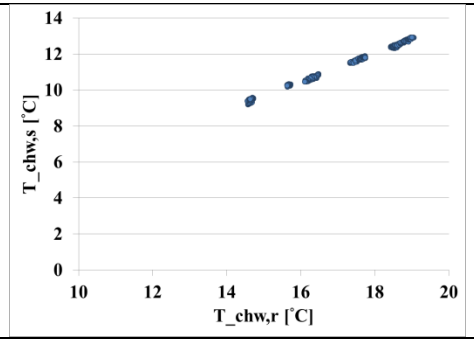	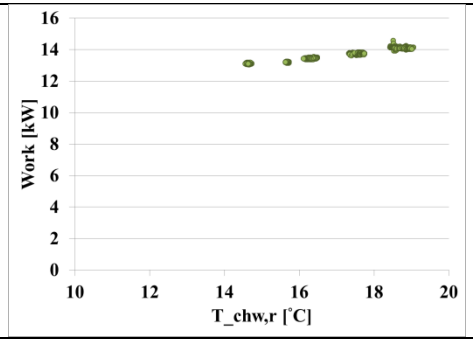
			Cooling capacity	COP
			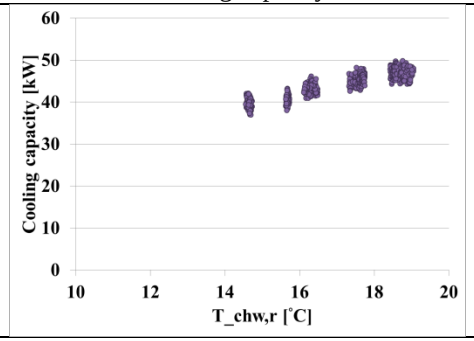	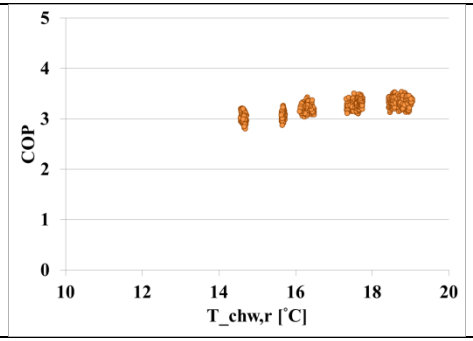

Table 4.6 continued

FR_cw	16	**0.84 -1.39**	T_chw,s 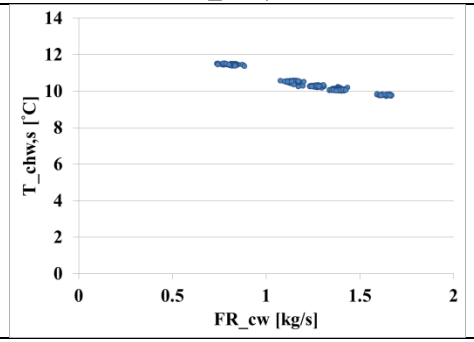	Work 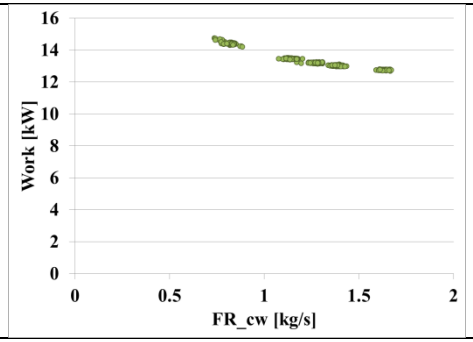
			Cooling capacity 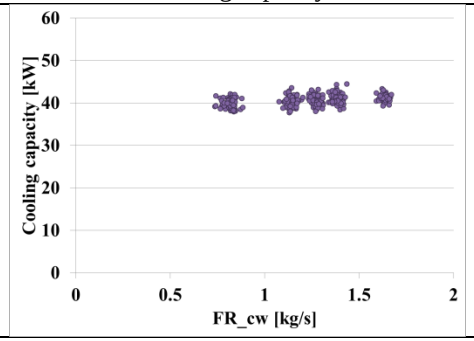	COP 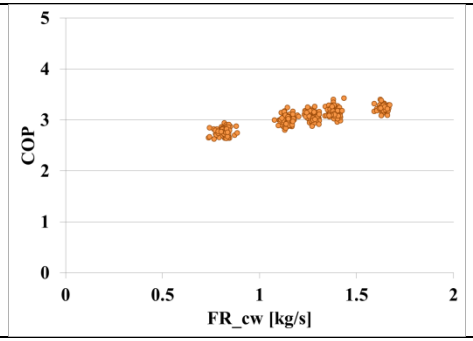

A higher FR_cw helped to remove the heat in the condenser and the refrigerant could thus absorb more heat in the evaporator, which increased the Q_e and reduced the T_chw,s. Also, the higher FR_cw decreased the condensing temperature so the W was reduced and the COP increased.

4.3.3 Test results of the ICASS

4.3.3.1 Steady state operation of the ICASS

At the beginning of the tests for the ICASS, it was found that the integrated system was hard to be operated at the steady state. Figure 4.10(a) shows a test results from an unstable operation of the ICASS. The AHP of the integrated system stopped when the chilled water temperatures of the AHP (T_ahp,chw,r and T_ahp,chw,s) were too low. The hot water temperature of the AHP (T_ahp,hw,r) dropped once the AHP stopped and could not generated heating power. The AHP repeated the on and off cycles for several times but could not stay at the steady state. From the individual test of the AHP, it was found that the chilled water temperature decreased as cooling load decreased. In the ICASS, the chilled water of the AHP absorbs heat in the subcooler. Accordingly, the heat transfer rate in the subcooler was not enough which made the AHP stop and the ICASS unstable.

Heat transfer rate in the subcooler was actually related to 1) the mass flow rate and 2) the temperature of the refrigerant of the VC. The mass flow rate of the refrigerant is related to the total cooling load at the evaporator of the VC. As mentioned previously, hot steam was used to simulate the cooling load. The steam pressure was thus raised to increase the

total cooling load. However, even with the maximum steam pressure, the temperature of the chilled water from the AHP was still low and the AHP stopped eventually.

Another control strategy was thus implemented. From the individual test of the VC, it was found that the condensing temperature of the VC (T_vc,cond) increased as the flow rate of the cooling water (FR_cw) decreased. The T_vc,cond was actually the same as the temperature of the refrigerant entering the subcooler. The refrigerant with higher temperature helped to increase the heat transfer rate in the subcooler. It can be observed in Figure 4.10(a), the T_vc,cond was around 40℃ but lower than 50℃. The FR_cw should be reduced to get higher T_vc,cond. The problem of decreasing the T_vc,cond was, the high side pressure of the VC also increased. The VC will stop if the high side pressure goes across the cut-off pressure. Therefore, there was a lower limit for the FR_cw to make sure the high side pressure of the VC stay in the safe range.

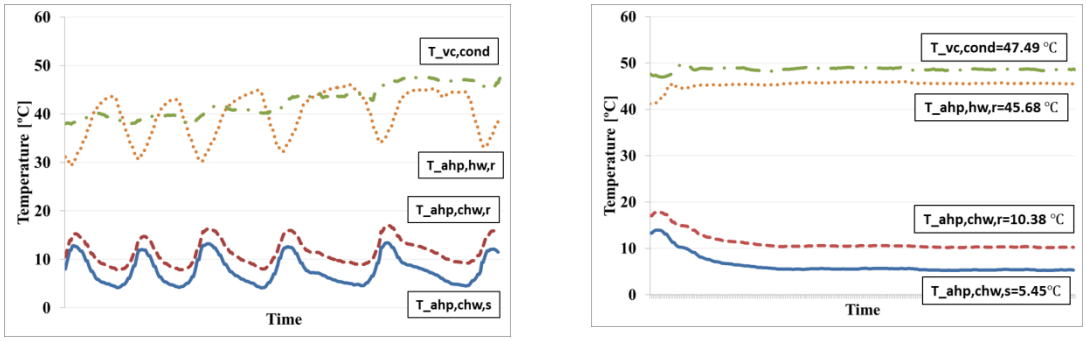

(a) unstable condition (b) steady state condition

Figure 4.10 The tests of the ICASS

The final strategy was adjusting the AHP. Again, from the individual test of the AHP, it was found that both the heating and cooling capacities of the AHP decreased as the hot water return temperature (T_ahp,hw,r) increased. Originally, the T_ahp,hw,r was controlled at 40℃, which is the design condition of the AHP. The T_ahp,hw,r was thus

increased to around 45℃ to reduce the cooling demand of the AHP. Finally, the ICASS became stable, as shown in Figure 4.10(b) with the maximum steam pressure, low FR_cw=0.55 kg/s, and T_ahp_hw,r around 45℃. Meanwhile, the T_vc,cond was around 47.5℃.

Some findings and comments via the test of the ICASS are summarized here:

1) The total cooling load of the ICASS is important to make the system operate at steady state condition. If the total cooling load is not enough, the AHP of the ICASS may stop. This means the ratio between the cooling capacity of the VCRS and the AHP is important.

2) If the total cooling load of the ICASS is not high enough, there are two methods to solve the issues. The first one is increasing the condensing temperature of the VCRS and the second one is decreasing the heating load of the AHP. These two methods can be implemented together or separately depends on different conditions.

3) In the ICASS, an air-cooled VCRS should be more suitable than a water-cooled VCRS since the condensing temperature of the air-cooled VCRS is usually higher.

4.3.3.2 Comparison between the ICASS and the VC alone

The tests of the comparison between the ICASS and the VC alone were conducted on August 13, 2014. Originally, the ICASS and the VC alone were planned to be tested at the same cooling capacity. However, as stated in the previous section, the ICASS could only be operated with low FR_cw. When the VC was tested individually with the same FR_cw, the high side pressure crossed the cut-off pressure and the VC stopped.

Table 4.7 The comparison between the ICASS and the VC alone

Parameter	Unit	ICASS	VC
Temperature			
VC			
Chilled water return	℃	19.37	15.94
Chilled water supply	℃	11.56	10.55
Cooling water at condenser inlet	℃	15.90	16.52
Cooling water at condenser outlet	℃	41.93	40.83
Compressor inlet	℃	10.79	8.41
Compressor outlet	℃	93.98	97.89
Condenser outlet		47.49	48.97
Subcooler outlet	℃	7.19	-
Evaporator outlet	℃	0.8	-1.17
AHP			
Hot water return	℃	45.68	-
Hot water supply	℃	56.92	-
Chilled water return	℃	10.38	-
Chilled water supply	℃	5.45	-
Pressure			
Compressor inlet	kPa	473.62	439.68
Compressor outlet	kPa	1844.18	1922.31
Receiver outlet	kPa	1833.77	1897.76
Expansion valve inlet	kPa	1799.67	1896.09
Expansion valve outlet	kPa	511.78	
Flow rate			
VC			
Chilled water	kg/s	1.82	1.79
Cooling water	kg/s	0.54	0.54
Refrigerant (R22)	kg/s	0.295	0.273
AHP			
Chilled water	kg/s	0.77	-
Hot water	kg/s	0.9	-
Power			
Electricity input at compressor	kW	16.03	16.04
Data analysis			
VC			
dT_chilled water	℃	7.81	5.39
dT_cooling water	℃	26.03	24.31
Cooling capacity	kW	59.54	40.31
Heat removed at condenser	kW	59.17	54.89
COP	n/a	3.71	2.51
AHP			
dT_hot water	℃	11.24	-
dT_chilled water	℃	4.93	-
Heating capacity	kW	42.33	-
Cooling capacity	kW	15.94	-

Accordingly, the comparison between the ICASS and the VC alone with same cooling capacity was changed to the comparison with the same electrical power input. Cooling capacity and COP of the two systems were compared to see the differences. The test results are listed in Table 4.7. The comparisons of the VC refrigerant circles are shown in the T-s and P-h diagrams (Figure 4.11 (a) and (b)).

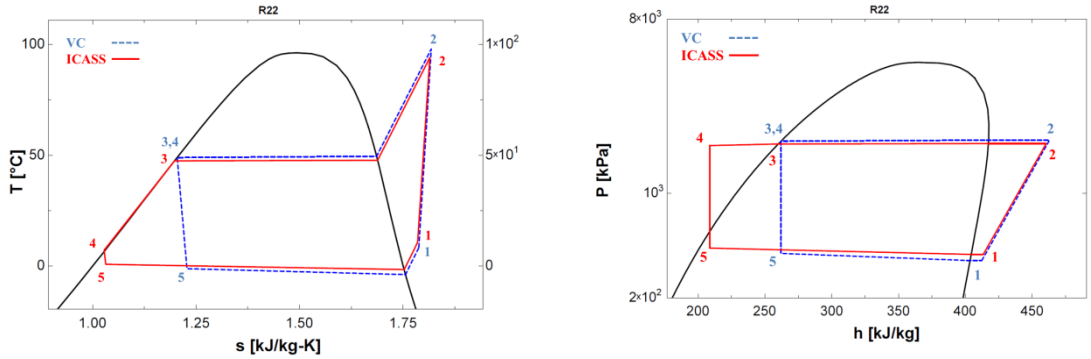

(a) T-s diagram (b) P-h diagram

Figure 4.11 The states of refrigerant in the ICASS and in the VC alone

The test results showed, when the electrical power inputs of the chiller and the integrated were the same around 16 kW, the cooling capacity of the ICASS and the VC alone were 59.54 kW and 40.31 kW respectively. The cooling capacity of the ICASS was 19.23 kW higher than the VC alone; the improvement was around 48%. Also, the COP of the chiller alone and chiller in the integrated system were 2.51 and 3.71 respectively; the improvement was also around 48%.

The comparisons between the refrigerant circles of the VC alone and the VC of the ICASS showed that the condensing and evaporating temperatures were at the same level as the figures show. The extra cooling capacity of the integrated system was actually coming from the AHP. The refrigerant exiting the condenser was subcooled to lower

temperature. After the refrigerant passing through the expansion, it had lower quality and thus could absorb more heat in the evaporator. The comparison between the two systems proved the assumptions stated in the front and showed the benefits of the technology.

CHAPTER 5. MODEL DEVELOPMENT AND VALIDATION

In this chapter, the developments of the VC, AHP, and ICASS models will be introduced first and the validations of the models will be presented next.

5.1 Model development of the AHP

Figure 5.1 shows the schematic diagram of the AHP model. It was drawn based on the working principle of the AHP installed.

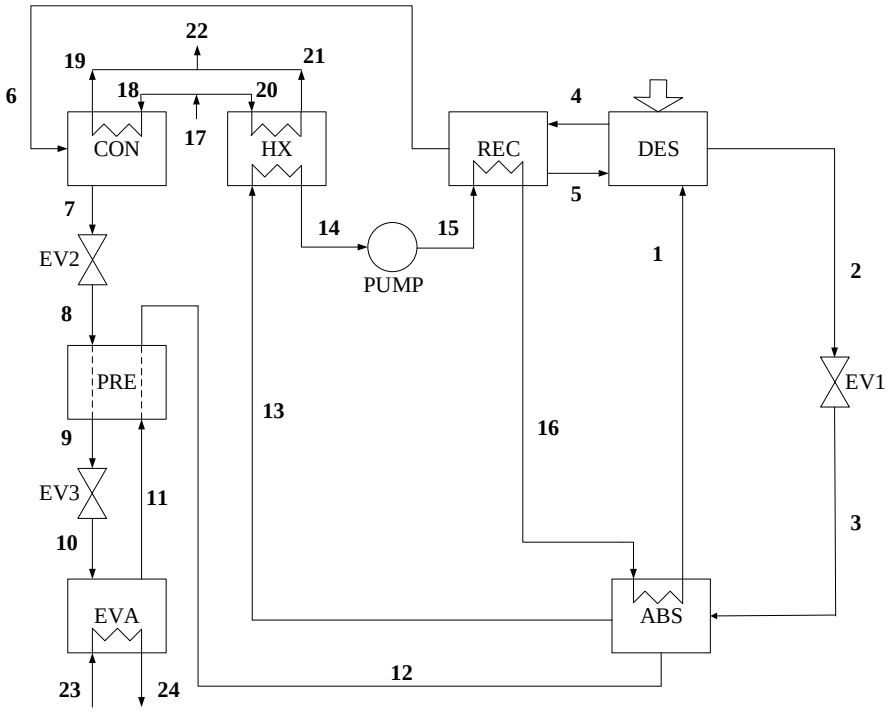

Figure 5.1 Schematic diagram of the AHP model

In the real machine of the AHP, three streams exchange heat in a heat exchanger called condenser/absorber. These three streams are the refrigerant vapor, the strong solution, and the hot water return. In the model developed, the condenser/absorber was separated into two independent heat exchangers and linked by an additional exchanger marked HX as shown in Figure 5.1. The refrigerant vapor and the strong solution both exchange heat with the hot water in parallel and mix together afterwards. In this configuration, it is assumed the condenser and the HX at same temperatures but different flow rates. The two separated hot water streams will combined together again when they exit the two heat exchangers. This change basically refers to other similar studies (Lazzarin et al., 1996; Horuz et al, 2003; Darwish et al, 2008; Rossa and Bazzo, 2009). It could simplify the models and is relatively close to the real situation.

The assumptions of the AHP model are listed as below:

1) Pressure drops of the components and along the pipes are neglected.
2) Heat losses of the components and along the pipes are neglected.
3) The condition of the fluid exiting one component is same as the condition when it enters the next component.
4) Weak solution exiting (state 2) and working fluid returning (state 5) the desorber are assumed as saturated liquids.
5) Working fluids exiting the desorber (state 4) and the rectifier (state 6) and are assumed as superheated and saturated vapors.
6) Mass fraction of the working fluid exiting the rectifier (state 6) is assumed as 99%.
7) Isenthalpic process is assumed across the expansion valve.

The inputs of AHP model include the return temperatures and flow rates of the hot and chilled waters, the effectiveness of each heat exchanger, thermal input at the desorber, mass flow rate of the strong solution entering the desorber (state 1), and the mass fraction of ammonia of the strong solution entering the desorber (state 1).

5.1.1 Properties of the ammonia-water solution

Some features of the ammonia water solution have been mentioned in the previous chapters. First, the freezing point of a 94.4% ammonia-water solution is around -80.56℃. This is much lower than the freezing point of the water so the absorption system using ammonia water solution can be used for low temperature application. Secondly, the affinity of ammonia and water is higher than the affinity of water and lithium bromide so a rectifier is required to remove the water vapor in the mixture as shown in Figure 5.2.

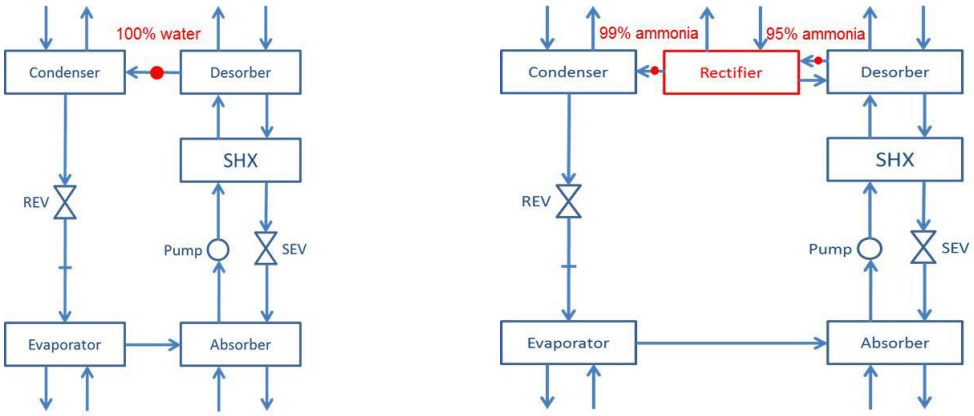

(a) lithium bromide water solution (b) ammonia water solution

Figure 5.2 Absorption system using different working fluids

Since the refrigerant of the ammonia absorption system is still the mixture, “temperature lift” will occur in the heat exchangers. Temperature lift is the phenomenon that the temperature of a mixture increases from boiling point to dew point during the two-phase region. Figure 5.3 shows the temperature-mass fraction (T-x) diagram of the ammonia water solution at constant pressure. The dew line and boiling line of ammonia water solution are shown in the diagram. Point A and B represent the pure water and ammonia respectively. Marked C is an example which shows the temperature lift of the ammonia water solution. The mass fraction of Marked C is around 0.51, the boiling and dew

temperatures are 78.67 and 168.9℃ respectively. It can be observed that the temperature of the mixture still increases in the two-phase region. Even if the mass fraction of the ammonia-water solution is 99%, temperature difference still exists between the boiling and dew points. Therefore, this phenomenon was taken into consideration while developing the AHP model.

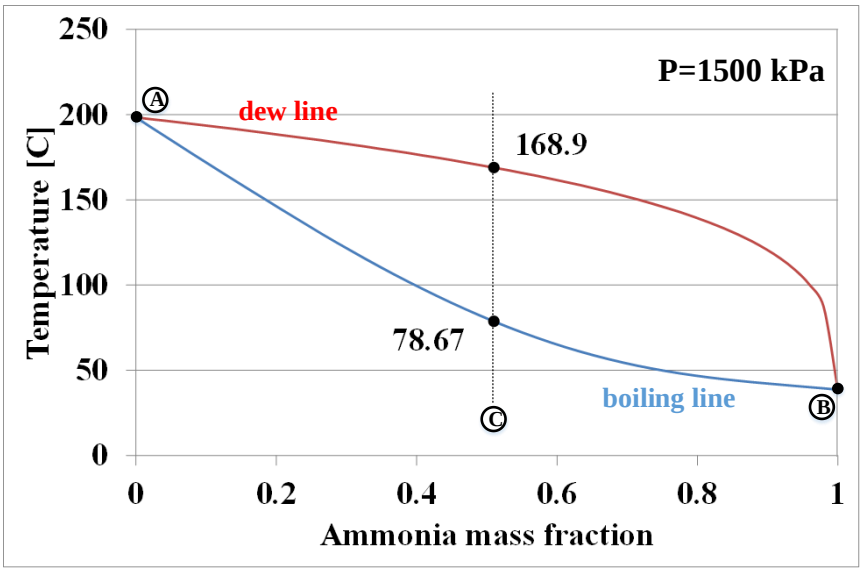

Figure 5.3 T-x diagram of the ammonia water solution at constant pressure

5.1.2 Component models of the AHP

The system model was composed of different component models. The most components of the AHP are heat exchangers. The model of evaporator, as shown in Figure 5.4, is used as an example here to illustrate the development process of the AHP model.

First of all, the numbers of variables were counted. Table 5.1 shows the numbers of variables of the evaporator model. For instance, the temperatures (T), enthalpies (h), mass flow rates (m), and quality of stream 23 and 24 were calculated by the model so there

were 4*2=8 variables of these two streams. The total numbers of variables of the evaporator model were counted and added as 34.

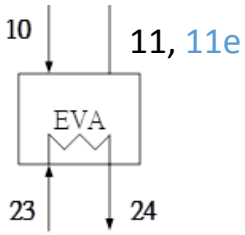

Figure 5.4 Schematic diagram of the evaporator model

Table 5.1 Numbers of variables of the evaporator model

State point	**Stream**	**Var. specified**	**Total SP var. #**
	10, 11	m, T, P, x, h, Q, v, s	8*2=16
	11e	h, Q, v, s	4*1=4
	23, 24	T, h, m, Q	4*2=8
Other	**Var. specified**		**Number of comp. var.**
	Qeva, Qeva(hs, cs, max), Eff_eva, Cp_w_23		6
Total numbers of variables: 16+4+8+6=34			

The numbers of equations were counted next. Table 5.2 shows the numbers of equations of the evaporator model. For example, there were 2 and 4 equations for the mass balance and heat transfer rate calculation respectively. The total numbers of equations of the evaporator model were counted and added as 28.

It should be noted that stream 11e was an imaged stream assuming stream 11 had the same temperature as stream 23. The enthalpy of stream 11e and the maximum possible heat transfer rate of the cold side were thus calculated. Effectiveness method was used for the heat exchanger. The smaller values between the maximum possible heat transfer rates of the cold and hot sides was selected as the maximum possible heat transfer rate of the

heat exchanger. The actual heat transfer rate of the heat exchanger was the product of effectiveness and maximum possible heat transfer rate.

Table 5.2 Numbers of equations of the evaporator model

	Eqn. specified	**Eqn. number**
Property	PL=P_{10}, P_{11} (2) T_{24}=f(h_{24}, Q_{24}) (2) h_{23}=f(T_{23}, Q_{23}) (2) Cp_w_23=f(T_{23}, Q_{23}) CALL: 10, 11, 11e (12)	19
Mass balance	m_{10}=m_{11} m_{23}=m_{24}	2
NH3 balance	X_{10}=X_{11}	1
Energy balance	m_{11}*h_{11}=m_{10}*h_{10}+Q_{eva} Q_{eva}=m_{23}*(h_{23}-h_{24})	2
Heat transfer	$Q_{eva,hs}$=m_{23}* Cp_w_23*(T_{23}-T_{10}) $Q_{eva,cs}$=m_{10}*(h_{11e}-h_{10}) $Q_{eva,max}$=min($Q_{eva,hs}$, $Q_{eva,cs}$) Q_{eva}=Eff_eva*$Q_{eva,max}$	4
Total numbers of equations: 19+2+1+2+4=28		

Finally, the numbers of assumptions and inputs were counted. Table 5.3 shows the numbers of assumptions and inputs of the evaporator model. There were no assumptions but 3 inputs for the evaporator so the total numbers of assumptions and inputs of the evaporator model were 3.

Table 5.3 Numbers of assumptions and inputs of the evaporator model

Assumptions
0
Inputs
T_{23}, m_{23}, Eff_eva
Total number of assumptions and inputs: 3

The total numbers of equations, assumptions, and inputs were 31 but the variables were 34. This meant the evaporator model was lack of 3 equations, assumptions, or inputs. These equations, assumptions, or inputs could be found in other components. After the component models were assembled together as the system model, the numbers of

variables should be the same as the total numbers of equations, assumptions, and inputs. Please refer to the Appendix A for the detailed of the AHP models.

5.1.3 Heat transfer rate calculations of the rectifier and absorber

In the previous section, the evaporator model was used as an example to illustrate the heat transfer rate calculation of the heat exchanger. However, the calculations were slightly different in the rectifier and absorber. The heat transfer rate calculations and some stream properties of the rectifier and absorber are described in Table 5.4 and Table 5.5.

Table 5.4 Heat transfer rate calculations of the rectifier and absorber

Rectifier		Absorber	
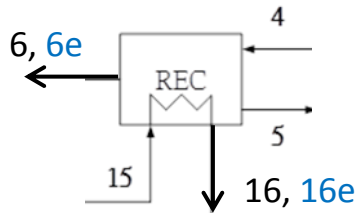		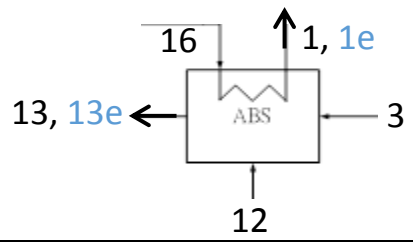	
Energy balance			
$m_4*h_4=m_5*h_5+m_6*h_6+Q_{rec}$ $m_{15}*h_{15}+Q_{rec}=m_{16}*h_{16}$	(5.1) (5.2)	$m_{16}*h_{16}+Q_{abs}=m_1*h_1$ $m_{12}*h_{12}+m_3*h_3=Q_{abs}+m_{13}*h_{13}$	(5.3) (5.4)
Heat transfer rate calculation			
$Q_{rec,hs}=m_4*(h_4-h_{6e})$ $Q_{rec,cs}=m_{15}*(h_{15}-h_{16e})$ $Q_{rec,max}=\min(Q_{rec,hs}, Q_{rec,cs})$ $Q_{rec}=Eff\_rec*Q_{rec,max}$	(5.5) (5.6) (5.7) (5.8)	**$Q_{abs,\ hs}=m_3*h_3+m_{12}*h_{12}-m_{13}*h_{13e}$** $Q_{abs,cs}=m_{16}*(h_{1e}-h_{16})$ $Q_{abs,max}=Q_{abs,cs}$ $Q_{abs}=Eff\_abs*Q_{abs,max}$	(5.9) (5.10) (5.11) (5.12)

For the rectifier, the hot side included the stream 4, 5, and 6. These three streams were all used for the calculation of energy balance. However, stream 5 was ignored in the calculation of maximum possible heat transfer rate of the hot side. It can be seen in Table 5.5, the energy carried by stream 5 was much smaller than stream 4 and 6 so it was negligible.

Table 5.5 The stream properties of the rectifier and absorber

Parameter	Rectifier			Absorber		
	stream 4	stream 5	stream 6	stream 3	stream 12	stream 13
h [kJ/kg]	1529.00	119.10	1416.00	663.70	1268.00	418.20
m [kg/s]	0.021	0.002	0.019	0.034	0.019	0.053
h*m [kW]	32.11	0.24	26.90	22.57	24.09	22.16

Situation was different in the absorber. The hot side of the absorber included the stream 3, 12, and 13. All of these streams were used for calculations of energy balance and maximum possible heat transfer rate of the hot side. It can be observed from the table of stream properties, energy carried by these three streams were pretty even so none of them could be ignored.

Actually, the effects of stream 12 were usually negligible in the absorption system using lithium bromide water solution as working fluid. The circulation ratio is usually larger of the absorption system using lithium bromide water solution than the one using ammonia water solution as working fluid. A larger circulation ratio makes the flow rate of stream 12 smaller so the effects were negligible. Circulation ratio of the absorption system will be introduced in the next section.

5.1.4 Circulation ratio

The circulation ration of the absorption system is defined as the flow rate of refrigerant vapor leaving the desorber over the flow rate of strong solution entering the desorber. This value is important for designing the absorption system. Herold et al. (1996) proposed a graphic method, as shown in Figure 5.5, which used the enthalpy-mass fraction (h-x) diagram to illustrate the desorption process and related equations of circulation ratio in the desorber.

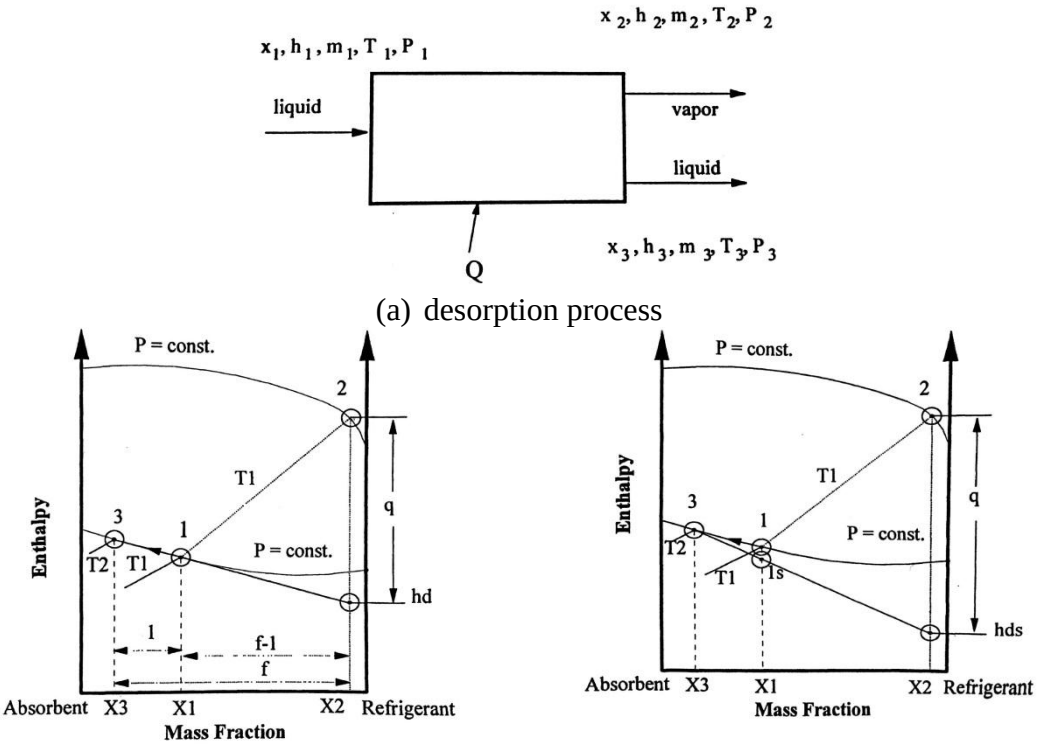

(a) desorption process

(b) desorption process with saturated inlet stream

(c) desorption process with subcooled inlet stream

(Herold et al., 1996)

Figure 5.5 Desorption process of the desorber

In Figure 5.5(a), stream 1 is the strong solution entering the desorber. Heat (Q) is added to the desorber so saturated refrigerant vapor (stream 2) and saturated weak solution (stream 3) are separated and exiting the desorber. Table 5.6 shows the equations of total mass balance, refrigerant mass balance, and energy balance for the desorber (Equation 5.13, 5.14, and 5.15). Equation 5.17 and 5.18 show the equations of total mass balance and refrigerant mass balance after introduced the circulation ratio (Equation 5.16). Based on Equation 5.18, the relations between the mass fractions of the streams and circulation ratio can be plotted on the h-x diagram, as shown in Figure 5.5(b) and (c), no matter stream 1 is saturated or subcooled liquid.

A point (h_d) can be found at the intersection of the extended line from point 3 and 1 with the vertical line of x_2. Equation 5.19 is yielded based on the graphic relationships shown in the h-x diagram. This equation can actually be derived from Equation 5.15 by letting the enthalpy difference (q) between h_2 and h_d equal to the heat over the mass flow rate of stream 2 (Equation 5.20 and 5.21). The circulation ratio and the mass flow rate of saturated refrigerant vapor exiting the desorber can be calculated by introducing the additional equations (Equation 5.16, 5.19, 5.20, and 5.21).

Table 5.6 Equations related to the circulation ratio

Total mass balance	$m_1=m_2+m_3$	(5.13)
Refrigerant mass balance	$m_1*x_1=m_2*x_2+m_3*x_3$	(5.14)
Energy balance	$m_1*h_1+Q=m_2*h_2+m_3*h_3$	(5.15)
Introduce circulation ratio: $\mathbf{f=m_1/m_2}$		(5.16)
Total mass balance	$m_3=(f-1)*m_2$	(5.17)
Refrigerant mass balance	$f=(x_2-x_3)/(x_1-x_3)$	(5.18)
Energy balance	$\mathbf{f=(h_d-h_3)/(h_1-h_3)}$, from the h-x diagram	(5.19)
	where,	
	$\mathbf{h_2-h_d=q}$	(5.20)
	$\mathbf{q=Q/m_2}$	(5.21)

The method mentioned above was modified slightly in the present study. Figure 5.6 shows the schematic diagram of the desorber and rectifier. The AHP installed has a rectifier so the refrigerant vapor exiting the rectifier (stream 6) was concerned instead of the refrigerant vapor exiting the desorber (stream 4).

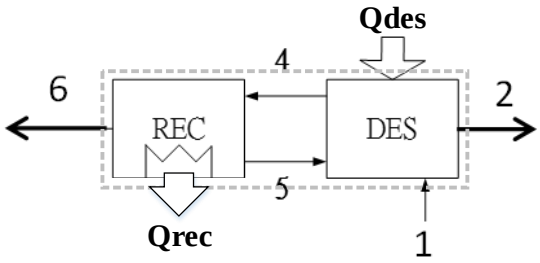

Figure 5.6 Schematic diagrams of the desorber and rectifier

If the desorber and rectifier were treated as one control volume, the equations of total mass balance, refrigerant mass balance, and energy balance are described in Table 5.7.

Table 5.7 Equations related to the circulation ratio of the AHP model developed

Total mass balance	$m_1=m_2+m_6$	(5.22)
Refrigerant mass balance	$m_1*x_1=m_2*x_2+m_6*x_6$	(5.23)
Energy balance	$m_1*h_1+Q_{des}=m_2*h_2+m_6*h_6+Q_{rec}$	(5.24)
Introduce circulation ratio: $\mathbf{f=m_1/m_6}$		(5.25)
Total mass balance	$m_2=(f-1)*m_6$	(5.26)
Refrigerant mass balance	$f=(x_6-x_2)/(x_1-x_2)$	(5.27)
Energy balance	$\mathbf{f=(h_d-h_2)/(h_1-h_2)}$, from the h-x diagram where,	(5.28)
	$\mathbf{h_6-h_d=q}$	(5.29)
	$\mathbf{q=(Q_{des}-Q_{rec})/m_6}$	(5.30)

The main difference was the equations of related to energy balance. Since rectifier was included in the control volume, the heat removed from it (Q_rec) was added to the equation of energy balance (Equation 5.24). Also, Equation 5.21 became Equation 5.30 of the AHP model developed by considering the Q_rec. The modeling results of stream 1, 2, and 6 were plotted in the h-x diagram as shown in Figure 5.7.

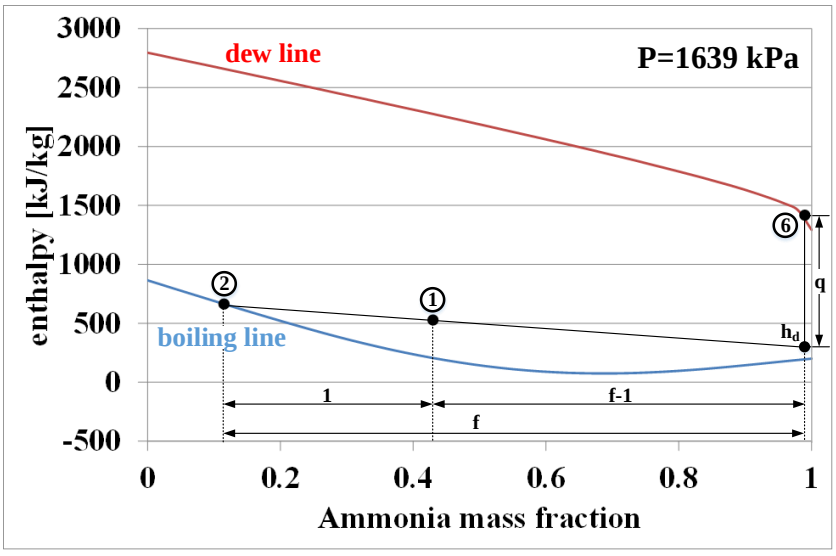

Figure 5.7 Desorption process of the AHP model developed on the h-x diagram

It can be seen from the diagram, even if the strong solution entering the desorber was in the two phase region, the graphic method was still very useful and well established the relationships of circulation ratio, enthalpies, and mass fractions. Again, the circulation ratio and the mass flow rate of saturated refrigerant vapor exiting the rectifier can be calculated by introducing the additional equations (Equation 5.25, 5.28, 5.29, and 5.30).

5.1.5 Validation of the AHP model

In this section, the AHP model results will be compared with the experimental data to see the accuracy.

5.1.5.1 The AHP model result at design condition

The values of the inputs at design condition are listed in Table 5.8. The primary outputs of the AHP model are the supply temperature of the hot and chilled waters.

Table 5.8 Inputs of the AHP model at design condition

water temperature [℃]	**hot water return**	39.39
	chilled water return	12.15
water flow rate [kg/s]	**hot water**	0.89
	chilled water	0.78
effectiveness of the heat exchanger	**absorber**	0.80
	evaporator	0.90
	precooler	0.56
	condenser	0.91
	HX	0.92
	rectifier	0.80
other	**thermal input at the desorber [kW]**	26
	mass flow rate of the strong solution entering the desorber [kg/s]	0.053
	mass fraction of ammonia of the strong solution entering the desorber[%]	43

Table 5.9 AHP model results at design condition

Properties					
	P [kPa]	**T [℃]**	**h [kJ/kg]**	**x [%]**	**m [kg/s]**
1	1639.0	117.90	527.10	43.00	0.0530
2	1639.0	172.30	663.70	11.51	0.0339
3	451.0	127.20	663.70	11.51	0.0339
4	1639.0	105.40	1529.00	95.47	0.0209
5	1639.0	78.27	119.10	53.58	0.0016
6	1639.0	78.27	1416.00	99.00	0.0191
7	1639.0	42.29	291.80	99.00	0.0191
10	451.0	1.62	163.80	99.00	0.0191
11	451.0	3.74	1140.00	99.00	0.0191
12	451.0	16.56	1268.00	99.00	0.0191
13	451.0	74.20	418.20	43.00	0.0530
14	451.0	48.00	-20.61	43.00	0.0530
15	1639.0	48.11	-19.19	43.00	0.0530
16	1639.0	66.76	64.14	43.00	0.0530
17	101.3	39.39	165.00	-	0.8900
18	101.3	39.39	165.00	-	0.4269
19	101.3	51.40	215.20	-	0.4269
20	101.3	39.39	165.00	-	0.4631
21	101.3	51.40	215.20	-	0.4631
22	101.3	51.40	215.2	-	0.8900
23	101.3	12.15	50.99	-	0.7800
24	101.3	6.45	27.12	-	0.7800
Heat transfer rates of the HXs [kW]					
$\dot{Q}_{DES}$	26.00	$\dot{Q}_{REC}$	4.42	$\dot{Q}_{CON}$	21.44
$\dot{Q}_{HX}$	23.26	$\dot{Q}_{PRE}$	2.44	$\dot{Q}_{EVA}$	18.62
$\dot{Q}_{ABS}$	24.54				

The thermal properties of the working fluid at different states and the heat transfer rates of the heat exchangers were calculated by the model developed. The AHP model results at design condition are shown in Table 5.9.

Table 5.9

5.1.5.2 The AHP model results at off-design condition

The AHP was tested at different operation conditions and the experimental data collected was used to validate the AHP model. The values of the inputs at different operation

conditions are listed in Table 5.10. The comparisons between the experimental and modeling results are shown in Table 5.11.

Table 5.10 Inputs of the AHP model at different operation conditions

water temperature [℃]	**hot water return**	30 - 50
	chilled water return	12 - 30
water flow rate [kg/s]	**hot water**	0.51 – 0.97
	chilled water	0.63 – 0.84
effectiveness of the heat exchanger	**absorber**	0.80
	evaporator	0.90
	precooler	0.56
	condenser	0.91
	HX	0.92 – 0.95
	rectifier	0.80 – 0.90
other	**thermal input at the desorber [kW]**	26
	mass flow rate of the strong solution entering the desorber [kg/s]	0.053
	mass fraction of ammonia of the strong solution entering the desorber[%]	43

As shown in the tables, the primary inputs of the model were the return temperatures and the flow rates of the waters. The primary outputs of the model were the water supply temperatures. The heating and cooling capacities of the AHP were calculated accordingly. It can be observed the errors between experimental and modeling results are all within 5% except the predicted T_chw,s and Q_c at FR_hw=0.51 kg/s. The largest error of the model usually locates at the extreme. The comparison results showed the accuracy of the AHP model. This validated model can thus be used for the following studies.

5.2 Model development of the VC

Figure 5.8 shows the schematic diagram of the VC. The structure of the chiller is simplified as the combination of the four basic components: the compressor, the condenser, the expansion valve, and the evaporator.

Table 5.11 Comparisons between the experimental and modeling results of the AHP

Test No.	Experimental data and primary inputs of the model				Experimental results				Model results				Error [%]			
	T_hw,r	T_chw,r	FR_hw	FR_chw	T_hw,s	T_chw,s	Q_h	Q_c	T_hw,s	T_chw,s	Q_h	Q_c	T_hw,s	T_chw,s	Q_h	Q_c
	℃	℃	kg/s	kg/s	℃	℃	kW	kW	℃	℃	kW	kW				
1	29.48	12.44	0.90	0.78	41.26	6.78	44.15	6.78	41.41	6.66	44.73	18.78	0.37	-1.82	1.13	2.18
2	33.32	11.91	0.91	0.79	45.20	6.32	45.08	18.33	45.13	6.21	44.75	18.70	-0.19	-1.79	-0.73	2.03
3	39.39	12.15	0.89	0.78	51.49	6.37	45.17	18.81	51.40	6.45	44.85	18.56	-0.17	1.24	-0.72	-1.37
4	45.32	12.08	0.92	0.78	56.48	7.00	43.02	16.55	56.35	7.08	42.53	16.28	-0.22	1.18	-1.13	-1.62
5	49.66	12.05	0.91	0.78	60.43	7.40	41.17	15.09	60.42	7.50	41.13	14.78	-0.02	1.30	-0.10	-2.07
6	39.82	15.44	0.91	0.78	51.58	9.68	44.82	18.81	51.58	9.72	44.82	18.68	0.00	0.41	0.00	-0.69
7	39.86	20.52	0.91	0.79	51.66	14.78	44.74	18.89	51.67	14.81	44.79	18.79	0.03	0.21	0.12	-0.54
8	39.67	25.50	0.91	0.79	51.49	19.78	44.75	18.90	51.53	19.73	44.90	19.05	0.08	-0.24	0.34	0.81
9	39.11	30.64	0.89	0.80	51.07	24.99	44.68	19.00	51.45	24.71	46.11	19.92	0.75	-1.10	3.20	4.87
10	39.75	12.39	0.51	0.78	59.99	7.08	43.49	17.29	60.68	6.71	44.97	18.50	1.14	-5.21	3.39	6.95
11	39.69	12.09	0.76	0.78	53.89	6.38	45.08	18.54	53.73	6.42	44.56	18.41	-0.30	0.65	-1.15	-0.72
12	39.43	12.23	0.81	0.78	52.75	6.40	45.21	18.95	52.62	6.54	44.79	18.50	-0.24	2.15	0.95	-2.37
13	39.44	12.22	0.97	0.78	50.19	6.45	43.48	18.78	50.45	6.53	44.53	18.51	0.52	1.29	2.41	-1.44
14	39.87	12.45	0.89	0.63	51.87	5.47	44.83	18.51	51.85	5.44	44.76	18.57	-0.03	-0.47	-0.15	0.37
15	39.15	11.81	0.89	0.70	51.17	5.42	44.92	18.58	51.14	5.48	44.81	18.41	-0.06	1.04	-0.24	-0.89
16	39.40	12.29	0.90	0.84	51.30	6.96	44.80	18.75	51.26	7.01	44.66	18.57	-0.08	0.71	-0.32	0.92
												Mean	0.10	-0.03	0.44	0.40
												σ	0.39	1.74	1.38	2.48
												Max	1.14	2.15	3.39	**6.95**
												Min	-0.30	**-5.21**	-1.15	-2.37

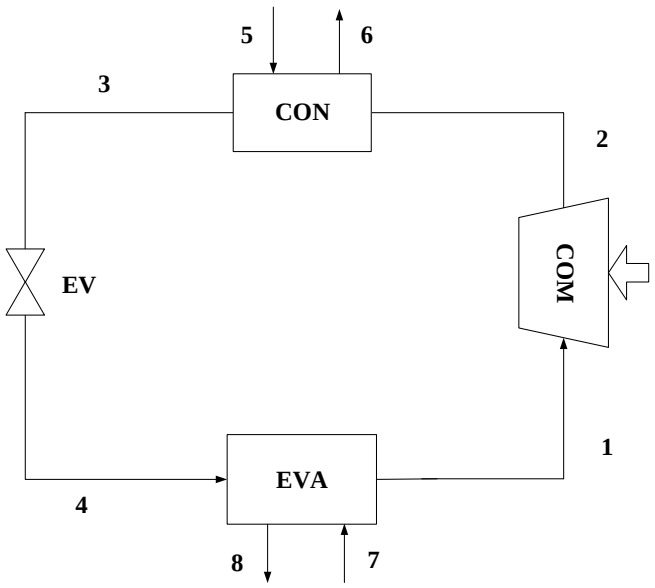

Figure 5.8 Schematic diagram of the VC

The assumptions of the VC model are listed as below:

1) Pressure drops of the components and along the pipes are neglected.
2) Heat losses of the components and along the pipes are neglected except the compressor.
3) The condition of the fluid exiting one component is same as the condition when it enters the next component.
4) Refrigerant exiting the condenser (state 4) is assumed as saturated liquid.
5) Refrigerant entering the compressor (state 1) is assumed as superheated vapor.
6) Isenthalpic process is assumed across the expansion valve.

The inputs of the VC model include the temperatures and flow rates of the chilled water return and cooling water inlet, the effectiveness of each heat exchanger, the superheated temperature of the refrigerant entering the compressor, and the isentropic efficiency.

5.2.1 Component models of the VC

The compressor model in this study is the model with statistical correlations based on system performance variables. The correlation equation is a ten-term polynomial

equation based on the same idea of developing the compressor map provided by AHRI stand 540 (2004). Equation 5.31 shows the polynomial equation. The mass flow rate of the refrigerant was calculated by the suction pressure and discharge pressure using the correlation equation.

$$\boldsymbol{X = C_1 \cdot (S) + C_2 \cdot (S^2) + C_3 \cdot (S^3) + C_4 \cdot (D) + C_5 \cdot (D^2) + C_6 \cdot (D^3) + C_7 \cdot (S \cdot D) + C_8 \cdot (S \cdot D^2) + C_9 \cdot (S^2 \cdot D) + C_{10}} \quad (5.31)$$

Where,

$\boldsymbol{X}$ = refrigerant mass flow rate, kg/s
$\boldsymbol{C}$ = equation coefficients
$\boldsymbol{S}$ = suction pressure, kPa
$\boldsymbol{D}$ = discharge pressure, kPa

However, Equation 5.31 was used to develop the compressor map or statistics model based on the same superheated and subcooling temperatures. Corrections have to be made for other superheated temperatures than specified in the compressor map or statistics model.

$$\frac{\dot{\boldsymbol{m}}_{\boldsymbol{new}}}{\dot{\boldsymbol{m}}_{\boldsymbol{map}}} = \boldsymbol{1} + \boldsymbol{F}\left(\frac{\boldsymbol{\rho}_{\boldsymbol{s,new}}}{\boldsymbol{\rho}_{\boldsymbol{s,map}}} - \boldsymbol{1}\right) \quad (5.32)$$

Where,

$\boldsymbol{F}$ = correction factor, 0.75 is used
$\dot{\boldsymbol{m}}$ = mass flow rate of the refrigerant, kg/s
$\boldsymbol{\rho_s}$ = suction density, kg/m^3

Equation 5.32 shows the correction equation. For this study, the experimental data was converted to the same superheated temperatures using Equation 5.32. The statistics model then could be developed based on the specified superheated temperature using Equation

5.31. In the model, Equation 5.32 was also used to convert the parameter for the desired superheated temperature.

Isentropic efficiency is also used for the compressor modeling in the VC. The isentropic efficiency is defined as the ratio of the enthalpy difference of isentropic process and the enthalpy difference of real process across the compressor as shown in Equation 5.33.

$$\eta_{isen} = \frac{h_{o(so=si)} - h_i}{h_o - h_i} \tag{5.33}$$

Where

η_{isen} = isentropic efficiency
$h_{o(so=si)}$ = enthalpy of the refrigerant exiting the compressor in isentropic process, kJ/kg
h_o = enthalpy of the refrigerant exiting the compressor in real process, kJ/kg
h_i = enthalpy of the refrigerant entering the compressor, kJ/kg

The developments of condenser and evaporator models for the VC were similar to the developments of heat exchanger models for the AHP. Please refer to the Appendix B for the details.

5.2.2 Validation of the VC model

The values of the inputs at different operation conditions are listed in Table 5.12. The coefficients of the correlation equations are described in Table 5.13. The comparisons between the experimental and modeling results are shown in Table 5.14.

As shown in the tables, the primary inputs of the model were the return/inlet temperatures and the flow rates of the waters. The primary outputs of the model were the chilled water supply temperature and electrical power. The cooling capacity and COP of the VC were calculated accordingly. For the T_chw,s, W, and COP, the errors between experimental and modeling results were all within 5% except one predicted T_chw,s. For the Q_e, the

errors are around 6%. The errors of the model results are mainly contributed from the neglected pressure drops and heat losses. However, the accuracy of the VC model was still validated by the experimental data.

Table 5.12 Inputs of the VC model at different operation conditions

water temperature [℃]	**chilled water return**	30 - 50
	cooling water inlet	12 - 30
water flow rate [kg/s]	**chilled water**	0.51 – 0.97
	cooling water	0.63 – 0.84
effectiveness of the heat exchanger	**condenser**	0.80
	evaporator	0.90
other	**superheated temperature of the refrigerant entering the compressor [℃]**	13.67 – 12.64
	isentropic efficiency	0.77 – 0.78

Table 5.13 Coefficients of the correlation equations

$m_r = C_1 \cdot (S) + C_2 \cdot (S^2) + C_3 \cdot (S^3) + C_4 \cdot (D) + C_5 \cdot (D^2) + C_6 \cdot (D^3) + C_7 \cdot (S \cdot D) + C_8 \cdot (S \cdot D^2) + C_9 \cdot (S^2 \cdot D) + C_{10}$					
C_1	6.2×10^{-3}	C_2	-1.72×10^{-5}	C_3	1.28×10^{-8}
C_4	-2.11×10^{-3}	C_5	1.05×10^{-6}	C_6	-1.76×10^{-10}
C_7	2.56×10^{-6}	C_8	-7.55×10^{-10}	C_9	-3.7×10^{-11}
C_{10}	0.27	-			

5.3 Model development of the ICASS

Figure 5.9 shows the schematic diagram of the ICASS model. The ICASS model was consisted of the VC model, the AHP model, and an additional subcooler model. The assumptions of the ICASS model were the same as the VC and AHP models. The inputs of the ICASS model are slightly different from the VC and AHP models. The T_chw,r is one of the inputs in the AHP model but it is replaced by the effectiveness of the subcooler. The correlation equation of the refrigerant mass flow rate was replaced by the mass flow rate of the refrigerant.

Table 5.14 Comparisons between the experimental and modeling results of the VC

Test No.	Experimental data and primary inputs of the model				Experimental results				Model results				Error [%]			
	T_chw,r	T_cw,r	FR_chw	FR_cw	T_chw,s	W	Q_e	COP	T_chw,s	W	Q_e	COP	T_chw,s	W	Q_e	COP
	℃	℃	kg/s	kg/s	℃	kW	kW	n/a	℃	kW	kW	n/a				
1	18.74	14.77	1.84	1.27	12.2	14.13	50.21	3.55	11.8	14.45	53.36	3.69	-3.30	2.26	6.27	3.92
2	17.58	14.7	1.84	1.27	11.2	13.74	48.79	3.55	10.9	14	51.82	3.70	-3.46	1.89	6.21	4.24
3	16.29	14.73	1.84	1.27	10.1	13.44	47.23	3.51	9.8	13.64	50.13	3.68	-3.61	1.49	6.14	4.58
4	14.64	14.91	1.83	1.28	8.7	13.11	45.3	3.46	8.4	13.31	48.02	3.61	-3.98	1.53	6.00	4.41
5	15.16	14.77	1.84	1.64	9.0	12.75	47.18	3.70	8.7	12.79	49.91	3.90	-3.83	0.31	5.79	5.46
6	15.51	14.54	1.81	1.39	9.3	13.02	46.9	3.60	9.0	13.1	49.6	3.79	-3.69	0.61	5.76	5.11
7	15.67	14.45	1.803	1.27	9.5	13.21	46.6	3.53	9.1	13.36	49.46	3.70	-3.89	1.14	6.14	4.95
8	15.86	14.53	1.81	1.14	9.7	13.46	46.66	3.47	9.3	13.61	49.45	3.63	-3.73	1.11	5.98	4.81
9	16.75	14.62	1.804	0.82	10.7	14.42	46	3.19	10.3	14.74	48.83	3.31	-3.50	2.22	6.15	3.85
10	19.36	15.18	1.864	1.37	12.8	13.85	50.88	3.67	12.5	14.1	53.92	3.82	-2.97	1.81	5.97	4.10
11	20.19	15.39	1.851	0.82	13.9	15.5	48.47	3.13	13.6	15.91	51.3	3.22	-2.53	2.65	5.84	3.11
12	18.57	15.38	1.848	0.8	12.6	15.16	46.45	3.06	12.2	15.49	49.08	3.17	-2.69	2.18	5.66	3.41
13	17.52	15.34	1.871	1.38	11.2	13.58	49.06	3.61	10.9	13.73	51.87	3.78	-3.09	1.10	5.73	4.57
14	16	15.23	1.843	1.7	9.6	13.12	49.37	3.76	9.2	13.2	52.27	3.96	-3.80	0.61	5.87	5.23
15	14.49	15	1.861	1.65	8.5	12.7	46.42	3.66	8.2	12.82	49.25	3.84	-4.17	0.94	6.10	5.10
16	14.87	15.03	1.857	1.39	8.9	13.08	46.52	3.56	8.5	13.22	49.28	3.73	-3.88	1.07	5.93	4.81
17	16.06	15.23	1.866	0.84	10.3	14.39	44.82	3.11	10.0	14.71	47.52	3.23	-3.32	2.22	6.02	3.72
18	14.5	15.34	1.87	0.82	9.0	14.12	43.03	3.05	8.7	14.45	45.52	3.15	-3.43	2.34	5.79	3.37
19	12.77	15.35	1.853	1.1	7.1	13.34	44.1	3.31	6.7	13.63	46.82	3.44	-4.74	2.17	6.17	3.91
20	11.07	15.03	1.833	1.92	5.5	12.02	42.62	3.55	5.2	12.23	45.38	3.71	-6.32	1.75	6.48	4.65
												Mean	-3.70	1.57	6.00	4.37
												σ	0.78	0.66	0.20	0.66
												Max	-2.53	2.65	6.48	5.46
												Min	-6.32	0.31	5.66	3.11

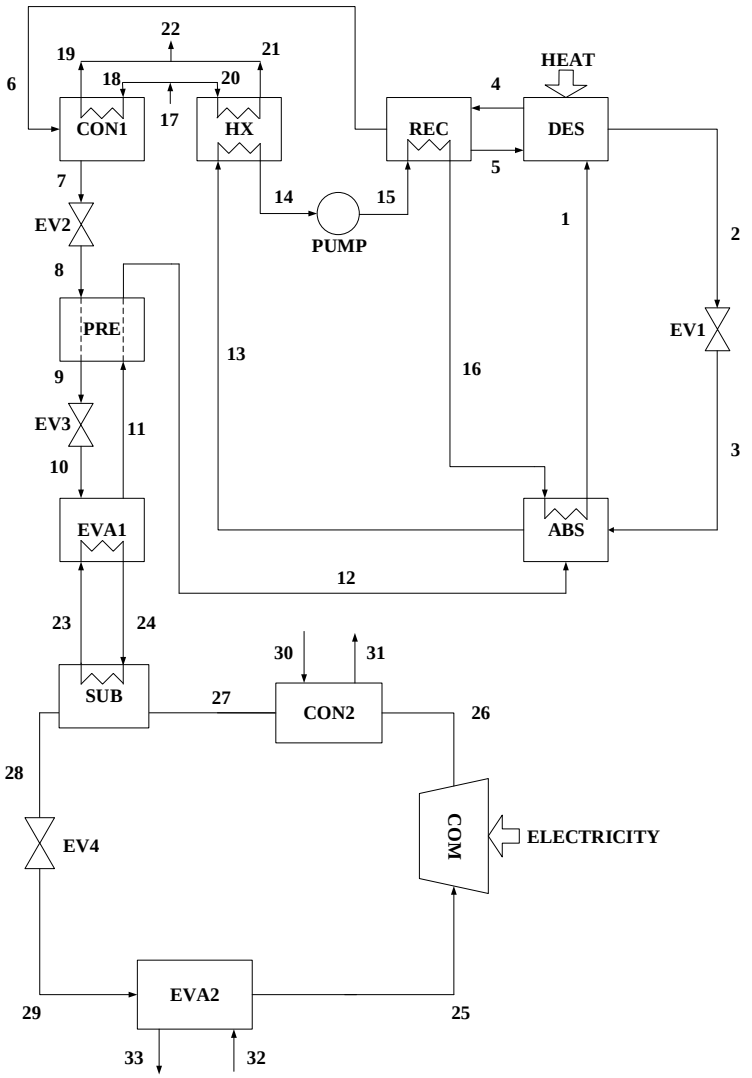

Figure 5.9 Schematic diagram of the ICASS model

5.3.1 Validation of the ICASS model

One steady state condition of the ICASS was tested and the experimental data was used to validate the ICASS model. The input values of the ICASS model are listed in Table 5.15. The modeling results of the ICASS are shown in Table 5.16. Table 5.17 shows the model validation of the ICASS model. It can be seen that the errors were all within 5%.

Table 5.15 Inputs of the ICASS model

water temperature [℃]	**AHP_hot water return**	45.68
	VC_chilled water	19.37
	VC_cooling water	15.9
water flow rate [kg/s]	**AHP_hot water**	0.90
	AHP_chilled water	0.77
	VC_chilled water	1.82
	VC_cooling water	0.54
effectiveness of the heat exchanger	**AHP_absorber**	0.80
	AHP_evaporator	0.90
	AHP_precooler	0.56
	AHP_condenser	0.91
	AHP_HX	0.92
	AHP_rectifier	0.80
	VC_condenser	0.85
	VC_evaporator	0.34
	subcooler	0.93
other	**thermal input at the desorber [kW]**	26
	mass flow rate of the strong solution entering the desorber [kg/s]	0.053
	mass fraction of ammonia of the strong solution entering the desorber[%]	43
	mass flow rate of the refrigerant [kg/s]	0.295
	superheated temperature of the refrigerant entering the compressor [℃]	12.9
	isentropic efficiency	0.77
	compressor heat loss ratio	0.12

Table 5.16 Results of the ICASS model

Properties					
	P [kPa]	**T [℃]**	**h [kJ/kg]**	**x [%]**	**m [kg/s]**
1	1820.0	113.00	399.10	0.430	0.0530
2	1820.0	158.10	559.70	0.192	0.0371
3	494.2	115.40	559.70	0.192	0.0371
4	1820.0	109.50	1535.00	0.953	0.0173
5	1820.0	81.06	134.40	0.547	0.0015
6	1820.0	81.06	14150	0.990	0.0158
7	1820.0	46.19	320.30	0.990	0.0158
10	494.2	4.12	174.50	0.990	0.0158
11	494.2	5.90	1119.00	0.990	0.0158
12	494.2	17.63	1265.00	0.990	0.0158
13	494.2	77.89	440.00	0.430	0.0530
14	494.2	50.98	-7.32	0.430	0.0530
15	1820.0	51.11	-5.73	0.430	0.0530
16	1820.0	67.74	68.69	0.430	0.0530
17	101.3	45.68	191.30	-	0.9000
18	101.3	45.68	191.30	-	0.3802
19	101.3	56.58	236.90	-	0.3802
20	101.3	45.68	191.30	-	0.5198

Table 5.16 continued

21	101.3	56.58	236.90	-	0.5198
22	101.3	56.58	236.90	-	0.9000
23	101.3	10.38	43.58	-	0.7700
24	101.3	5.75	24.15	-	0.7700
25	438.8	9.07	412.80	-	0.2950
26	1824.0	96.28	462.70	-	0.2950
27	1824.0	47.26	259.60	-	0.2950
28	1824.0	7.33	208.90	-	0.2950
29	438.8	-3.84	208.90	-	0.2950
30	101.3	15.90	66.68	-	0.5400
31	101.3	42.44	177.70	-	0.5400
32	101.3	19.37	81.20	-	1.8200
33	101.3	11.46	48.11	-	1.8200
Heat transfer rates [kW]					
$\dot{Q}_{DES}$	26.00	$\dot{Q}_{REC}$	3.94	$\dot{Q}_{CON1}$	17.34
$\dot{Q}_{HX}$	23.71	$\dot{Q}_{PRE}$	2.31	$\dot{Q}_{EVA1}$	14.96
$\dot{Q}_{ABS}$	17.51	$\dot{Q}_{CON2}$	59.91	$\dot{Q}_{EVA2}$	60.16
$\dot{Q}_{SUB}$	14.96	$\dot{W}_{COM}$	16.72		

Table 5.17 Model validation of the ICASS

Parameter	**Unit**	**Exp.**	**Mod.**	**Error [%]**
Primary inputs of the model				
VC_chilled water return	℃	19.37		-
VC_cooling water at condenser inlet	℃	15.90		-
VC_chilled water	kg/s	1.82		-
VC_cooling water	kg/s	0.54		-
VC_refrigerant (R22)	kg/s	0.295		-
AHP_hot water return	℃	45.68		-
AHP_hot water	kg/s	0.90		-
AHP_chilled water	kg/s	0.77		-
Primary outputs of the model				
VC_chilled water supply	℃	11.56	11.46	-0.86
VC_power input at the compressor	kW	16.03	16.72	4.31
AHP_hot water supply	℃	56.92	56.58	-0.6
Calculated values				
VC_cooling capacity	kW	59.54	60.29	1.26
VC_COP	n/a	3.71	3.61	-2.92
AHP_heating capacity	kW	42.33	41.04	-3.04

CHAPTER 6. MODEL-BASED ANALYSIS

In this chapter, the analyses were based on the models of VC, AHP, and ICASS. The validated models described in the previous sections were used to conduct the sensitivity analysis. The key parameters of the systems were identified via the sensitivity analysis. In the ideal case, the key parameters of the systems should be found through the tests. However, the test ranges of the systems are sometimes limited. For example, although the manufacturer claims that the lowest T_chw,r of the AHP installed is around 8℃, it was found during the tests that the AHP tended to stop when the T_chw,r was lower than 12℃. The validated model can thus help to predict the performances of the AHP when the T_chw,r is lower than 12℃.

6.1 Analysis of the AHP

Four parameters were tested and the results were discussed in the previous chapter. However, some of the parameters had limited test ranges. The validated model was thus used to conduct the sensitivity analysis of the AHP.

6.1.1 Sensitivity analysis of the AHP

As same as the tests, only one parameter changed at one time, the other parameters remained at the design values. Each of the parameters was varied at least 20% from its

design value and the results are shown in Figure 6.1(a) to (d). It can be observed that the model results showed agreement and same trends with the test results presented in the previous chapter. Tornado charts were drawn accordingly to compare the influences of the four parameters.

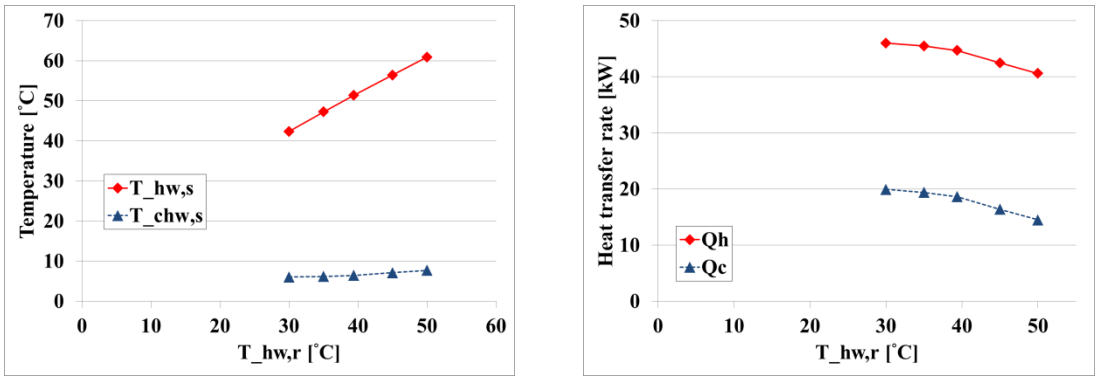

(a) T_hw,r

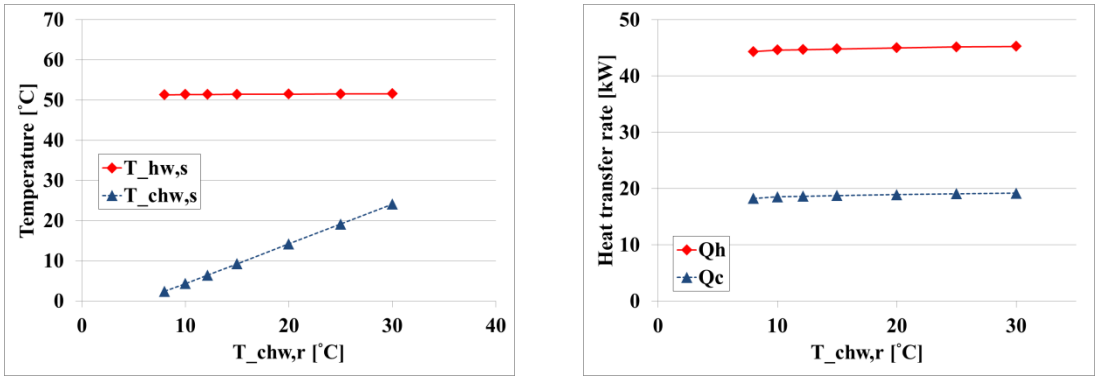

(b) T_chw,r

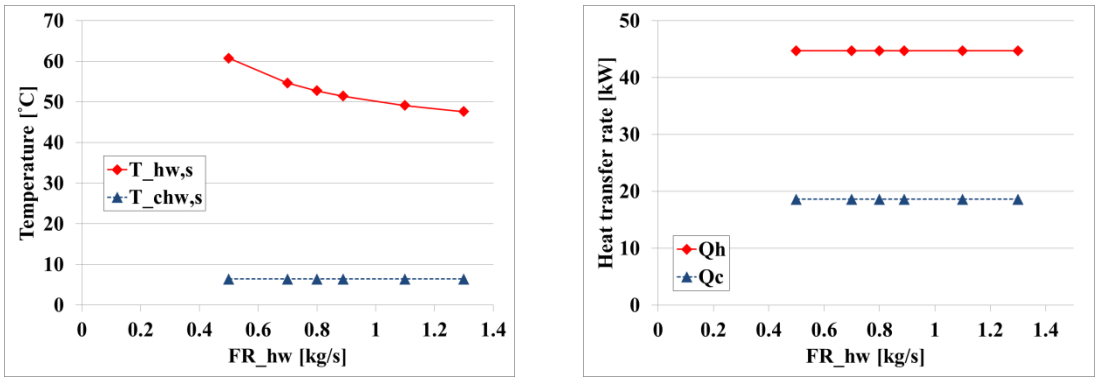

(c) FR_hw

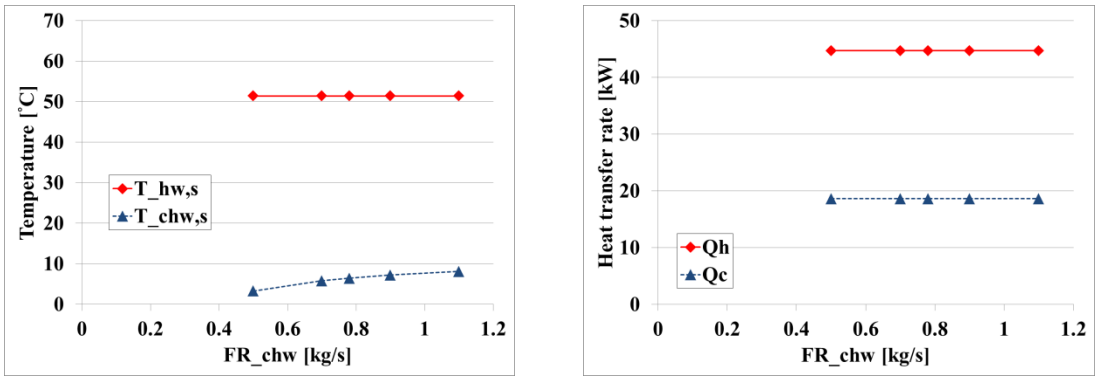

(d) FR_chw

Figure 6.1 Modeling results of the four tested parameters

Figure 6.2(a) to (d) show the results on the tornado charts. In the charts, the solid black bars represent the changes of the performance indicator while the tested parameters increase 20%; the bars with slashes represent the changes of the performance indicator while the tested parameters decrease 20%. For instances, the T_hw,s increased 14.79% when the T_hw,r increased 20%; the T_hw,s increased 5.94% when the FR_hw decreased 20%. Some studies used Kelvin as the unit of temperature when the sensitivity analysis was conducted. However, in this study, Celsius Degree was still used as the unit of temperatures because 1) the design values of the water temperatures were not zero and 2) the influences of the water temperatures were compared with the water flow rate. Using Celsius Degree as the unit of water temperatures gave more proper studied ranges. For the T_hw,s, the T_hw,r and FR_hw had significant influences on it, especially the T_hw,r. For the T_chw,s, the T_chw,r and FR_chw affected more than the T_hw,r. For the Q_h, the T_hw,r had larger effect than the T_chw,r. Also, for the Q_c, the T_hw,r had the most impact.

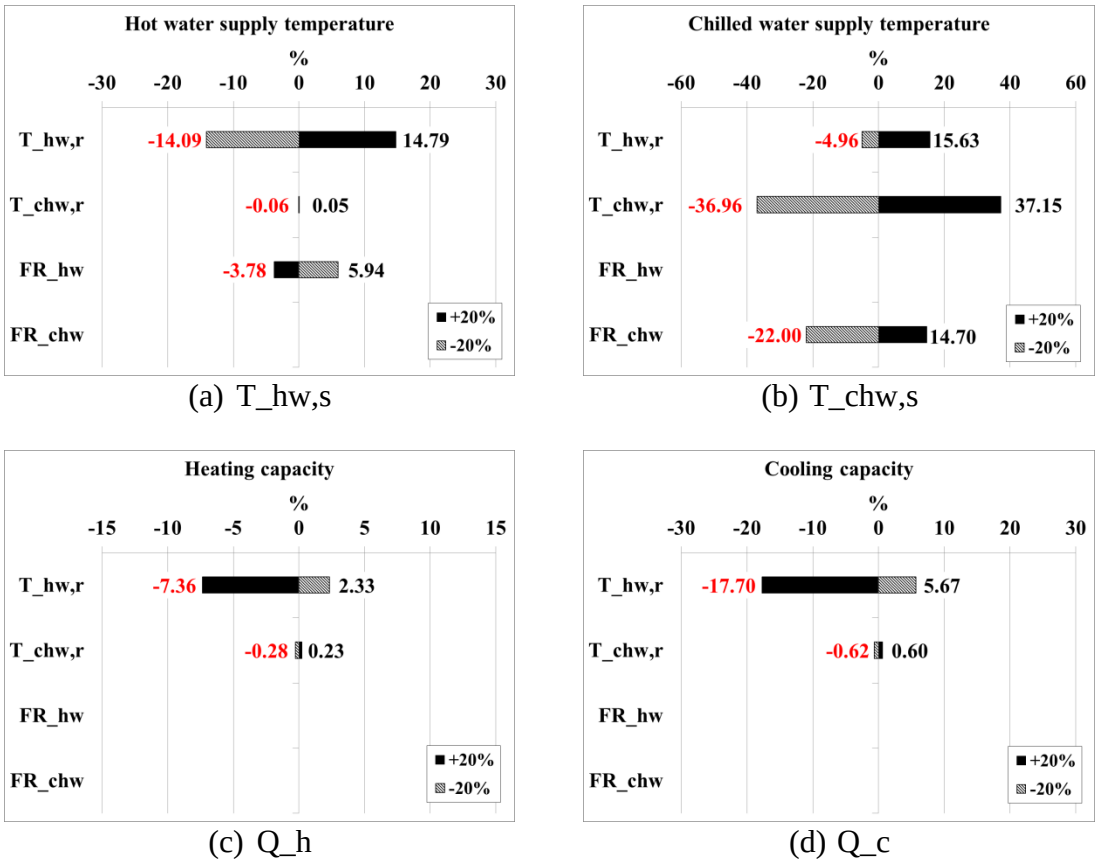

(a) T_hw,s (b) T_chw,s

(c) Q_h (d) Q_c

Figure 6.2 Sensitivity analysis of the AHP

6.1.2 Discussion of the AHP

The results of the sensitivity analysis will be discussed in this section. Detailed analyses were carried out to illustrate the influences of the four tested parameters.

6.1.2.1 Influences of the FR_hw and FR_chw

The FR_hw and FR_chw have nearly no influences on the Q_h and Q_c from both the experimental and modeling results. This could be explained by using the effectiveness method mentioned in the previous chapter. The actual heat transfer rate of a heat exchanger is the product of the effectiveness and the maximum possible heat transfer rate.

And the maximum possible heat transfer rate is the smaller value among the maximum possible heat transfer rates of the hot and cold fluids. If the inlet temperatures of the hot and cold fluids remain the same, the maximum possible heat transfer rates of the hot and cold fluids are only related to the flow rates.

Table 6.1(a) to (c) show the comparisons of the maximum possible heat transfer rates for the hot and cold fluids in the CON, HX, and EVA. It can be observed from the tables, no matter how the hot/chilled water flow rate changed, the smaller maximum possible heat transfers were always determined by the working fluid. This explained why the FR_hw and FR_chw had no influences on the Q_h and Q_c since the Q_h and Q_c are only affected by the two inlet temperatures and the flow rates of the working fluids.

Table 6.1 Heat transfer rates in the CON, HX, and EVA

(a) condenser

CON	FR_hw [kg/s]	Hot side [kW]	Cold side [kW]
		Fluid	
		99% ammonia-water	water
Design condition	0.43	23.56	69.41
Off-design condition	0.24 – 0.62	23.56	39.00 – 101.40

(b) HX

HX	FR_hw [kg/s]	Hot side [kW]	Cold side [kW]
		Fluid	
		43% ammonia-water	Water
Design condition	0.46	25.28	67.43
Off-design condition	0.26 – 0.68	25.25	37.88 – 98.49

(c) evaporator

EVA	FR_hw [kg/s]	Hot side [kW]	Cold side [kW]
		Fluid	
		water	99% ammonia-water
Design condition	0.78	34.39	20.69
Off-design condition	0.5 – 1.1	22.04 – 48.5	20.69

6.1.2.2 Influences of the T_chw,r

In the sensitivity analysis of the AHP, the low side pressure only changed from 450.1 to 454 kPa when the T_chw,r changed from 8 to 30℃ and the T_hw,r remained the same. Figure 6.3 shows the enthalpy-temperature (h-T) diagram of the working fluid (99% ammonia-water solution) at different T_chw,r. In the diagram, the enthalpies and temperatures of the working fluids entering the evaporator were plotted. Since the pressures were almost the same, the enthalpies and temperatures of the working fluids entering the evaporator thus had similar values. The enthalpies of the working fluids leaving the evaporator at different T_chw,r were also shown in the diagram.

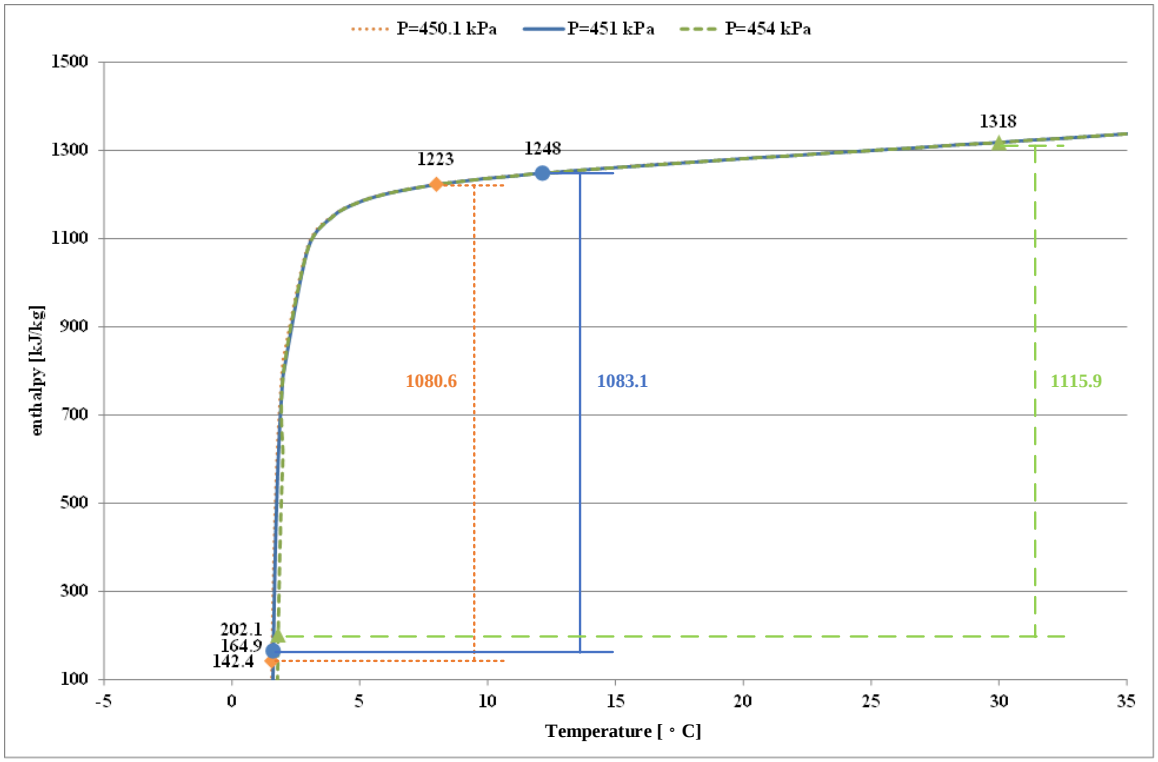

Figure 6.3 h-T diagram of the 99% ammonia water solution at different T_chw,r

The enthalpy difference between this point and the working fluids entering the evaporator was the maximum possible enthalpy difference of the heat exchanger. And the product of the maximum possible enthalpy difference and the mass flow rate of the working fluid was the maximum possible heat transfer rate of the heat exchanger. It can be seen from the diagram, even the T_chw,r increased from 8 to 30℃, the maximum possible enthalpy difference only increased 35.3 kJ/kg from 1080.6 to 1115.9 kJ/kg. The value became smaller after the increased maximum possible enthalpy difference timed the mass flow rate of the working fluid (around 0.02 kg/s) and the effectiveness of the evaporator (0.9). The discussion above illustrated why the T_chw,r only had small influences on the system performances. The low side pressure of the AHP did not change a lot while the T_hw,r remained the same. The maximum possible heat transfer rates of the evaporator were also only affected a little by the T_chw,r. Since the flow rate of the working fluid and the effectiveness of the HX remianed at the same level, the heat transfer rates of the evaporator remained pretty much the same.

6.1.2.3 Influences of the T_hw,r

Unlike the T_chw,r, the variations of the T_hw,r significantly affected the pressures of the AHP. When the T_hw,r increased from 30 to 50℃, the high side and low side pressures varied from 1,190 to 2,041 kPa and 332.6 to 552 kPa respectively. The decreased high side pressure reduced the temperature of the working fluid entering the desorber. More ammonia water vapor was boiled out due to the lower temperature. The mass flow rate of the working fluid passing through the condenser and evaporator thus

increased. This implied the potential increments of heat transfer rates in the condenser and the evaporator. On the other hand, the increased high side pressure raised the temperature of the working fluid entering the desorber which reduced the mass flow rate of the working fluid passing through the condenser and evaporator. The heat transfer rates in the condenser and the evaporator thus potentially decreased.

Moreover, the changes of the low side pressure also affected the heat transfer rate in the evaporator. Similar analysis was shown in Figure 6.4 as the analysis of the T_chw,r. When the T_chw,r were the same, the working fluid with higher pressure had lower maximum possible enthalpy difference. The heat transfer rate of the evaporator thus became lower with the decreased mass flow rate and maximum possible enthalpy difference.

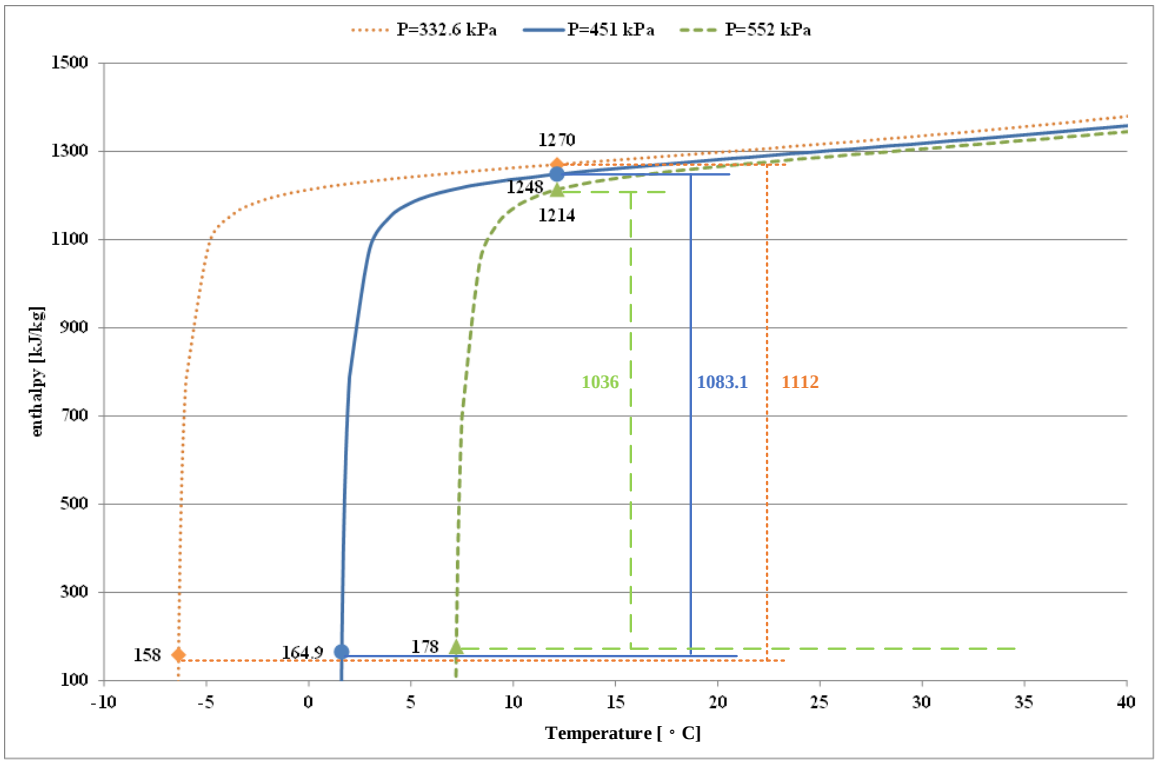

Figure 6.4 h-T diagram of the 99% ammonia-water solution at different T_hw,r

The discussions above described how the T_hw,r influenced the Q_h and Q_c of the AHP. The points were the changes of the pressures. The variation of the high side pressure affected the mass flow rate of the working fluid passing through the condenser and evaporator. The changes of the maximum possible enthalpy difference were related to the changes of the low side pressure. Both the mass flow rate and maximum possible enthalpy difference increased or decreased at the same time which enlarged the changes of the Q_h and Q_c.

6.2 Analysis of the VCRS

The test results of the ICASS showed that the capacity of the VC installed was insufficient for the integrated system. Additionally, an air-cooled VCRS will be more suitable for the ICASS because the condensing temperature is usually higher. Therefore, another model of an air-cooled VCRS was developed. The structure of the VCRS model is the same as Figure 5.8showed. The main differences between the VC and the VCRS models are the heat transfer fluids. For the VC, R22 is the refrigerant; water is used as chilled and cooling mediums. For the VCRS model, R410A is assumed as the refrigerant; air is used as the chilled and cooling mediums.

Another difference is the compressor model. Volumetric efficiency was used to replace the correlation equation of the refrigerant since experimental data was not available. The volumetric efficiency is defined as the ratio between the actual volume flow rate at the compressor inlet and the maximum theoretical flow rate as shown in Equation 6.1.

$$\eta_V = \frac{\dot{V}_{act}}{\dot{V}_{max}} = \frac{\dot{m}_r \cdot v_i}{\dot{N}_c \cdot V_s} \tag{6.1}$$

Where

η_V = volumetric efficiency
$\dot{V}_{act}$ = the actual volume flow rate at the compressor inlet, m^3/s
$\dot{V}_{max}$ = the maximum theoretical flow rate, m^3/s
$\dot{m}_r$ = mass flow rate of the refrigerant entering the compressor, kg/s
v_i = specific volume of the refrigerant entering the compressor, m^3/kg
$\dot{N}_c$ = number of intake strokes per unit time, 1/s
V_s = maximum volume of the suction process, m^3

The assumptions of the VCRS model are listed as below:

1) Pressure drops of the components and along the pipes are neglected.
2) Heat losses of the components and along the pipes are neglected.
3) The condition of the fluid exiting one component is same as the condition when it enters the next component.
4) Refrigerant exiting the condenser is assumed as saturated liquid.
5) Refrigerant entering the compressor is assumed as superheated vapor.

6.2.1 The VCRS model results

The inputs of the VCRS model include the properties of the indoor and outdoor airs, effectiveness of each heat exchanger, superheated temperature of the refrigerant entering the compressor, isentropic efficiency, and volumetric efficiency. The values of the inputs are listed in Table 6.2. The model results are shown in Table 6.3.

Table 6.2 Inputs of the VCRS model at different operation conditions

air temperature [℃]	**outdoor dry bulb**	35
	outdoor wet bulb	23.9
	indoor dry bulb	26.7
	indoor wet bulb	19.4
air flow rate [kg/s]	**outdoor air**	11.26
	indoor air	3.47
effectiveness of the heat exchanger	**condenser**	0.80
	evaporator	0.8
other	**superheated temperature of the refrigerant entering the compressor [℃]**	5
	isentropic efficiency	0.8
	volumetric efficiency	0.8

This VCRS model was used to conduct sensitivity analysis and for the development of another ICASS model.

Table 6.3 Results of the VCRS model

Properties					
	P [kPa]	**T [℃]**	**m [kg/s]**	**h [kJ/kg]**	**s [kJ/kg-℃]**
1	808.3	5.40	0.4984	427.00	1.830
2	2759.0	76.46	0.4984	470.60	1.855
3	2759.0	45.39	0.4984	276.50	1.252
4	808.3	0.33	0.4984	276.50	1.280
5	101.3	35.00	11.2600	71.35	-
6	101.3	37.66	11.2600	79.94	-
7	101.3	26.70	3.4700	55.16	-
8	101.3	17.51	3.4700	33.55	-
Calculated values [kW]					
$\dot{Q}_{CON}$	96.71	$\dot{Q}_{EVA}$	75.00	$\dot{W}_{COM}$	21.71
COP	3.46				

6.2.2 Sensitivity analysis of the VCRS

Assuming the air flow rates across the condenser and the evaporator are constant, the influences of the outdoor (T_amb) and indoor (T_ia,r) temperatures are plotted in Figure 6.5(a) to (d). For the charts, the X axis is the T_ia,r, the Y axis is the performance indicators which are the indoor air supply temperature (T_ia,s), cooling capacity (Q_e), power consumption (W), and COP. The different lines in the charts represent different outdoor (ambient) temperatures.

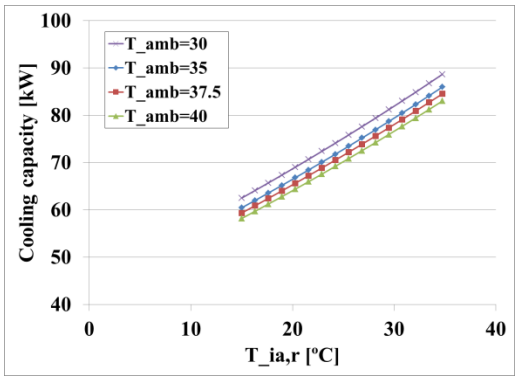

(a) Q_e

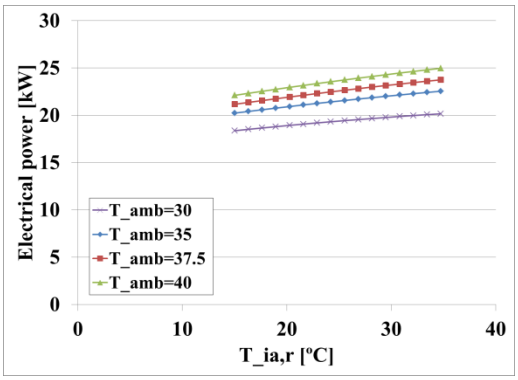

(b) W

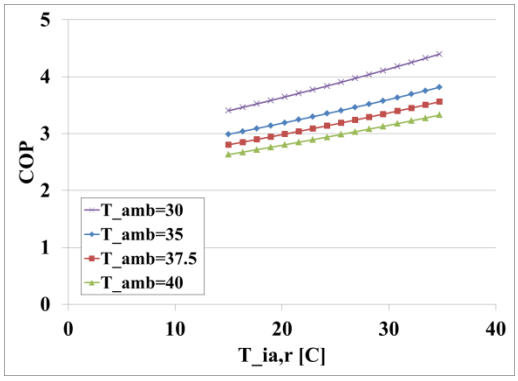

(c) COP

Figure 6.5 Influences of the T_amb and T_ia,r on the system performances

It was found from the charts, the T_ia,r had more impacts on the Q_e but the T_amb affected more on W and COP. The influences of the T_ia,r and the T_amb were also compared in the tornado charts as shown in Figure 6.6(a) to (d).

As same as the sensitivity analysis of the AHP, only one parameter changed at one time. The two tested parameters were varied 20% from the original values to see their influences. The sensitivity analysis of the VCRS confirmed that the T_ia,r had more impacts on the Q_e but the T_amb affected more on W and COP.

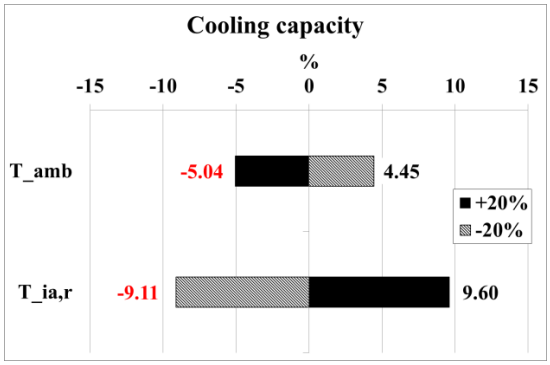

(a) Q_e

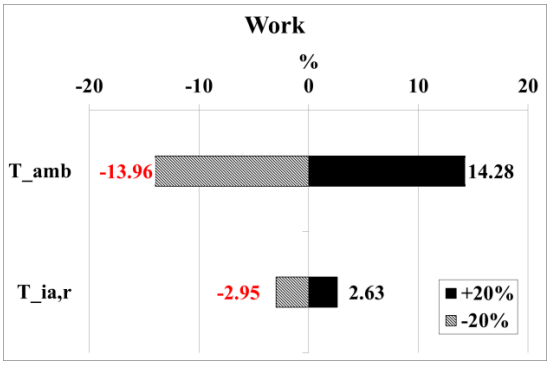

(b) W

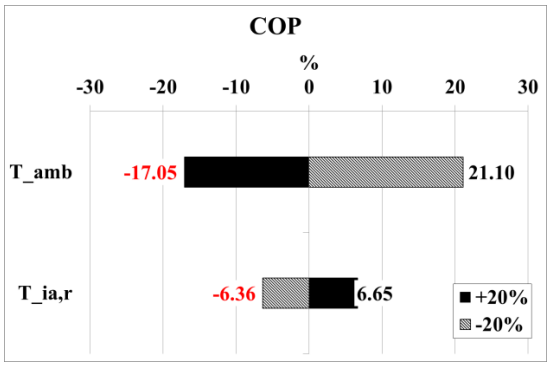

(c) COP

Figure 6.6 Sensitivity analysis of the VCRS

6.2.3 Discussion of the VCRS

In order to explain why the T_ia,s had more influences on the Q_e and the T_amb affected more on the W and COP, the changes of the condensing temperature (T_cond), the evaporating temperature (T_evap), and the refrigerant flow rate (m_r) are shown in Figure 6.7(a) to (d).

It can be observed from Figure 6.7(a) and (c) that the T_cond and T_evap increased as the T_ia,r and T_amb increased. Besides, the T_ia,r affected more on the T_evap while the T_amb had more influence on the T_cond. Moreover, the T_amb had more impact on the temperature differences between the T_cond and T_evap. This explained why the T_amb affected more on the W and COP.

Figure 6.7(b) and (d) show the changes of the m_r. The m_r is related to the specific volume of the refrigerant entering the compressor according to the equation of the volumetric efficiency. The changes of the T_ia,r actually influenced the T_evap and also the thermal properties of the refrigerant entering the compressor. The m_r was thus affected more by the changes of T_ia,r. And the Q_e was influenced by the m_r so that explained why the T_ia,r had more impact on the Q_e.

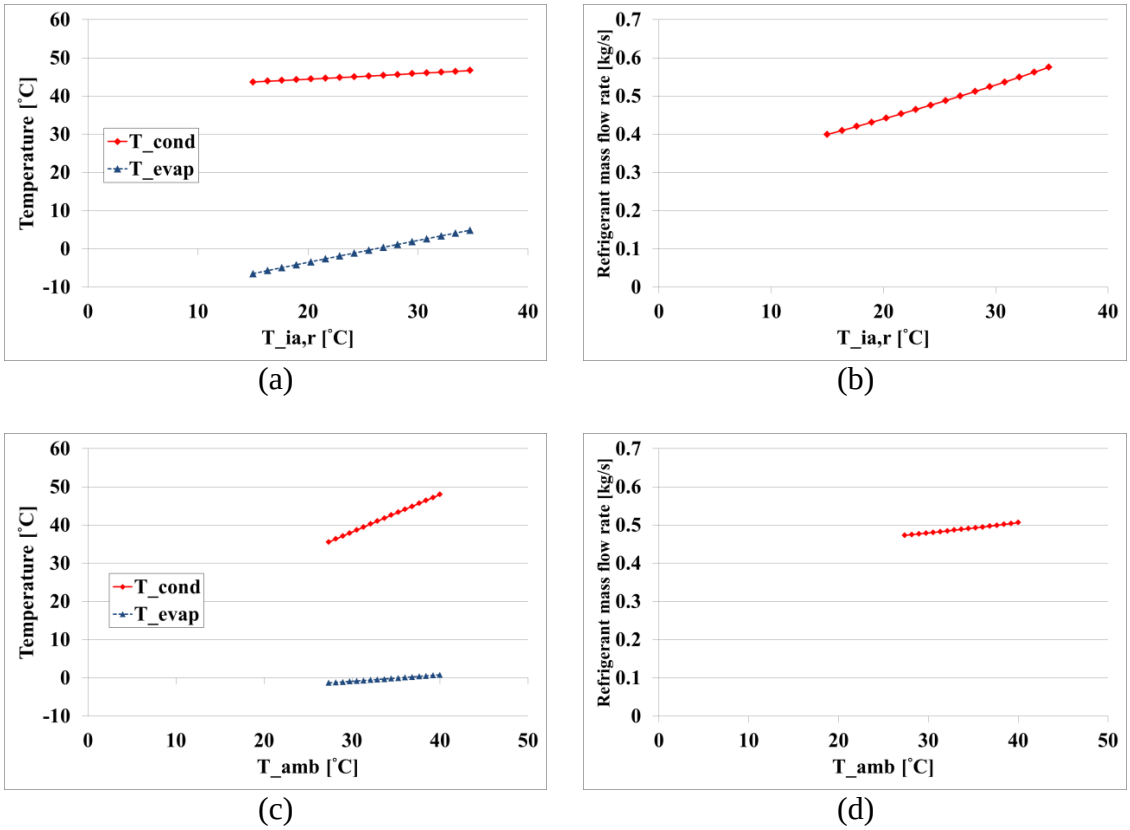

Figure 6.7 Influences of the T_amb and T_ia,r on the refrigerant properties

6.3 Analysis of the ICASS

The ICASS model discussed here was the integration of the VCRS and the AHP models via an additional subcooler model. The assumptions were the same as the VCRS and the

AHP models. The T_chw,r is one of the inputs in the AHP model but it is replaced by the effectiveness of the subcooler.

6.3.1 The results of the ICASS model using air-cooled VCRS

Table 6.4 shows the input values of the ICASS model using air-cooled VCRS. The model results are listed in Table 6.5.

Table 6.4 Inputs of the ICASS model using air-cooled VCRS

Air/water temperature [℃]	**outdoor dry bulb**	
	outdoor wet bulb	
	indoor dry bulb	26.7
	indoor wet bulb	19.4
	hot water return	39.39
Air/water flow rate [kg/s]	**AHP_hot water**	0.89
	AHP_chilled water	0.78
	Outdoor air	11.26
	Indoor air	3.47
effectiveness of the heat exchanger	**AHP_absorber**	0.80
	AHP_evaporator	0.90
	AHP_precooler	0.56
	AHP_condenser	0.91
	AHP_HX	0.92
	AHP_rectifier	0.80
	VCRS_condenser	0.8
	VCRS_evaporator	0.8
	subcooler	0.8
other	**thermal input at the desorber [kW]**	26
	mass flow rate of the strong solution entering the desorber [kg/s]	0.053
	mass fraction of ammonia of the strong solution entering the desorber[%]	43
	superheated temperature of the refrigerant entering the compressor [℃]	5
	isentropic efficiency	0.8
	volumetric efficiency	0.8

Table 6.5 Results of the ICASS model using air-cooled VCRS

Properties					
	P [kPa]	**T [℃]**	**h [kJ/kg]**	**x [%]**	**m [kg/s]**
1	1652.0	118.10	525.90	0.4300	0.0530
2	1652.0	172.20	662.00	0.1171	0.0340
3	451.8	127.00	662.00	0.1171	0.0340
4	1652.0	105.90	1530.00	0.9541	0.0206
5	1652.0	78.47	120.20	0.5366	0.0016
6	1652.0	78.47	1416.00	0.9900	0.0190
7	1652.0	42.58	291.80	0.9900	0.0190
10	451.8	1.67	172.30	0.9900	0.0190
11	451.8	4.14	1156.00	0.9900	0.0190
12	451.8	18.59	1276.00	0.9900	0.0190
13	451.8	74.47	421.50	0.4300	0.0530
14	451.8	48.06	-20.35	0.4300	0.0530
15	1652.0	48.17	-18.91	0.4300	0.0530
16	1652.0	67.06	65.49	0.4300	0.0530
17	101.3	39.39	165.00	-	0.8900
18	101.3	39.39	165.00	-	0.4244
19	101.3	51.42	215.30	-	0.4244
20	101.3	39.39	165.00	-	0.4656
21	101.3	51.42	215.30	-	0.4656
22	101.3	51.42	215.30	-	0.8900
23	101.3	16.05	67.31	-	0.7800
24	101.3	10.32	43.34	-	0.7800
25	808.4	5.40	427.00	-	0.3613
26	2585.0	72.36	468.20	-	0.3613
27	2585.0	42.65	271.20	-	0.3613
28	2585.0	12.67	219.50	-	0.3613
29	808.4	0.40	219.50	-	0.3613
30	101.3	35	71.35	-	11.2600
31	101.3	36.99	77.67	-	11.2600
32	101.3	26.7	55.17	-	3.4700
33	101.3	17.51	33.55	-	3.4700
Heat transfer rates [kW]					
$\dot{Q}_{DES}$	26.00	$\dot{Q}_{REC}$	4.47	$\dot{Q}_{CON1}$	21.35
$\dot{Q}_{HX}$	23.42	$\dot{Q}_{PRE}$	2.27	$\dot{Q}_{EVA1}$	18.69
$\dot{Q}_{ABS}$	24.40	$\dot{Q}_{CON2}$	71.18	$\dot{Q}_{EVA2}$	75.00
$\dot{Q}_{SUB}$	0.8	$\dot{W}_{COM}$	14.87		

6.3.2 Sensitivity analysis of the ICASS

Three parameters were tested to see their influences on the system performances. The three parameters were the T_amb, the T_ia,r, and the T_hw,r. Again, only one parameter

changed at one time; the three parameters were varied 20% from the original values to see their influences. The comparisons are shown in Figure 6.8(a) to (d).

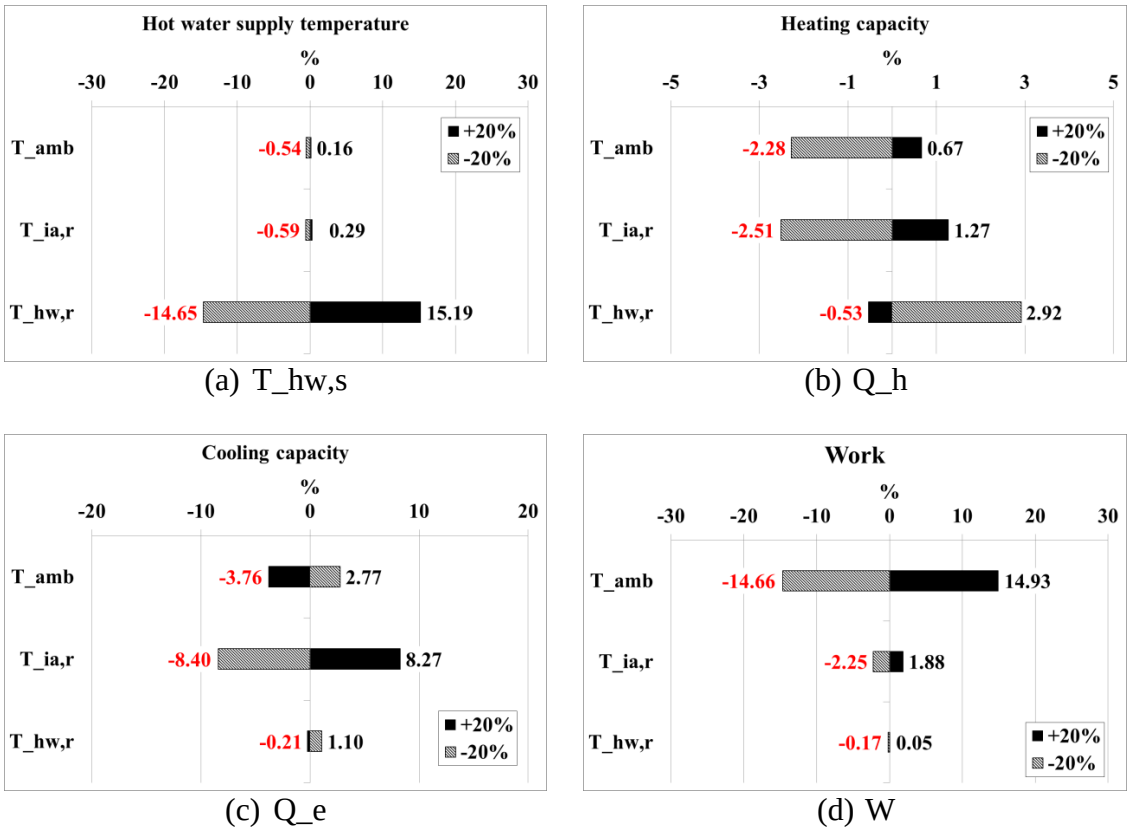

(a) T_hw,s (b) Q_h

(c) Q_e (d) W

Figure 6.8 Sensitivity analysis of the ICASS

It can be observed from the results, the T_hw,r affected the most on the T_hw,s. For the Q_e, W, and COP, the results were the same as the analysis of the VCRS. The T_amb influenced the W and COP the most while the T_ia,r significantly affected the Q_e. However, the three parameters had about the same influences on the Q_h. Even the T_hw,r had only slightly influence on the Q_h which yielded different results from the AHP. The sensitivity analysis of the AHP showed when the T_hw,r increased 20% from the design value, the Q_h decreased 7.36%. However, the sensitivity analysis of the

ICASS showed when the T_hw,r increased 20% from the design value, the Q_h only decreased 0.53%.

Table 6.6 shows the modeling results of the ICASS at different T_ahp,hw,r. Although the system balance process is complicated and dynamic but it can be simplified into several steps as shown in Figure 6.9. The simplified process was illustrated based on the modeling results. The left part of the figure illustrates the balance process while the T_hw,r decreases and the right part of the figure illustrates the balance process while the T_hw,r increases. Although the two processes have opposite reactions but the sequences are similar so only one process are described as the example.

From the experimental and modeling results of the AHP, the Q_h and Q_c decreased when the T_ahp,hw,r increased. The T_ahp,chw,s increased since the Q_c decreased. This higher T_ ahp,chw,s increased the temperature of the refrigerant exiting the subcooler (T_vc,sub); the T_vc,evap and T_vc,cond thus increased as well. Since the T_ahp,chw,s and T_vc,cond were higher, the T_ahp,chw,r increased as well. However, the increased T_ahp,chw,r actually increased the Q_h and Q_c of the AHP. Therefore, the total decrements of the Q_h and Q_c became less.

Table 6.6 Influences of the T_ahp,hw,r in the ICASS

Parameter	Unit	T_ahp,hw,r = 30℃	T_ahp,hw,r = 40℃	T_ahp,hw,r = 50℃
T_ahp,chw,s	℃	7.10	10.32	11.02
T_ahp,chw,r	℃	13.30	16.05	16.64
T_vc,cond	℃	42.58	42.65	42.66
T_vc,sub	℃	9.37	12.67	13.37
T_vc,evap	℃	0.06	0.40	0.48
Q_h	kW	46.33	44.77	44.45
Q_c	kW	20.28	18.69	18.35

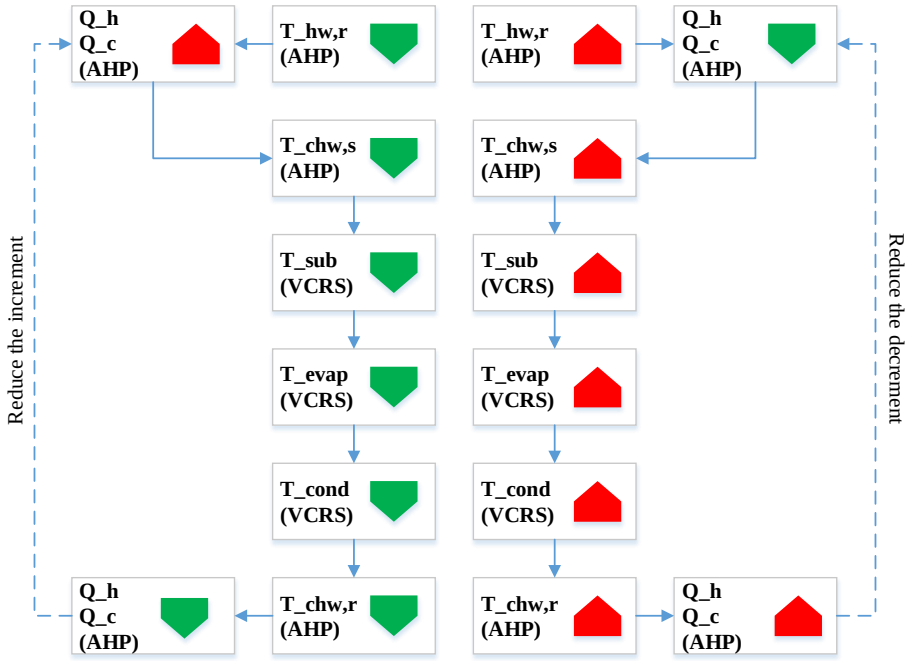

Figure 6.9 Simplified balance process of the ICASS while changing the T_hw,r

Another feature of the AHP can thus be found from the modeling results of the ICASS. When the heating load of the AHP is higher than the design condition (T_hw,r < 40℃), the T_chw,r has nearly no influences on the system performances. However, when the heating load of the AHP is lower than the design condition (T_hw,r > 40℃), the influences of the T_chw,r became larger. This also applied to the cooling load of the AHP. When the cooling load of the AHP is higher than the design condition (T_chw,r > 12℃), the T_hw,r has less influences on the system performances. But when the cooling load of the AHP is lower than the design condition (T_chw,r < 12℃), the T_hw,r significantly affects the system performances.

6.3.3 Cooling capacity ratio of the ICASS

From the tests of the ICASS, it was found that the total cooling capacity of the ICASS was an important factor for the stable operation. If the total cooling capacity of the ICASS is not enough, the chilled water temperature of the AHP will keep decreasing till the machine stops. In this section, assuming the ICASS provide the same unit cooling ($Q_{icass,c}$), different cooling capacity ratios of the ICASS were modeled to compare the performances. The results can be found in Table 6.7. Two different scenarios were compared. The first one was assumed that free thermal energy was used. The calculated power inputs for the ICASS were also used for the VCRS alone to calculate the cooling capacity ($Q_{vcrs,c}$). The capacity ratio was then calculated by the $Q_{vcrs,c}$ over the heat transfer rate of the AHP ($Q_{ahp,c}$). $COP_{icass,c}$, which did not consider the thermal input, was used as the performance indicator. It can be observed from the results that the $COP_{icass,c}$ increased from 3.89 to 5.36 when the capacity ratio decreased from 10.72 to 2.28. Therefore, if free thermal energy is utilized, the capacity ratio should be as small as possible to get the higher efficiency.

The previous discussions were assuming that the ICASS utilizes free thermal energy so the thermal input of the AHP was ignored. If natural gas is used for the ICASS, the thermal input should also be taken into account. For the calculations of COP for the ICASS, the consumptions of electricity and natural gas (site energy) were converted to primary energy (source energy) and the resource COP were calculated (Jain et al, 2013). The convert factor of the electricity and natural gas were 3.365 and 1.092 respectively (Deru and Torcellini, 2007). For example, the primary energy (PE) consumptions for 1 kW of electricity and 1 kW of natural gas are 3.365 kW and 1.092 kW, respectively.

Table 6.7 Analysis of the capacity ratio of the ICASS

ICASS						
Q_icass,c [kW]	1	1	1	1	1	1
Q_ahp,c [kW]	0.285	0.266	0.249	0.163	0.150	0.083
T_ahp,chw,s [℃]	3.18	7.03	10.33	25.09	26.98	36.06
Work [kW]	0.187	0.193	0.198	0.228	0.233	0.26
Thermal input [kW]	0.4	0.371	0.347	0.217	0.2	0.111
PE_work [kW]	0.63	0.65	0.67	0.77	0.783	0.87
PE_thermal [kW]	0.44	0.41	0.38	0.24	0.218	0.12
PE_total	1.07	1.06	1.05	1.00	1.001	0.98
COP_ahp,c	0.712	0.716	0.719	0.752	0.752	0.745
COP_icass,c	5.36	5.20	5.04	4.38	4.30	3.89
COP_PE,icass,c	0.939	0.949	0.956	0.996	0.999	1.01
Electricity cost [$/hr]	0.0281	0.029	0.0297	0.0342	0.035	0.039
NG cost [$/hr]	0.015	0.014	0.013	0.008	0.0074	0.004
Total cost [$/hr]	0.043	0.043	0.0427	0.0422	0.0424	0.043
Capacity ratio	2.28	2.52	2.77	4.85	5.36	10.72
VCRS alone						
COP_vcrs	3.46	3.46	3.46	3.46	3.46	3.46
Work [kW]	0.187	0.193	0.198	0.228	0.233	0.26
Q_vcrs,c [kW]	0.65	0.67	0.69	0.79	0.81	0.89

The results showed that the resource COP of the ICASS for cooling (COP_PE,icass,c) increased as the capacity ratio increased. This was actually reversed from the previous results assuming free thermal energy is used. Additionally, it was found, the COP_PE,icass,c had the largest value when the capacity ratio was 10.72. The chilled water return temperature of the AHP approached the maximum allowed value which is 45℃. The operation costs for the different scenarios were also calculated to see the differences. Using Chicago as the example, the price of the electricity and natural gas are 0.15 and 0.037 $/kWh, respectively (BLS, 2015). For the free thermal energy condition, the trend of the electricity cost made agreement with the COP_icass,c. However, when thermal input was taken into account, the total cost had the lowest value when the cooling capacity ratio was 4.85.

The cooling COP of the AHP (COP_ahp,c) was introduced to explain the results. Although the COP_PE,icass,c increased as the cooling capacity ratio increased, however,

the COP_ahp,c was the highest when the cooling capacity ratio was 4.85. Therefore, if thermal input is taken into account and the total cost is used as the indicator, the best cooling capacity ratio of the ICASS should be 4.85.

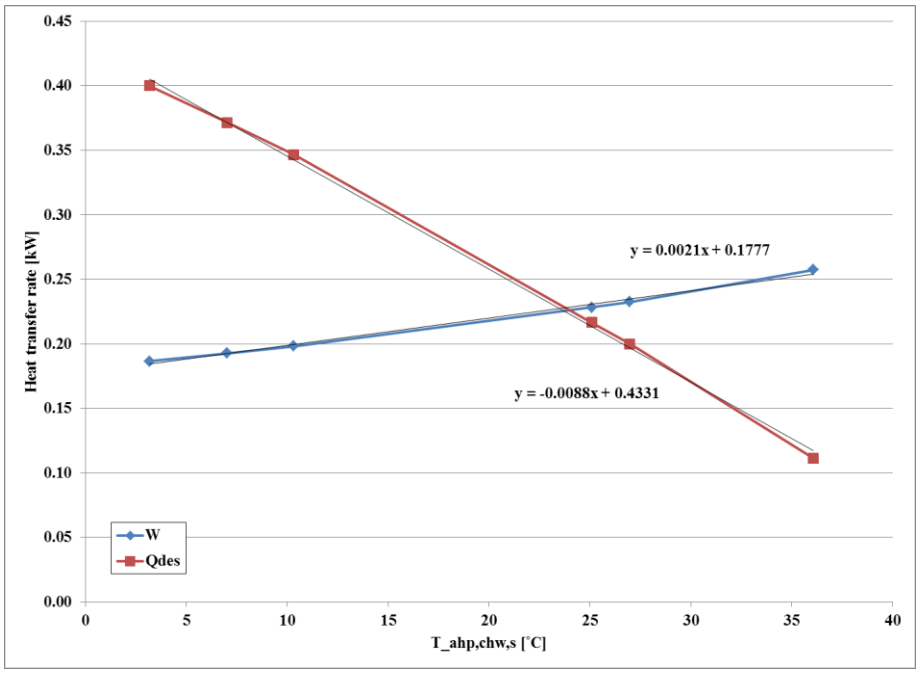

Figure 6.10 The energy inputs of the ICASS as the functions of T_ahp,chws

It was also found, if the COP_vcrs was converted to COP_PE,vcrs, the value (1.03) was higher than the COP_PE,icass,c (1.01) at the cooling capacity ratio of 10.72. In order to explore the highest value of the COP_PE,icass,c, the electrical and thermal inputs of the ICASS as the functions of T_ahp,chws are plotted in Figure 6.10. The relationships were almost linear so the equations could be calculated. Using the two equations listed in the figure, the T_ahp,chw,s for making COP_PE,icass,c larger than COP_PE,vcrs was found at 43.08℃. However, this condition is hard to reached because 1) the condensing temperature is around 45℃, and 2) the limitation of the T_ahp,chw,r is also 45℃.

6.4 Exergy analysis of the ICASS

In the previous chapters, the models developed and the analyses were based on the energy method, also known as the first-law analysis. In this section, exergy method is used for the second-law analysis of the ICASS. The definition of exergy is: the maximum useful work that can be achieved for a system by reducing the system losses in environmental conditions. Exergy reduction is due to the friction and other irreversibilities. The reduction in the exergy content of energy will decrease the efficiency of the system. The exergy losses should thus be minimized for increasing the system efficiency (Moran. 2010).

6.4.1 Irreversibility

In the real world, any system is irreversible. The irreverisibilities (or exergy destruction/loss) of the components and systems can be addressed via the second-law analysis which provides the clue for improving the systems. Specific exergy should be calculated first in order to know the irreversibility. The specific exergy of a fluid is defined as Equation 6.2 shows.

$$\boldsymbol{e = (h - h_o) - T_0(s - s_0)} \tag{6.2}$$

Where,
$\boldsymbol{e}$ = specific exergy of the fluid, kJ/kg
$\boldsymbol{T_0}$ = temperature of the environment (dead state), K
$\boldsymbol{h}$ = enthalpy of the fluid, kJ/kg
$\boldsymbol{h_o}$ = enthalpy of the fluid at the dead state, kJ/kg
$\boldsymbol{s}$ = entropy of the fluid, kJ/kg-K
$\boldsymbol{s_0}$ = entropy of the fluid at the dead state, kJ/kg-K

And the irreversibility of the component is defined as Equation 6.3 shows. The first two terms represent the exergy carried by the fluids entering and exiting the component. The following two terms are the exergy caused by the heat entering and exiting the component. The last term is the work provided to the component.

$$\boldsymbol{I = \sum \dot{m}_i e_i - \sum \dot{m}_o e_o + \sum \dot{Q}_i \left(1 - \frac{T_0}{T}\right) - \sum \dot{Q}_o \left(1 - \frac{T_0}{T}\right) + \sum W} \qquad (6.3)$$

Where,

$\boldsymbol{I}$ = irreversibility, kW
$\boldsymbol{\dot{m}_i}$ = mass flow rate of the fluid entering the component, kg/s
$\boldsymbol{\dot{m}_o}$ = mass flow rate of the fluid exiting the component, kg/s
$\boldsymbol{e_i}$ = specific exergy of the fluid entering the component, kJ/kg
$\boldsymbol{e_o}$ = specific exergy of the fluid exiting the component, kJ/kg
$\boldsymbol{\dot{Q}_i}$ = heat added to the component, kW
$\boldsymbol{\dot{Q}_o}$ = heat rejected from the component, kW
$\boldsymbol{T}$ = temperature of the component, K
$\boldsymbol{W}$ = work provided to the component, kW

One should notice that the unit of the temperature is always in kelvin for the second-law calculation.

6.4.2 Selection of the control volume

Although the irreversibility of the component is clearly defined as the Equation 6.3 shows, it is sometimes confused because of the control volume selection. Again, take the evaporator of the AHP as an example, Figure 6.11 shows two different selections of control volumes.

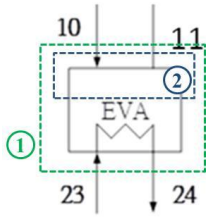

Figure 6.11 Control volume selection of the evaporator

The first selection of control volume (marked 1) include stream 10, 11, 23 and 24 while the second selection (marked 2) only include stream 10 and 11. The equations for calculating the irreversibility of evaporator for the two different control volumes are listed in Table 6.8. Although the selections of control volumes are different, the calculated results should be the same. One can select the most suitable control volume based on the available conditions.

Table 6.8 Calculation of the irreversibility of evaporator

Control volume 1	
$\mathbf{I_{eva}=m_{10}*e_{10}-m_{11}*e_{11}+m_{23}*e_{23}-m_{24}*e_{24}}$	(6.4)
Control volume 2	
$\mathbf{I_{eva}= m_{10}*e_{10}-m_{11}*e_{11}-Q_{eva}*(1-T_0/T_{eva})}$	(6.5)

For the second type of control volume selection, another question is how to define the temperature of the component. For the VCRS, temperature of the air entering the condenser and evaporator can be directly selected as the temperature of the component. However, for example, the heat exchanged mediums of all the components for the AHP are liquids, it is thus important to well define the temperature of the component. Three different methods were used to define the temperature of the component. The first one directly used the inlet temperature of the fluid as the temperature of the component. The

second one took average of the inlet and outlet temperatures of the fluids as the temperature of the component. The third one used the concept of effective temperature to define the temperature of the component (Colorado and Velazquez, 2013). The calculated results of the AHP evaporator based on these three definitions were compared and listed in Table 6.9 to see the differences.

It can be observed from the results that the second and third definitions yielded similar results. And the results were pretty much the same as the calculated result for the selection of control volume 1. In this study, the third method was used to calculate the temperature of the component.

Table 6.9 Comparison of the calculated irreversibility of evaporator

Control volume 1		
I_{eva} = 0.4407 kW		
Control volume 2		
Definition	T_{eva} [K]	I_{eva} [kW]
1	T_{23}	0.6439
2	$(T_{23}+T_{24})/2$	0.4411
3	$(T_{23}-T_{24})/\ln(T_{23}/T_{24})$	0.4404

6.4.3 Irreversibility of the ICASS

Table 6.10 shows the equations for calculating the COP, the exergy efficiency, and the irreversibilities of the components of the ICASS. The state points are the same as shown in Figure 5.9. The total irreversibility of the ICASS was the sum of the irreversibilities of the components. The equations were also used for the calculations of the VCRS and AHP.

Table 6.10 Equations for irreversibility calculation of the ICASS

Component	Equation	Note
Desorber (DES)	$I_{des}=m_1*e_1+m_5*e_5-m_2*e_2-m_4*e_4+Q_{des}*(1-T_0/T_{des})$	$T_{des}=T_2$; $T_0=T_{30}$
Rectifier (REC)	$I_{rec}=m_4*e_4+m_{15}*e_{15}-m_5*e_5-m_6*e_6-m_{16}*e_{16}$	
Condenser & HX (CONHX)	$I_{conhx}=m_6*e_6+m_{13}*e_{13}+m_{17}*e_{17}-m_7*e_7-m_6*e_6-m_{16}*e_{16}-m_{22}*e_{22}$	
Expansion valve 2 (EV2)	$I_{ev2}=m_7*e_7-m_8*e_8$	
Precooler (PRE)	$I_{pre}=m_8*e_8+m_{11}*e_{11}-m_9*e_9-m_{12}*e_{12}$	
Expansion valve 3 (EV3)	$I_{ev3}=m_9*e_9-m_{10}*e_{10}$	
Evaporator 1 (EVA1)	$I_{eva}=m_{10}*e_{10}+m_{23}*e_{23}-m_{11}*e_{11}-m_{24}*e_{24}$	
Absorber (ABS)	$I_{abs}=m_3*e_3+m_{12}*e_{12}+m_{16}*e_{16}-m_{13}*e_{13}-m_1*e_1$	
Pump	$I_{pump}=m_{14}*e_{14}-m_{15}*e_{15}+W_{pump}$	
Expansion valve 1 (EV1)	$I_{ev1}=m_2*e_2-m_3*e_3$	
Compressor (COM)	$I_{com}=m_{25}*e_{25}-m_{26}*e_{26}+W_{com}$	
Condenser (CON)	$I_{con}=m_{26}*e_{26}-m_{27}*e_{27}$	
Subcooler (SUB)	$I_{sub}=m_{24}*e_{24}+m_{27}*e_{27}-m_{23}*e_{23}-m_{28}*e_{28}$	
Expansion valve 4 (EV4)	$I_{ev4}=m_{28}*e_{28}-m_{29}*e_{29}$	
Evaporator 2 (EVA2)	$I_{eva2}=m_{29}*e_{29}-m_{25}*e_{25}-Q_{eva2}*(1-T_0/T_{eva2})$	$T_{eva2}=T_{32}$
$I_{total}=I_{des}+I_{rec}+I_{conhx}+I_{ev2}+I_{pre}+I_{ev3}+I_{eva1}+I_{abs}+I_{pump}+I_{ev1}+I_{com}+I_{con}+I_{sub}+I_{ev4}+I_{eva2}$		
COP & exergy efficiency		
$COP_{PE,C}=\frac{Q_{eva2}}{PE_W+PE_Q}$		$PE_W=W_{com}\times 3.365$ $PE_Q=Q_{des}\times 1.092$
$\eta_{II,c}=\frac{Q_{eva2}*(\frac{T_0}{T_{eva2}}-1)}{W_{com}+Q_{des}*(1-\frac{T_0}{T_{des}})}$		
$COP_{PE,H}=\frac{Q_{conhx}}{PE_W+PE_Q}$		
$\eta_{II,h}=\frac{Q_{conhx}*(1-\frac{T_0}{T_{conhx}})}{W_{com}+Q_{des}*(1-\frac{T_0}{T_{des}})}$		$T_{conhx}=(T_{22}-T_{17})/\ln(T_{22}/T_{17})$

Several points should be noticed from the table. First, the T_0 was selected as the same as the ambient temperature (T_{30}). The value of T_0 was thus changed with the $T_{30.}$ For the desorber, the temperature of the weak solution leaving the desorber (T_2) was selected as the temperature of the desorber (Ezzine et al., 2004).The calculated irreversibilities of the ICASS, VCRS, and AHP are shown in Figure 6.12. The blue bars show the irreversibilities of ICASS while the red bars show the irreversibilities of VCRS and AHP.

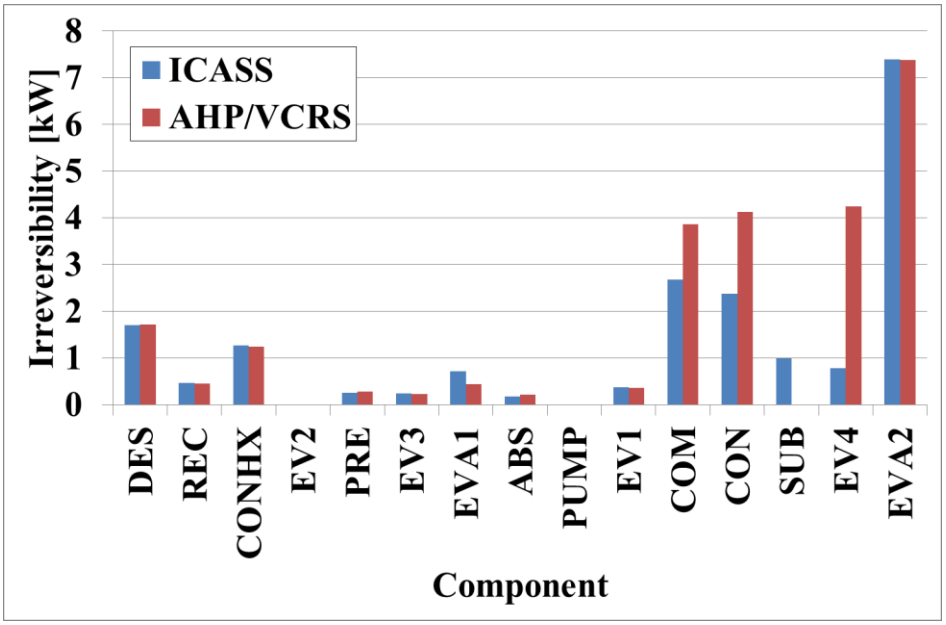

Figure 6.12 Irreversibilities of the ICASS, VCRS, and AHP

For the VCRS part, the largest irreversibility occurred at the evaporator both in the ICASS and the VCRS alone. This was due to the large temperature difference between the refrigerant and the air in the evaporator. However, it can be observed that the subcooling effect significantly reduced the irreversibility of compressor, condenser, and especially expansion valve. For the condenser, some of the irreversibility was shifted to

the subcooler. Additionally, the subcooler installed in the ICASS helped to reduce the condensing temperature as well as the temperature difference between the refrigerant and the air in the condenser. The irreversibility of the condenser was thus decreased. For the compressor and expansion valve, the subcooler helped to reduce the entropy difference across the two components. The irreversibilities of the compressor and expansion valve were thus decreased.

For the AHP, the amounts of the irreversibilities were pretty much the same in the ICASS and the AHP alone. The largest irreversibility occurred at the desorber due to the largest temperature difference between the desorber and the environment. The irreversibility of the evaporator was larger in the ICASS than that in the AHP alone. This was due to the higher chilled water temperature which increased the temperature difference between the working fluid and the chilled water in the evaporator.

The COP and exergy efficiency for heating and cooling of the ICASS, VCRS, and AHP are listed in Table 6.11. It can be seen from the comparison, the cooling COP of the ICASS was lower than the VCRS alone. However, the exergy efficiencies of cooling were pretty much the same. The detailed comparisons between the ICASS and different separated systems will be discussed in the next chapter.

Table 6.11 COP and exergy efficiency of the ICASS and the VCRS alone

	ICASS	VCRS
$COP_{PE,C}$	0.96	1.03
$\eta_{II,c}$	0.09	0.10
$COP_{PE,H}$	0.52	-
$\eta_{II,h}$	0.06	-

The changes of the irreversibilities and the exergy efficiencies of the ICASS for different operation and design conditions will be discussed in the following sections.

6.4.4 Exergy analysis of the ICASS at different operation conditions

In this section, the changes of the resource COPs, the exergy efficiencies, and the irreversibilities and of the ICASS along with the ambient temperature (T_amb), the indoor air temperature (T_ia,r), and the hot water return temperature (T_hw,r) will be discussed.

6.4.4.1 Influences of the ambient temperature

The changes of resource COP and exergy efficiencies of the ICASS along with the T_amb are shown in Figure 6.13(a) and (b). For the cooling of the ICASS, the resource COP decreased and exergy efficiency increased as the T_amb increased. The trends were the same as that in the VCRS as shown in Figure 6.13(c) and (d). The exergy efficiency increased due to the irreversibility ratio (IR) shown in Figure 6.13(d) decreased. The IR is defined as the total irreversibility over the power input at the compressor.

For the heating of the ICASS, both the resource COP and exergy efficiency decreased as the T_amb increased. Actually, the chilled water return temperature of the AHP (T_chw,r) increased as the T_amb increased. The changes of resource COP and exergy efficiency of the AHP along with T_chw,r are shown in Figure 6.13(e). The heating resource COP and exergy efficiency of the AHP remained pretty much the same as the T_chw,r increased.

Therefore, the decrements of the resource COP and exergy efficiencies of the ICASS were due to the consideration of the electrical power.

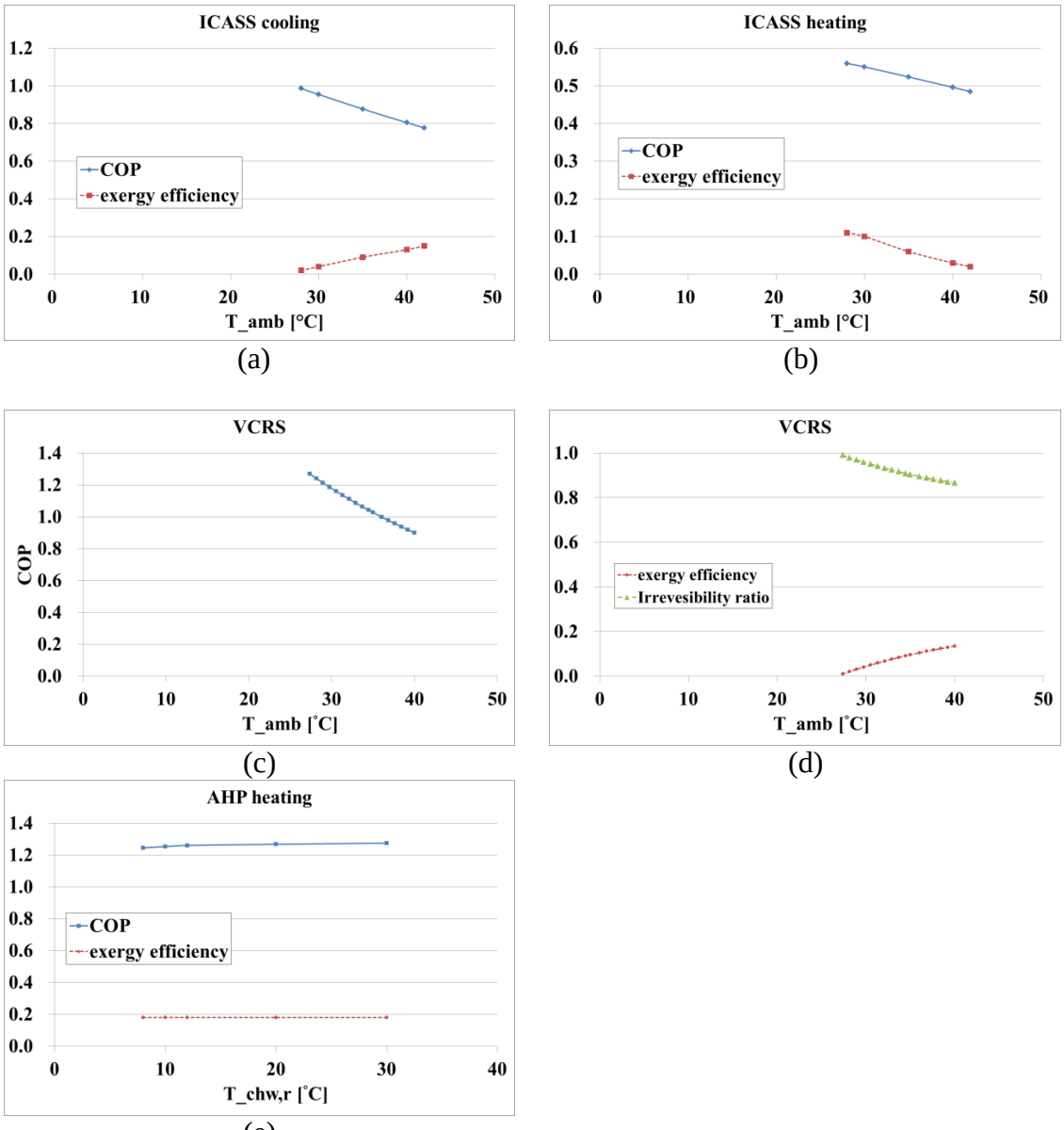

Figure 6.13 COP and exergy efficiency changed along with the T_amb and T_chw,r

The changes of the irreversibilities of ICASS along with the T_amb are shown in Figure 6.14(a), the changes of the irreversibilities of VCRS along with the T_amb are shown in Figure 6.14(b), and The changes of the irreversibilities of AHP along with the T_chw,r are shown in Figure 6.14(c). The total irreversibility of the ICASS increased as the T_amb increased. This trend is the same as that shown in Figure 6.14(b) and (c). The total irreversibility of the VCRS increased with the T_amb was mainly due to the increment of the capacity. And the total irreversibility of the AHP increased with the T_chw,r was mainly due to the increment of the irreversibility of evaporator. The higher T_chw,r increased the temperature difference between the working fluid and the chilled water in the evaporator. The irreversibility of evaporator thus increased.

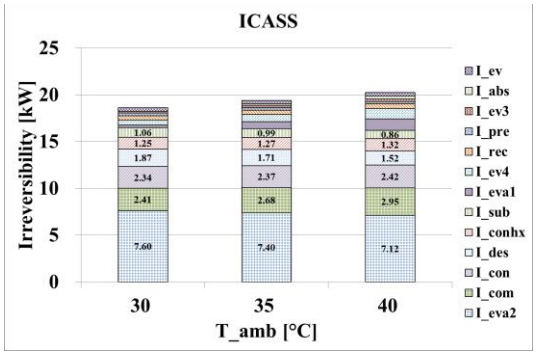

(a)

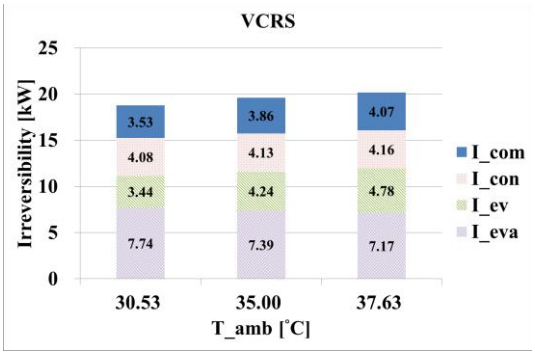

(b)

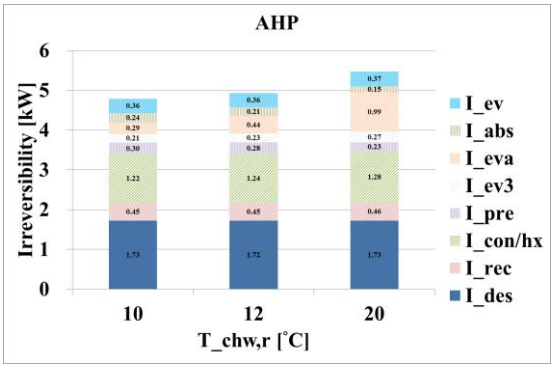

(c)

Figure 6.14 Changes of the irreversibilities along with the T_amb and T_chw,r

6.4.4.2 Influences of the indoor air return temperature

The changes of resource COP and exergy efficiencies of the ICASS along with the T_ia,r are shown in Figure 6.15(a) and. For the cooling of ICASS, the resource COP increased and exergy efficiency decreased as the T_ia,r increased. These trends were the same as that in the VCRS as shown in Figure 6.15(c) and (d). The exergy efficiency decreased due to the IR increased.

For the heating of the ICASS, the resource COP and exergy efficiency remained pretty much the same as the T_ia,r increased. The T_chw,r also increased as the T_ia,r increased. So the changes were the same as the trend shown in Figure 6.13(e).

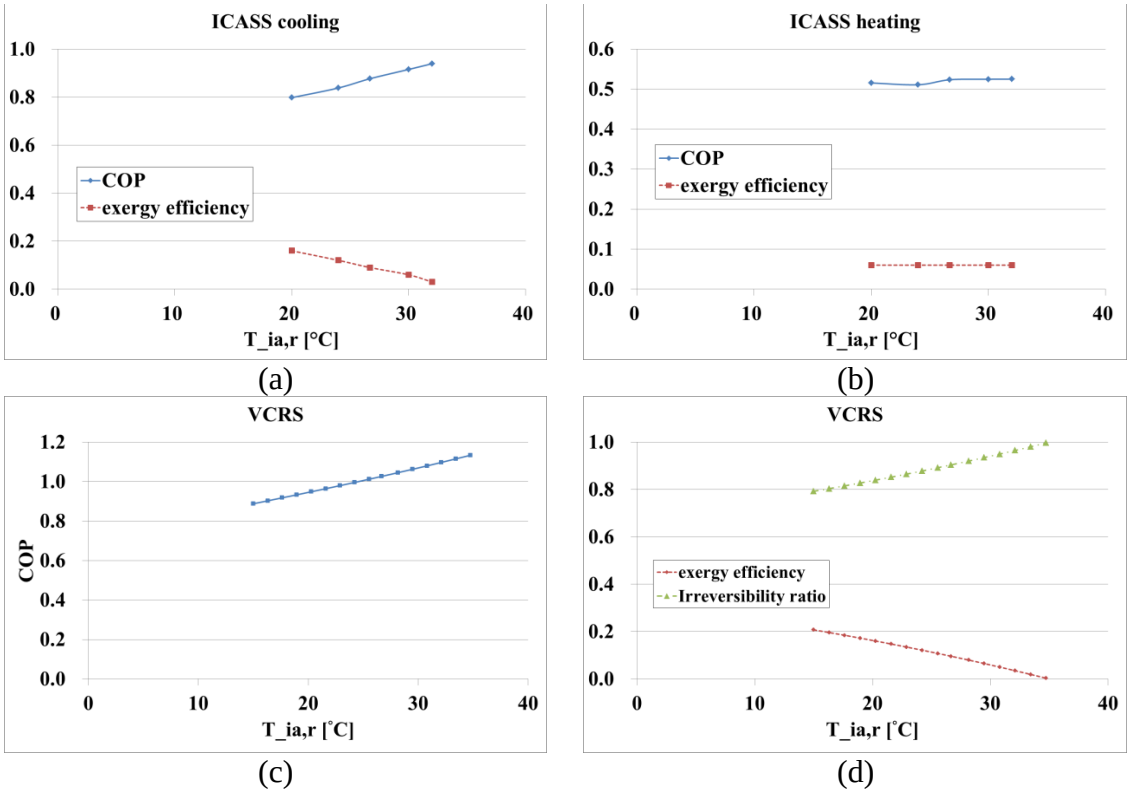

Figure 6.15 COP and exergy efficiency changed along with the T_ia,r

The changes of the irreversibilities of the ICASS along with the T_ia,r are shown in Figure 6.16(a). The total irreversibility of the ICASS increased as the T_ia,r increased. This trend is the same as that shown in Figure 6.16(b). The total irreversibility of the VCRS increased with the T_ia,r was mainly due to the increment of the capacity. The total irreversibility of the AHP increased was also due to the increment of T_chw,r as stated previously .

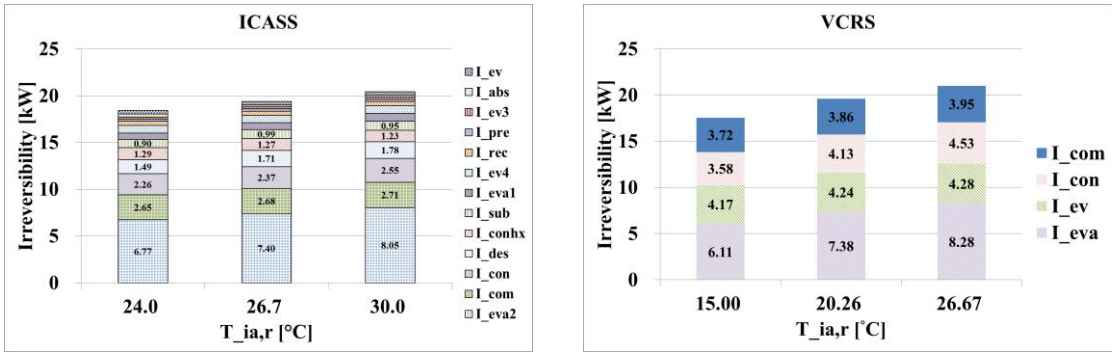

(a) (b)

Figure 6.16 Changes of the irreversibilities along with the T_ia,r

6.4.4.3 Influences of the hot water return temperature

The changes of resource COP and exergy efficiencies of the ICASS along with the T_hw,r are shown in Figure 6.17(a). For the cooling of ICASS, the COP and exergy efficiency did not change with the T_hw,r. For the heating of the ICASS, the COP slightly decreased and the exergy efficiency increased as the T_hw,r increased. The trend was the same as that in the AHP as shown in Figure 6.17(c).

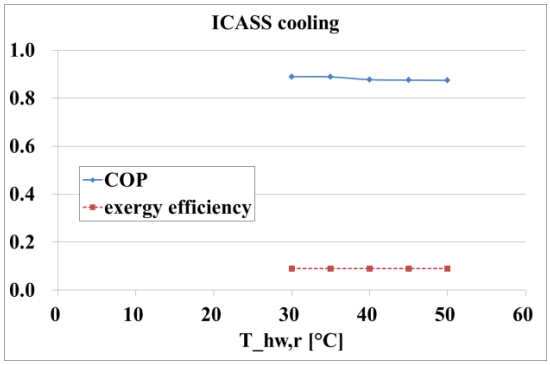

(a)

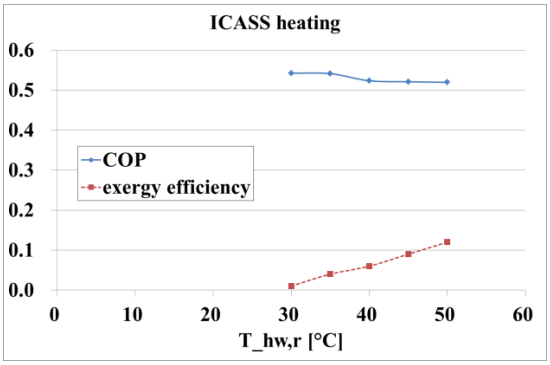

(b)

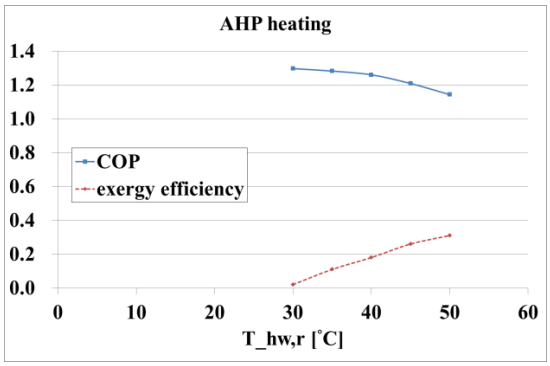

(c)

Figure 6.17 COP and exergy efficiency changed along with the T_hw,r

The changes of the irreversibilities of the ICASS along with the T_hw,r are shown in Figure 6.18(a). The total irreversibility of the ICASS decreased as the T_hw,r increased. This trend was the same as that in the AHP as shown in Figure 6.18(b). The total irreversibility of the AHP decreased as the T_hw,r increased was mainly due to the decrement of the irreversibility of evaporator. The higher T_hw,r reduced the temperature difference between the working fluid and the chilled water in the evaporator. The irreversibility of evaporator thus decreased.

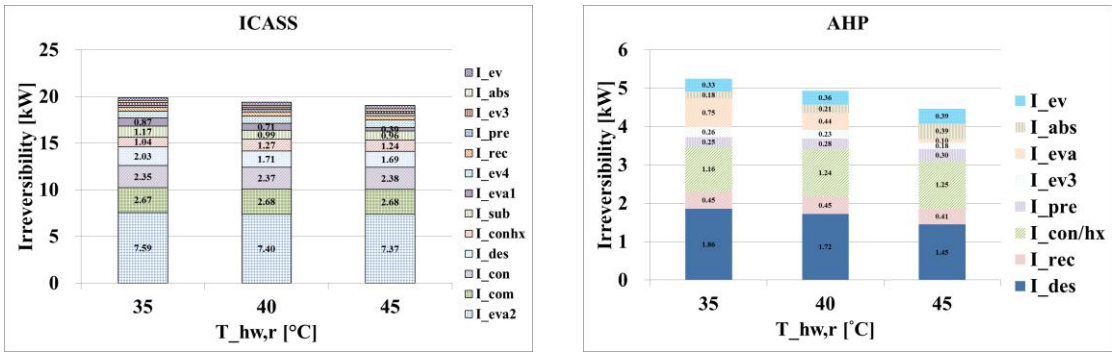

(a) (b)

Figure 6.18 Changes of the irreversibilities along with the T_hw,r

CHAPTER 7. ENERGY AND ECONOMIC BENEFITS OF THE ICASS

In this chapter, the energy and economic benefits of the ICASS will be discussed. The ICASS was compared with different other systems to evaluate the improvements of energy consumptions and efficiency. Building energy simulations were also carried out to estimate which scenario is most suitable for the application of ICASS.

7.1 Comparisons between the integrated and separated systems

In this section, the comparisons focus on the performances between the ICASS and the conventional separated systems. The energy consumptions and efficiencies of the integrated and separated systems were compared assuming that the heating and cooling capacities were the same.

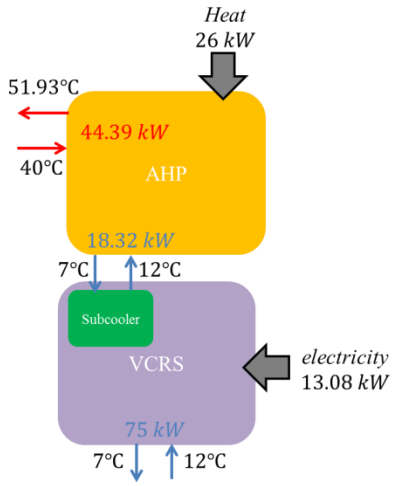

Figure 7.1 The base case of ICASS

Figure 7.1 shows the schematic diagram of the base case for the ICASS. The VCRS of the ICASS was an air-cooled chiller and the AHP was the one used in the previous chapters. The chilled water supply/return temperature of the VC and the AHP were the same as 7/12℃. The hot water supply and return temperature of the AHP were 51.93 and 40℃ respectively. In the following sections, this base case will be compared with different combinations of VCRS, absorption chiller (AC), AHP, and water heater(WH). The separated systems were assumed to provide the same amounts of heating and cooling capacities. The supply/return temperatures of the hot and chilled waters were also the same. The energy consumptions and the efficiencies of the systems were compared. Different COPs were used to compare the efficiencies of the systems. The definitions are summarized in Table 7.1.

Table 7.1 Definitions of the different COP

Term	Definition
COP_{VCRS}	The heat transfer rate at the evaporator over the work input at the compressor of the VCRS
COP_{AC}	The heat transfer rate at the evaporator over the heat transfer rate at the desorber of the AC
$COP_{AHP,C}$	The heat transfer rate at the evaporator over the heat transfer rate at the desorber of the AHP
$COP_{AHP,H}$	The heating capacity over the heat transfer rate at the desorber of the AHP
COP_{PE}	The sum of heating and cooling capacities over the sum of primary energy consumptions
$COP_{PE,C}$	The sum of cooling capacity over the sum of primary energy consumptions
$COP_{PE,H}$	The sum of heating capacity over the sum of primary energy consumptions
COP_{WH}	The heating capacity over the natural gas consumption of the water heater

7.1.1 Comparisons between the ICASS and the VCRS plus water heater

Figure 7.2 shows the chart of comparisons between the ICASS and the VCRS plus water heater. The combination of VCRS and water heater is the most common separated system

used to provide cooling and hot water respectively. The results of comparisons are listed in Table 7.2.

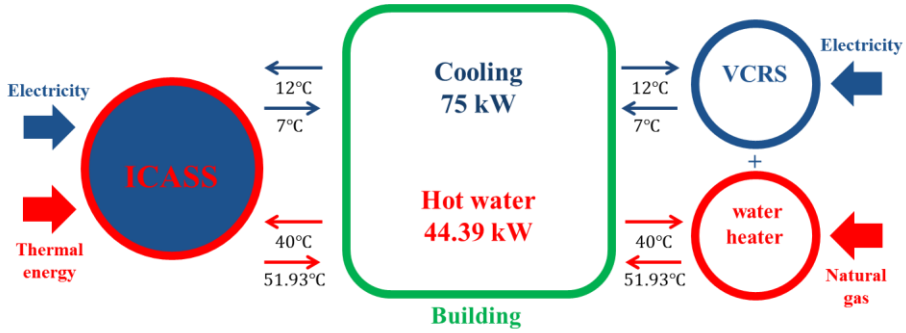

Figure 7.2 Comparisons between the ICASS and the VCRS plus water heater

It can be observed from the results, the electricity and natural gas consumptions of the ICASS were lower while the COP_{VCRS}, $COP_{AHP,H}$/ $COP_{WH,}$ and COP_{PE} of the ICASS was higher than the separated system. If the heating capacity was ignored, the $COP_{PE,C}$ was slightly lower than the VCRS. However, if the ICASS utilizes free thermal energy, the $COP_{PE,C}$ will be higher than the VCRS.

Table 7.2 Comparisons between the ICASS and the VCRS plus water heater

	ICASS	ICASS (free thermal input)	VCRS	WH	VCRS+WH
Cooling capacity [kW]	75.00	75.00	75.00	-	75.00
Heating capacity [kW]	44.39	44.39	-	44.39	44.39
Electricity consumption [kW]	13.08	13.08	19.34	-	19.34
Natural gas consumption [kW]	26.00	0.00	-	52.22	52.22
PE_electricity [kW]	44.01	44.01	65.08	-	65.08
PE_natural gas [kW]	28.39	0.00	-	57.03	57.03
Total PE consumption [kW]	72.41	44.01	65.08	57.03	122.11
COP_{VCRS}	5.73	5.73	3.88	-	-
$COP_{AHP,H}$/ COP_{WH}	1.71	-	-	0.85	-
COP_{PE}	1.65	2.71	-	-	0.98
$COP_{PE,C}$	1.04	1.70	1.15	-	0.62
$COP_{PE,H}$	0.61	1.01	-	0.78	0.36

7.1.2 Comparisons between the ICASS and the AC plus water heater

Figure 7.3 shows the chart of comparisons between the ICASS and the AC plus water heater. The AC and water heater were used to provide cooling and hot water respectively. The compared results are listed in Table 7.3.

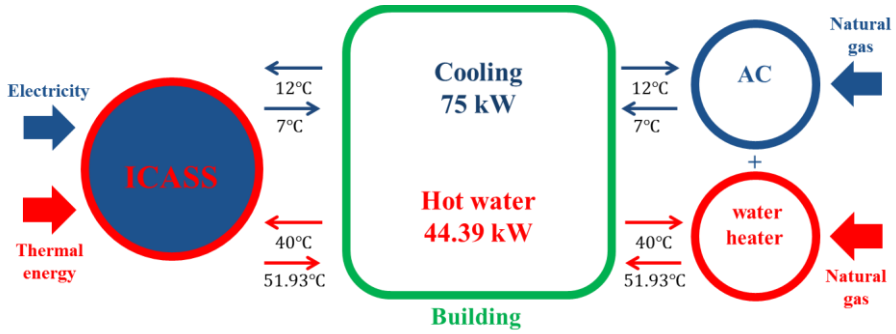

Figure 7.3 Comparisons between the ICASS and the AC plus water heater

It can be observed from the results, the energy consumptions were lower and the COPs were higher of the ICASS than that of the separated system.

Table 7.3 Comparisons between the ICASS and the AC plus WH

	ICASS	AC	WH	AC+WH
Cooling capacity [kW]	75.00	75.00	-	75.00
Heating capacity [kW]	44.39	-	44.39	44.39
Electricity consumption [kW]	13.08	-	-	-
Natural gas consumption [kW]	26.00	107.14	52.22	159.36
PE_electricity [kW]	44.01	-	-	-
PE_natural gas [kW]	28.39	117.00	57.03	174.03
Total PE consumption [kW]	72.41	117.00	57.03	174.03
COP_{VCRS}	5.73	-	-	-
$COP_{AHP,H}$/ COP_{WH}	1.71	-	0.85	-
COP_{PE}	1.65	-	-	0.69
$COP_{PE,C}$	1.04	0.64	-	0.43
$COP_{PE,H}$	0.61	-	0.78	0.26

7.1.3 Comparisons between the ICASS and the AC plus AHP

Figure 7.4(b) shows the chart of comparisons between the ICASS and the AC plus AHP. The AC and AHP were both used to provide cooling. They were placed in parallel as shown in Figure 7.4(a) while the AHP was also used to provide hot water. The compared results are listed in Table 7.4.

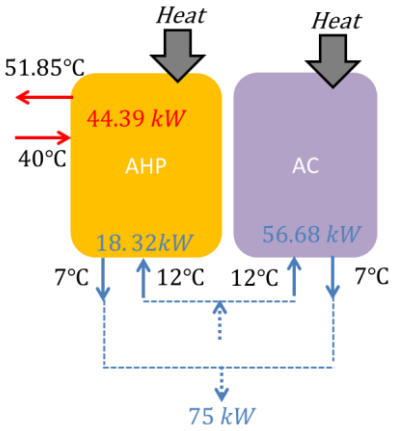

(a) Configuration of the AC plus AHP

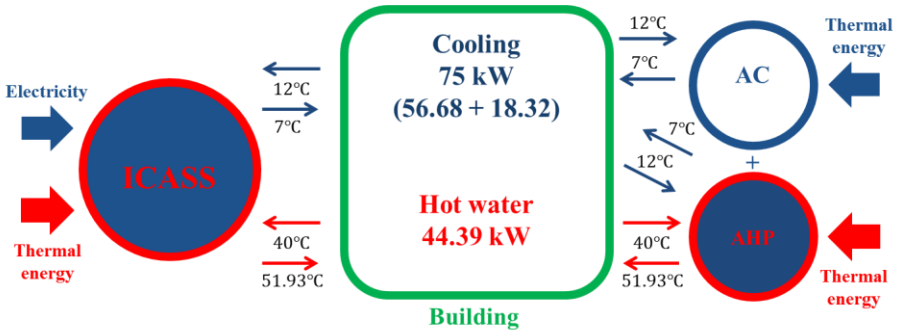

(b) Comparisons between the ICASS and the AC plus AHP

Figure 7.4 The charts of the AC plus AHP

The $COP_{PE,}$ $COP_{PE,C}$, and $COP_{PE,H}$ of the separated system were higher when the water heater was replaced by the AHP but still could not compete with the ICASS.

Table 7.4 Comparisons between the ICASS and the AC plus AHP

	ICASS	AC	AHP	AC+AHP
Cooling capacity [kW]	75.00	56.68	18.32	75.00
Heating capacity [kW]	44.39	-	44.39	44.39
Electricity consumption [kW]	13.08	-	-	-
Natural gas consumption [kW]	26.00	80.97	26.00	106.97
PE_electricity [kW]	44.01	-	-	-
PE_natural gas [kW]	28.39	88.42	28.39	116.81
Total PE consumption [kW]	72.41	88.42	28.39	116.81
COP_{VCRS}	5.73	-	-	-
$COP_{AHP,H}$	1.71	-	0.85	-
COP_{PE}	1.65	-	-	1.02
$COP_{PE,C}$	1.04	0.64	0.65	0.64
$COP_{PE,H}$	0.61	-	1.56	0.38

7.1.4 Comparisons between the ICASS and the VCRS plus AHP

The last comparison was between the ICASS and the VCRS plus AHP as shown in Figure 7.5(b). The VCRS and AHP were both used to provide cooling. They were placed in parallel as shown in Figure 7.5(a) while the AHP was also used to provide hot water. The compared results are listed in Table 7.5.

Table 7.5 Comparisons between the ICASS and the VCRS plus AHP

	ICASS	ICASS (free thermal input)	VCRS	AHP	VCRS+ AHP
Cooling capacity [kW]	75.00	75.00	56.68	18.32	75.00
Heating capacity [kW]	44.39	44.39	-	44.39	44.39
Electricity consumption [kW]	13.08	13.08	14.62	-	14.62
Natural gas consumption [kW]	26.00	0.00	-	26.00	26.00
PE_electricity [kW]	44.01	44.01	49.20	-	49.20
PE_natural gas [kW]	28.39	0.00	-	28.39	28.39
Total PE consumption [kW]	72.41	44.01	49.20	28.39	77.59
COP_{VCRS}	5.73	5.73	3.88	-	-
$COP_{AHP,H}$/ COP_{WH}	1.71	-	-	0.85	-
COP_{PE}	1.65	2.71	-	-	1.54
$COP_{PE,C}$	1.04	1.70	1.15	0.65	0.97
$COP_{PE,H}$	0.61	1.01	-	1.56	0.57

Although the energy consumptions were lower and COPs were higher of the ICASS than that of the separated system, the results were very close. The main advantage of the ICASS was coming from the reduction of electricity consumption. The comparison results proved that the performance is better when the AHP is integrated with the VCRS as the ICASS.

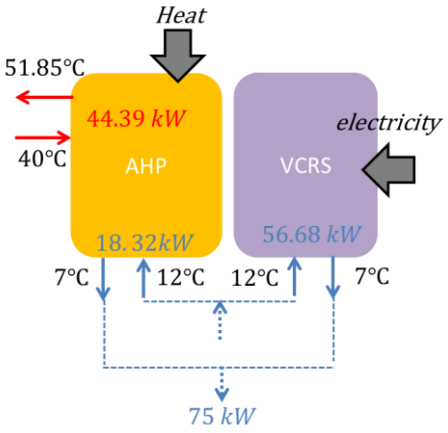

(a)

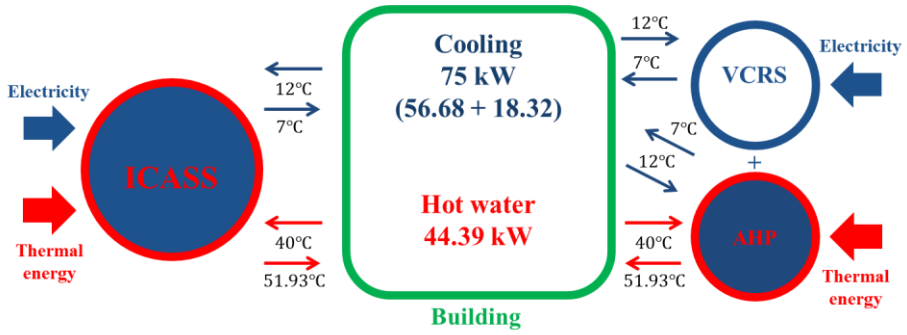

(b)

Figure 7.5 Comparisons between the ICASS and the VCRS plus AHP

7.1.5 Summary of the comparison

The comparison results discussed in the previous sections were summarized in Table 7.6. The operation costs of the systems for six different cities are also showed in the table. The corresponding prices of electricity and natural gas are listed in Table 7.7 (BLS, 2015).

The rate for NG in dollar per kWh was calculated from the original unit in dollar per therm. It can be seen from the table, Los Angeles has the highest electricity price while Baltimore has the highest NG price.

Table 7.6 Summary of the comparisons between ICASS and other systems

	ICASS	**VCRS+AHP**	**AC+AHP**	**VCRS+WH**	**AC+WH**
Electricity [kW]	13.08	14.62	0.00	19.34	0.00
NG [kW]	26.00	26.00	106.97	52.22	159.37
PE_electricity [kW]	44.01	49.20	0.00	65.08	0.00
PE_NG [kW]	28.39	28.39	116.81	57.03	174.03
PE_total [kW]	72.41	77.59	116.81	122.11	174.03
COP_{PE}	1.65	1.54	1.02	0.98	0.69
$COP_{PE,C}$	1.04	0.97	0.64	0.62	0.43
$COP_{PE,H}$	0.61	0.57	0.38	0.36	0.26
Baltimore [$/hr]	2.85	3.06	4.17	4.74	6.22
Chicago [$/hr]	2.92	3.16	3.96	4.83	5.90
Houston [$/hr]	2.66	2.86	3.96	4.45	5.90
LA [$/hr]	3.71	4.03	3.96	5.99	5.90
Miami [$/hr]	2.53	2.72	3.96	4.25	5.90
Seattle [$/hr]	2.27	2.42	3.96	3.87	5.90

It can be observed from the table, from the energy and economic aspects, the performance of the ICASS was better than the other systems. The combination of VCRS and AHP ranked at the second place and followed by the AC plus AHP, the VCRS plus WH, and the AC plus WH. The only exception was the cost in LA. The AC cost less than the VCRS due to the high electricity price in LA.

Table 7.7 Utility fees for different cities

	Electricity [$/kWh]	Natural gas [$/kWh]	Natural gas [$/therm]
Baltimore	0.14	**0.039**	**1.14**
Chicago	0.15	0.037	1.08
Houston	0.13	0.037	1.08
Los Angeles	**0.21**	0.037	1.08
Miami	0.12	0.037	1.08
Seattle	0.10	0.037	1.08

7.2 Building energy simulation

The comparisons between the ICASS and separated systems were described in the previous section. The building energy simulations were conducted in order to evaluate the economic savings of the ICASS in the real case.

7.2.1 The target building

Since the ICASS can provide cooling and hot water at the same time, it is very suitable for buildings with both requirements such as restaurants and hotels. The building energy simulations were conducted in EnergyPlus which provides many benchmark models of commercial-reference buildings (DOE, 2009).

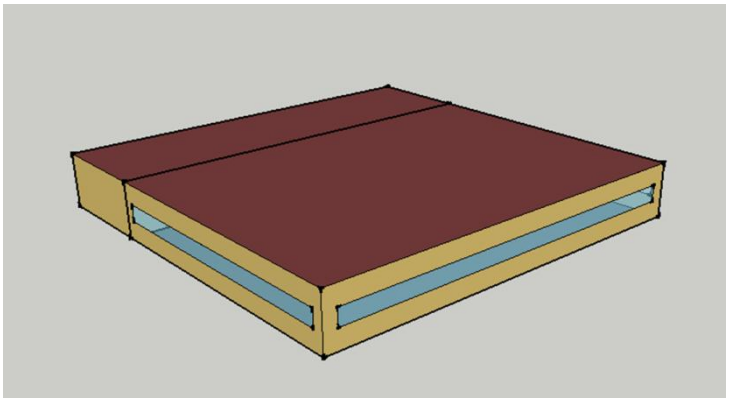

(DOE, 2009)

Figure 7.6 DOE Commercial Building Benchmark - Full Service Restaurant

Table 7.8 Geometric information of the target building

Zone Name	Area [m^2]	Volume [m^3]	Floor-to-Ceiling Height [m]	Gross Wall Area [m^2]	Window Glass Area [m^2]
Dining	371.75	1133.39	3.05	169.19	47.17
Kitchen	139.41	425.02	3.05	106.53	0
Total	**511.16**	**1558.41**	**n/a**	**275.72**	**47.17**

Table 7.9 Information of the target building in different cities

		Miami	Houston	Los Angeles	Baltimore	Seattle	Chicago
Fabric	**Exterior walls**						
	Construction Type	Steel frame wall	Steel frame wall	Steel frame wall	Steel frame wall	Steel frame wall	Steel frame wall
	R-value [m^2·K / W]	0.77	0.77	0.77	0.99	1.01	1.13
	Roof						
	Construction Type	IEAD	IEAD	IEAD	IEAD	IEAD	IEAD
	R-value [m^2·K / W]	1.76	1.76	1.76	2.04	2.07	2.50
	Window						
	U-Factor [W / m^2·K]	5.84	5.84	5.84	5.84	5.84	3.53
	SHGC	0.54	0.54	0.54	0.54	0.54	0.41
	Visible transmittance	0.38	0.38	0.38	0.38	0.38	0.32
	Foundation						
	Foundation Type	Mass Floor	Mass Floor	Mass Floor	Mass Floor	Mass Floor	Mass Floor
	Construction	4in slab-on-grade	4in slab-on-grade	4in slab-on-grade	4in slab-on-grade	4in slab-on-grade	4in slab-on-grade
	R-value [m^2·K / W]	0.32	0.32	0.32	0.32	0.32	0.32
HVAC	**Type**						
	Zone 1	DX-single speed	DX-single speed	DX-single speed	DX-single speed	DX-single speed	DX-single speed
	Zone 2	DX-single speed	DX-single speed	DX-single speed	DX-single speed	DX-single speed	DX-single speed
	COP						
	Zone 1	3.46	3.46	3.46	3.46	3.46	3.46
	Zone 2	3.50	3.50	3.50	3.50	3.67	3.50
	Economizer						
	Zone 1	No Economizer	No Economizer	No Economizer	No Economizer	No Economizer	No Economizer
	Zone 2	No Economizer	No Economizer	Differential Dry Bulb	No Economizer	No Economizer	No Economizer

The full service restaurant was taken as the example to evaluate the savings of the ICASS. The geometric information of the target building was shown in Figure 7.6 and Table 7.8. The restaurant was divided into the dining and kitchen zones. The analyses of cooling device were only focused on the dining zone.

Table 7.9 shows the information of the target building in different in different cities. It includes the sizes and efficiencies of the HVAC system and some parameters of the fabric. EnergyPlus provides models for the buildings which are constructed before 1908, in or after 1980, and new constructed. The information described in this section was for the building constructed before 1980.

7.2.2 Building simulation results

The annual simulation results for the annual cooling energy and cooling electrical consumption for the dining zone of the target building in different cities were shown in Figure 7.7. It can be observed from the charts, Miami had the highest annual cooling energy and consumed the most electricity for cooling.

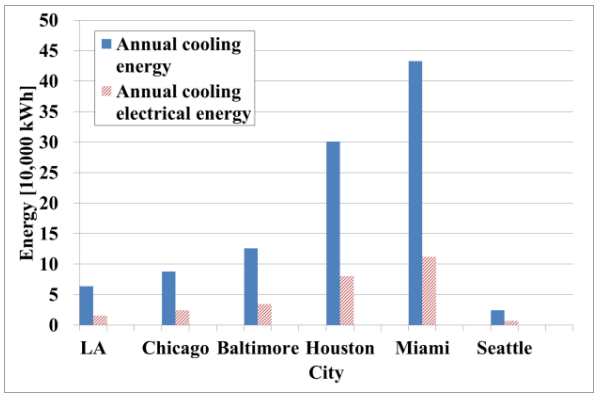

Figure 7.7 Annual simulation results of the target building

From the previous modeling results, it can be assumed that the ICASS can reduce around 30% of electricity consumption. This assumption was used to calculate the savings of ICASS in the six cities. It can found in Table 7.10, although the percentages of saving were the same, Miami had the most savings while Seattle had the least. The results were identical with the annual cooling energy of the cities. Additionally, the useful hot water generated by the ICASS was also calculated. The results were also the same as the electrical savings that Miami could provide the most heating energy while Seattle produced the least.

Table 7.10 Benefits of the ICASS

		Cost for electricity [$]	Additional hot water [kWh]
Baltimore	VCRS	4,096.04	-
	ICASS	2,867.23	55,350.12
	Difference	1,228.81	-
Chicago	VCRS	3,027.42	-
	ICASS	2,119.19	42,476.95
	Difference	908.23	-
Houston	VCRS	8,938.36	-
	ICASS	6,256.85	118,806.29
	Difference	2,681.51	-
LA	VCRS	2,978.25	-
	ICASS	2,084.77	32,127.61
	Difference	893.47	-
Miami	VCRS	11,533.87	-
	ICASS	8,073.71	174,966.56
	Difference	3,460.16	-
Seattle	VCRS	576.46	-
	ICASS	403.52	15,127.38
	Difference	172.94	-

Another notable point is the savings in LA. Comparing Chicago and LA, although LA has lower annual cooling energy but the savings were closed to Chicago due to the high

electricity price. The discussions above showed that the most ideal location for applying the ICASS was the place with high cooling demands and high electricity price. Additionally, more hot water can be generated if the cooling demands are higher.

CHAPTER 8. CONCLUSION

The summary and contributions of this research and the suggestions of future research are discussed in this chapter.

8.1 Summary and contributions of the research

The research investigated the ICASS by conducting the experiments, modeling, and evaluations of energy and economic savings.

8.1.1 Summary of the tests

A prototype of the ICASS was designed and constructed in the Herrick Labs at Purdue University. The test bed is primary composed by a VC, an AHP, and other auxiliary equipment and devices. The VC and AHP were tested individually and then the ICASS was tested.

For the AHP, four parameters were tested: hot water return temperature, the chilled water return temperature, the hot water flow rate, and the chilled water flow rate. The test results showed that, for the hot and chilled water, the return temperature and flow rate influenced the supply temperature. However, hot water return temperature was the only parameter which had significant influences on the heating and cooling capacities. The reasons may be because of the fixed thermal input at the desorber. The fixed thermal

input at the desorber. The fixed thermal input also limited the operation ranges of the AHP. For the VC, two parameters were tested: the chilled water return temperature and the cooling water flow rate. A higher chilled water return temperature directly increased the chilled water supply temperature, the power consumption, and the cooling capacity. However, the COP did not influenced a lot by the chilled water return temperature. And a higher cooling water flow rate increased the COP and decreased the water supply temperature and the power consumption while the cooling capacity remained the same. For the ICASS, it was found the total cooling capacity of the ICASS was an important factor. If the total cooling capacity is not enough, the AHP of the ICASS may stop and the system will not be operated at the steady state. If there is the limitation of the total cooling capacity, there are two methods to solve the issues. The first one is increasing the condensing temperature of the VCRS and the second one is decreasing the heating load of the AHP. These two methods can be implemented together or separately depends on the different conditions. Based on this, an air-cooled VCRS should be more suitable than a water-cooled VCRS for the ICASS since the condensing temperature of the air-cooled VCRS is usually higher.

The tests of the AHP, VC, and ICASS can contribute to the field of study. The test results of the VC, AHP, and ICASS are the valued references for researchers who study the similar integrated systems.

8.1.2 Summary of the model-based analysis

The experimental data collected from the test bed was used to develop and validate the models of the VC, AHP, and ICASS. For the AHP and ICASS models, the errors of the

predicted values were all within 5%. For the VC model, the largest errors of the predicted values were around 6%. For the system level modeling, the errors were accepted so the models were validated.

The validated models were used for the further analyses. For the AHP, the effectiveness method was used to analyze the influences of the hot and chilled water flow rates. It was found that, in the condenser, evaporator, and HX, the heat transfer rates were only determined by the two inlet temperatures and the flow rate of the working fluid. That explained why the hot and chilled water flow rates had no influences on the capacities. Also, it was found from the modeling results that the properties of the ammonia water solution helped to explain why the hot water return temperature had more influences than the chilled water return temperature.

Another VCRS model was developed and used for the analyses since the capacity of the VC installed in the test bed was not enough. The influences of the ambient temperatures and indoor return temperature were analyzed. The modeling results yielded similar results as the test results of the VC. The ambient temperature influenced more on the power consumption and COP while the indoor return temperature affected more on the cooling capacity.

Sensitivity analyses were carried out for the VC, AHP, and ICASS. For the ICASS, the influences of the ambient temperature, the indoor return temperature, and the hot water return temperature were compared. The results were similar to the results of the sensitivity analyses for the VC and AHP. The only exception was the influences of the increased hot water temperature. It was found in the analysis of AHP, the heating capacity decreased as the hot water return temperature increased. However, when the

AHP was integrated with the VCRS, the chilled water return temperature increased as the hot water return temperature increased. The increased chilled water return temperature actually reduced the decrement of the heating capacity. The AHP can thus provide higher temperature of hot water without losing much of the capacity. Therefore, it is beneficial for the AHP to integrate with the VCRS as the ICASS.

The cooling capacity ratio of the ICASS was studied. It was found, for the given AHP, the suggestion of cooling capacity ratio ranged from 2.28 to 10.72. If free thermal energy was used, the cooling COP of ICASS increased as the cooling capacity ratio decreased. However, if the energy consumption of thermal input was taken into account, the resource COP increased as the cooling capacity ratio increased. The results were reversed for the two different scenarios. Furthermore, if total cost was selected as the indictor, the lowest operation cost occurred when the cooling capacity ratio was 4.85. This was due to the changing of cooling COP of the AHP.

Since the ICASS utilized both electricity and thermal energy as inputs, the resource COP and exergy efficiency were used to represent the efficiency of the ICASS. For the calculations of resource COP, the electricity and thermal energy were converted to primary energy. Also, exergy analyses of the ICASS, VCRS, and AHP were conducted in order to calculate the exergy efficiency and irreversibilities. The equations for calculating the specific exergy, the selection of control volume, the calculation of the irreversibility for each component, and the equations of the resource COP and exergy efficiency were introduced and discussed. How did the irreversibilities, resource COPs, and exergy efficiencies of the ICASS, VCRS, and AHP change along with T_amb, T_ia,r, and T_hw,r were also analyzed.

The models developed for the VC, VCRS, AHP, and ICASS are the valued references for the researchers who try to develop the similar models. The details of the AHP model are especially useful for developing the absorption chiller/heat pump with ammonia water solution as the working fluid. Some critical points such as the properties of the ammonia water solution and the calculations of the circulation ratio were pointed out in this study. This help to save a lot of time for the researchers who are modeling the similar systems. Also, the energy and exergy analyses of the VCRS, AHP, and ICASS were clearly stated in this study. One can refer the equations and use the methods to conduct similar analyses. Also, the results of the model-based analyses are the valued references for the researchers to evaluate their analyses.

8.1.3 Summary of the energy and economic benefits of the ICASS

The energy consumptions and COPs of ICASS were compared with other conventional separated systems assuming the heating and cooling outputs were the same. The separated systems were the different combinations of VCRS, AC, AHP, and WH. The ICASS had advantages over any of the combinations. The combination of single-effect AC and WH had the worst performances among them. The comparison between the ICASS and the combination of VCRS plus AHP proved that the overall efficiency of the ICASS was higher than that when the VCRS and AHP were used in parallel. The comparisons also pointed out, if the heating capacity was ignored, the VCRS and double-effect AC had higher cooling efficiency than the ICASS. However, if the ICASS utilizes double-effect AC to subcool the VCRS, the cooling efficiency may compete with the VCRS and double-effect AC.

The last part of the research was the building energy simulation. The energy and economic savings of the ICASS were evaluated via the simulations conducted in EnergyPlus. The full service restaurant was selected as the target building since it requires both cooling and hot water at the same time. The benchmark models of the full service restaurant were thus used and simulations were carried out in six different cities. The results showed that the ICASS had the most savings in Miami. From the simulation results, it was found that the ICASS should be installed in the location with long cooling hours and high cooling demand. The savings of the ICASS will be higher if the hot water demand is higher since the operation time of the ICASS is limited by it.

8.2 Suggestions of the future research

8.2.1 Using double-effect ARS for the ICASS

In this research, the AHP available on the market was purchased and installed. However, the AHP is still a single-effect machine. From the results of comparisons, if the heating capacity was ignored, the cooling efficiency of the ICASS was slightly lower than the VCRS or the double-effect AC. If a double-effect AC or AHP can be used for the ICASS, even if the heating capacity is not taken into account, the cooling efficiency of the ICASS can compete with the VCRS or the double-effect AC.

8.2.2 Case study of the ICASS

In the present study, the VC was selected for the VCRS. Also, the cooling load was simulated by the hot steam. A better situation for the case study is installing an AHP to the air-conditioning system of a restaurant or a hotel as the ICASS. The test data

collected can be directly compared with the original condition. Conducting the test in the psychrometric room is another option. The psychrometric room can simulate the indoor and outdoor conditions of different locations. The performances of ICASS at different locations and conditions can thus be tested in the psychrometric room.

8.2.3 Dynamic modeling and control strategy

In this research, the models developed were the static models so only the steady state conditions could be simulated. A dynamic model can give more details about the changing process of the ICASS. Control strategy can be established based on the dynamic model. Although two different strategies were used in this study for the building energy simulation to predict the savings of the ICASS, they were still based on some assumptions and the calculations were static. The dynamic model may yield simulation results more closed to the real conditions. Different control strategies applied may also increase the savings of ICASS.

8.2.4 Life cycle assessment

In the present work, the evaluations of the benefits for ICASS were focused on the energy and economic aspects. However, the performance at the environmental aspect of ICASS shall be studied. The 3E (energy, economic, and environmental) life cycle assessment shall be discovered to provide more insights of the sustainability of the ICASS for convincing people to pursue this technology.

8.2.5 Utilization of the hot water

Since the ICASS can produce cooling and heating at the same time, different utilizations of the hot water should be taken into consideration in order to increase the value of ICASS. For example, the value of ICASS can be enlarged if the hot water produced from the ICASS is used to drive the liquid desiccant system.

REFERENCES

REFERENCES

Ahamed, J. U., Saidur, R., & Masjuki, H. H. (2011). A review on exergy analysis of vapor compression refrigeration system. Renewable and Sustainable Energy Reviews, 15(3), 1593-1600.

AHRI. (2000). Absorption Water Chilling and Water Heating Packages.

AHRI. (2004). Standard For Performance Rating Of Positive Displacement Refrigerant Compressors And Compressor Units.

AHRI. (2013). Performance Rating Of Water-Chilling and Heat Pump Water-Heating Packages Using the Vapor Compression Cycle

Aspen Plus.(2004). Aspen Technology, Inc., Ten Canal Park, Cambridge, MA, USA. From www.aspentech.com.

Ataer, Ö. E., & Göğüs, Y. (1991). Comparative study of irreversibilities in an aqua-ammonia absorption refrigeration system. International Journal of Refrigeration, 14(2), 86-92.

Benouali, J., Chang, Y. S., & Clodic, D. (2000). Analysis of the Sub-Cooling on Refrigerating Systems Using R-410A or R-404A.

Berlitz, T., Plank, H., Ziegler, F., & Kahn, R. (1998). An ammonia-water absorption refrigerator with a large temperature lift for combined heating and cooling. International Journal of Refrigeration, 21(3), 219-229.

Boian, I., Serban, A., Fota, S., & Chiriac, F. (2009, October). NH_3-H2O Absorption Systems Used for Research and Student Activities. In Proceedings of 8th WSEAS International Conference on System Science and Simulation in Engineering, Mathematics and Components in Science and Engineering, Ed. Revetria, R., Mladenov, V., Mastorakis, N., Genova, Italy, World Scientific Publ. CO PTE LTD., PO BOX (Vol. 128, pp. 131-136).

Cimsit, C., & Ozturk, I. T. (2012). Analysis of compression–absorption cascade refrigeration cycles. Applied Thermal Engineering, 40, 311-317.

Chien, Z. J., Cho, H. P., Jwo, C. S., Chien, C. C., Chen, S. L., & Chen, Y. L. (2013). Experimental Investigation on an Absorption Refrigerator Driven by Solar Cells. International Journal of Photoenergy, 2013.

Colorado, D., & Velazquez, V. M. (2013). Exergy analysis of a compression–absorption cascade system for refrigeration. International Journal of Energy Research, 37(14), 1851-1865.

Couvillion, R. J., Larson, M. W., & Somerville, M. H. (1988). Analysis of a vapor-compression refrigeration system with mechanical subcooling. ASHRAE transactions, 94, 641-660.

Darwish, N. A., Al-Hashimi, S. H., & Al-Mansoori, A. S. (2008). Performance analysis and evaluation of a commercial absorption–refrigeration water–ammonia (ARWA) system. International Journal of Refrigeration, 31(7), 1214-1223.

Deru, M. P., & Torcellini, P. (2007). Source energy and emission factors for energy use in buildings. Golden, CO: National Renewable Energy Laboratory.

Dincer, I., & Dost, S. (1996). Energy analysis of an ammonia-water absorption refrigeration system. Energy Sources, 18(6), 727-733.

DOE, U. (2009). Getting started with EnergyPlus.

DOE, U. (2010). Energyplus engineering reference. The Reference to EnergyPlus Calculations.

DOE, U. (2010). EnergyPlus Input Output Reference. US Department of Energy.

DOE, U (2011) Buildings Energy Data Book. Retrieved June 14, 2013, from http://buildingsdatabook.eren.doe.gov

El May, S., Boukholda, I., & Bellagi, A. (2010). Modular simulation and thermodynamic analysis of absorption heat pumps. Engineering with Computers, 26(2), 185-192.

Ezzine, N. B., Barhoumi, M., Mejbri, K., Chemkhi, S., & Bellagi, A. (2004). Solar cooling with the absorption principle: first and Second Law analysis of an ammonia—water double-generator absorption chiller. Desalination, 168, 137-144.

Fumo, N., Mago, P., & Luck, R. (2010). Methodology to estimate building energy consumption using EnergyPlus Benchmark Models. Energy and Buildings, 42(12), 2331-2337.

Gadalla, M. A., Ibrahim, T. A., & Hassan, M. A. (2013). Performance characteristics of an ammonia–water absorption heat pump system. International Journal of Energy Research.

Gordon, J. M., & Ng, K. C. (1995). A general thermodynamic model for absorption chillers: theory and experiment. Heat Recovery Systems and CHP, 15(1), 73-83.

Grossman, G., & Zaltash, A. (2001). ABSIM—modular simulation of advanced absorption systems. International Journal of Refrigeration, 24(6), 531-543.

Herold, K. E., & Radermacher, R. (1989). Absorption heat pumps. Mechanical Engineering, 111(8), 68-71.

Herold, K. E., Radermacher, R., & Klein, S. A. (1996). Absorption chillers and heat pumps. CRC press.

Horuz, I. (1998). A comparison between ammonia-water and water-lithium bromide solutions in vapor absorption refrigeration systems. International communications in heat and mass transfer, 25(5), 711-721.

Horuz, I., & Callander, T. M. S. (2004). Experimental investigation of a vapor absorption refrigeration system. International Journal of Refrigeration, 27(1), 10-16.

Hwang, Y. (2004). Potential energy benefits of integrated refrigeration system with microturbine and absorption chiller. International Journal of Refrigeration, 27(8), 816-829.

Incropera, F. P. (2011). Fundamentals of heat and mass transfer. John Wiley & Sons.

Jain, V., Kachhwaha, S. S., & Sachdeva, G. (2013). Thermodynamic performance analysis of a vapor compression–absorption cascaded refrigeration system. Energy Conversion and Management, 75, 685-700.

Jain, V., Kachhwaha, S. S., & Sachdeva, G. (2014). Exergy analysis of a vapour compression–absorption cascaded refrigeration system using modified Gouy–Stodola equation. International Journal of Exergy, 15(1), 1-23.

Jawahar, C. P., & Saravanan, R. (2011). Experimental studies on air-cooled NH3H2O based modified gax absorption cooling system. International Journal of Refrigeration, 34(3), 658-666.

Kairouani, L., & Nehdi, E. (2006). Cooling performance and energy saving of a compression–absorption refrigeration system assisted by geothermal energy. Applied thermal engineering, 26(2), 288-294.

Kim, B., & Park, J. (2007). Dynamic simulation of a single-effect ammonia–water absorption chiller. International Journal of Refrigeration, 30(3), 535-545.

Kung, Y. S., Qu, M., and Peng, S. (2013). Model based analysis of an integrated system of vapor-compression chiller and absorption heat pump. International Conference on Energy Sustainability.

Lazzarin, R. M., Gasparella, A., & Longo, G. A. (1996). Ammonia-water absorption machines for refrigeration: theoretical and real performances. International Journal of Refrigeration, 19(4), 239-246.

Lee, S. F., & Sherif, S. A. (2001). Thermodynamic analysis of a lithium bromide/water absorption system for cooling and heating applications. International Journal of Energy Research, 25(11), 1019-1031.

Mansoori, G. A., & Patel, V. (1979). Thermodynamic basis for the choice of working fluids for solar absorption cooling systems. Solar Energy, 22(6), 483-491.

Marcriss, R. A., Gutraj, J. M., & Zawacki, T. S. (1988). Absorption fluid data survey: final report on worldwide data, ORLN/sub/8447989/3, Inst. Gas Tech.

Minh, N. Q., Hewitt, N. J., and Eames, P. C.. 2006. Improved Vapour Compression Refrigeration Cycles: Literature Review and Their Application to Heat Pumps. International Refrigeration and Air Conditioning Conference, Paper 795.

Modahl, R. J., & Hayes, F. C. (1992). Development and proof-testing of advanced absorption refrigeration cycle concepts (No. ORNL/Sub-86-17498/1). Oak Ridge National Lab., TN (United States); Trane Co., La Crosse, WI (United States). Applied Unitary/Refrigeration Systems Div.

Moran, M. J., Shapiro, H. N., Boettner, D. D., & Bailey, M. B. (2010). Fundamentals of engineering thermodynamics. John Wiley & Sons.

Mustafa, H. (2013, March). Experimental and Analytical Investigation of Ammonia Absorption into Ammonia-Water Solution: Free Absorption. In Defect and Diffusion Forum (Vol. 334, pp. 167-170).

NAEA. 2005. Final Report to Oak Ridge National Laboratory Under Subcontract Number 4000016141

Radermarcher, R., & Klein, S. A. (1996). Absorption chillers and heat pumps. CRC press.

Ramaraj, S. (2012). Vapor compression cycle enhancements for cold climate heat pumps.

Rasmussen, B. D., & Jakobsen, A. (2000). Review of compressor models and performance characterizing variables.

ROBUR. Retrieved June 14, 2013, from http://www.roburcorp.com/products/gahp-line/water-to-water-heat-pump-w-series/description.html

Rossa, J. A., & Bazzo, E. (2010). Thermodynamic modeling of an ammonia-water absorption system associated with a microturbine. International Journal of Thermodynamics, 12(1), 38-43.

Şencan, A., Yakut, K. A., & Kalogirou, S. A. (2005). Exergy analysis of lithium bromide/water absorption systems. Renewable energy, 30(5), 645-657.

Sözen, A., Altıparmak, D., & Usta, H. (2002). Development and testing of a prototype of absorption heat pump system operated by solar energy. Applied Thermal Engineering, 22(16), 1847-1859.

Srikhirin, P., Aphornratana, S., & Chungpaibulpatana, S. (2001). A review of absorption refrigeration technologies. Renewable and sustainable energy reviews, 5(4), 343-372.

Talbi, M. M., & Agnew, B. (2000). Exergy analysis: an absorption refrigerator using lithium bromide and water as the working fluids. Applied Thermal Engineering, 20(7), 619-630.

Tarique, S. M., & Siddiqui, M. A. (1999). Performance and economic study of the combined absorption/compression heat pump. Energy conversion and management, 40(6), 575-591.

Thornton, J. W., Klein, S. A., & Mitchell, J. W. (1994). Dedicated mechanical subcooling design strategies for supermarket applications. International Journal of Refrigeration, 17(8), 508-515.

Qiao, H., Radermacher, R., & Aute, V. (2010). A Review for Numerical Simulation of Vapor Compression Systems.

Qureshi, B. A., & Zubair, S. M. (2012). The effect of refrigerant combinations on performance of a vapor compression refrigeration system with dedicated mechanical sub-cooling. International Journal of Refrigeration, 35(1), 47-57.

Qureshi, B. A., Inam, M., Antar, M. A., & Zubair, S. M. (2013). Experimental energetic analysis of a vapor compression refrigeration system with dedicated mechanical sub-cooling. Applied Energy, 102, 1035-1041.

Yin, H. (2006). An absorption chiller in a micro BCHP application: model based design and performance analysis (Doctoral dissertation, Ph. D. Thesis, Carnegie Mellon University, Pittsburgh, PA, USA).

Yumrutaş, R., Kunduz, M., & Kanoğlu, M. (2002). Exergy analysis of vapor compression refrigeration systems. Exergy, An international journal, 2(4), 266-272.

Zhao, L. X., Zhang, C. L., Gu, B., (2009). Neural-Network-Based Polynomial Correlation of Single- and Variable-Speed Compressor Performance. HVAC&RESEARCH, 15(2), 255-268

Zubair, S. M., Yaqub, M., & Khan, S. H. (1996). Second-law-based thermodynamic analysis of two-stage and mechanical-subcooling refrigeration cycles. International Journal of Refrigeration, 19(8), 506-516.

Zubair, S. M. (2000). Design and rating of dedicated mechanical-subcooling vapour compression refrigeration systems. Proceedings of the Institution of Mechanical Engineers, Part A: Journal of Power and Energy, 214(5), 455-471.

APPENDICES

Appendix A The AHP model

Please refer to Figure 5.1 for the schematic diagram of the AHP model.

Desorber

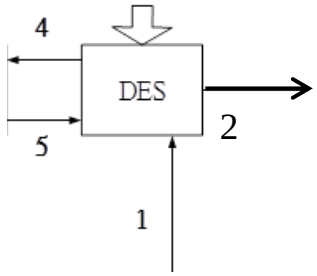

1. Variable

State point	Var. per state point	Var. specified	# of SPs	Total SP var. #
	8	m, T, P, x, h, Q, v, s	4	8*4=32
Other	**Var. specified**		**Number of comp. var.**	
	PH, Qdes		2	

Total number of variables: 32+2=34

2. Equation

	Eqn. specified	Eqn. number
Property	PH=P1,P2,P4,P5 (4) CALL: 1, 2, 4, 5 (16)	20
Mass balance	m1+m5=m2+m4	1
NH3 balance	m1*x1+m5*x5=m2*x2+m4*x4	1
Energy balance	m1*h1+m5*h5+Qdes=m2*h2+m4*h4	1
Heat transfer		0

Total number of equations: 20+1+1+1=23

3. Assumption

Q2=0, Q4=1.001, Q5=0

Total assumptions: 3

4. Input

Design model
T1, PH, m1, m2, x1, Qdes, ~~T5(REC)~~, ~~x4(REC)~~
Performance model
m1, x1, Qdes

Design: ~~8~~, 6

Performance: 3

EV1

1. Variable

State point	Var. per state point	Var. specified	# of SPs	Total SP var. #
	8	m, T, P, x, h, Q, v, s	1	8*1=8
Other	**Var. specified**		**Number of comp. var.**	
	PL		1	

Total number of variables: 8+1=9

2. Equation

	Eqn. specified	Eqn. number
Property	PL=P3 CALL: 3 (4)	5
Mass balance	m2=m3	1
NH3 balance	x2=x3	1
Energy balance	h2=h3	1
Heat transfer		0

Total number of equations: 5+1+1+1=8

3. Assumption

Total assumptions: 0

4. Input

Design model
PL
Performance model

Design: 1
Performance: 0

Rectifier

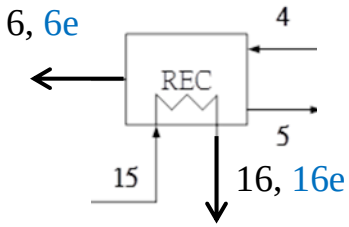

1. Variable

State point	**Var. per state point**	**Var. specified**	**# of SPs**	**Total SP var. #**
	8	m, T, P, x, h, Q, v, s	3	8*3=24
	4	h, Q, v, s	2	4*2=8
	Other		**Number of var.**	
Other	**Var. specified**		**Number of comp. var.**	
	Qrec, Qrec(hs, cs, max), Eff_rec		5	

Total number of variables: 24+8+5=37

2. Equation

	Eqn. specified	**Eqn. number**
Property	PH=P6, P15, P16 (3) CALL: 15, 16, 6, 16e, 6e (20)	23
Mass balance	m4=m5+m6 m15=m16	2
NH3 balance	m4*x4=m5*x5+m6*x6 x15=x16	2
Energy balance	m4*h4=m5*h5+m6*h6+Qrec m15*h15+Qrec=m16*h16	2
Heat transfer	Qrec,hs=m4*(h4-h6e) Qrec,cs=m15*(h15-h16e) Qrec,max=min(Qrec,hs, Qrec,cs) Qrec=Eff_rec*Qrec,max	4

Total number of equations: 23+2+2+2+4=33

3. Assumption

x6=0.99, Q6=1, T5=T6(PRE); Total assumptions: 3

4. Input

Design model
~~T15(pump), m15, x15(ABS)~~
Performance model
Eff_rec

Design: ~~3~~, ~~1~~, 0
Performance: 1

Circulation ratio

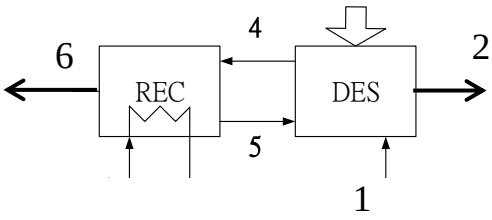

1. Variable

State point	**Var. per state point**	**Var. specified**	**# of SPs**	**Total SP var. #**
	Other		**Number of var.**	
Other	**Var. specified**		**Number of comp. var.**	
	h_d, f, q		3	

Total number of variables: 3

2. Equation

	Eqn. specified	**Eqn. number**
Other	f=m1/m6 f=(h_d-h2)/(h1-h2) Qdes-Qrec=m6*q Q=h6-h_d	4

Total number of equations: 4

5. Assumption

Total assumptions: 0

6. Input

Design model
Performance model

Design: 0
Performance: 0

Condenser

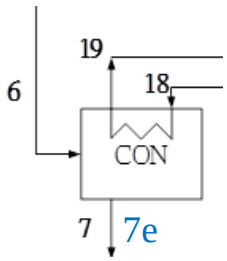

1. Variable

	Var. per state point	Var. specified	# of SPs	Total SP var. #
State point	8	m, T, P, x, h, Q, v, s	1	8*1=8
	4	h, Q, v, s	1	4*1=4
	4	T, h, m, Q	2	4*2=8
	Other		**Number of var.**	
	Cp_w_18		1	
Other	**Var. specified**		**Number of comp. var.**	
	Qcon, Qcon(hs, cs, max), Eff_con		5	

Total number of variables: 8+4+8+1+5=26

2. Equation

	Eqn. specified	Eqn. number
Property	PH=P7 T19=f(h19, Q19) (2) h18=f(T18, Q18) (2) Cp_w_18=f(T18,Q18) CALL: 7, 7e (8)	14
Mass balance	m6=m7 m18=m19	2
NH3 balance	x6=x7	1
Energy balance	m6*h6=m7*h7+Qcon Qcon=m18*(h19-h18)	2
Heat transfer	Qcon,hs=m6*(h6-h7e) Qcon,cs=m18* Cp_w_18*(T6-T18) Qcon,max=min(Qcon,hs ,Qcon,cs) Qcon=Eff_con*Qcon,max	4

Total number of equations: 14+2+1+2+4=23

3. Assumption

T19=T21; Total assumptions: 1

4. Input

Design model
~~T18(HW)~~, T19
Performance model
Eff_con

Design: ~~2,~~ 1
Performance: 1

Precooler

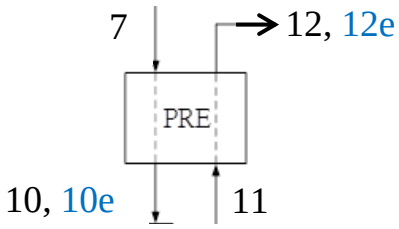

1. Variable

State point	**Var. per state point**	**Var. specified**	**# of SPs**	**Total SP var. #**
	8	m, T, P, x, h, Q, v, s	3	8*3=24
	4	h, Q, v, s	2	4*2=8
	Other		**Number of var.**	
Other	**Var. specified**		**Number of comp. var.**	
	Qpre, Qpre(hs, cs, max), Eff_pre		5	

Total number of variables: 24+8+5=37

2. Equation

	Eqn. specified	**Eqn. number**
Property	PL=P10, P11, P12 (3) CALL: 9, 11, 12, 9e, 12e (20)	23
Mass balance	m7=m10 m11=m12	2
NH3 balance	x7=x10 x11=x12	2
Energy balance	m7*h7=m10*h10+Qpre m11*h11+Qpre=m12*m12	2
Heat transfer	Qpre,hs=m7*(h7-h10e) Qpre,cs=m11*(h12e-h11) Qpre,max=min(Qpre,hs ,Qpre,cs) Qpre=Eff_pre*Qpre,max	4

Total number of equations: 23+2+2+2+4=33

3. Assumption

Total assumptions: 0

4. Input

Design model
T9, ~~T11, m11, x11(EVA)~~
Performance model
Eff_pre

Design: **4**, 1
Performance: 1

Evaporator

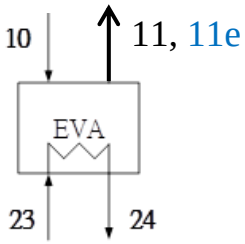

1. Variable

	Var. per state point	Var. specified	# of SPs	Total SP var. #
State point	8	m, T, P, x, h, Q, v, s	0	
	4	h, Q, v, s	1	4*1=4
	4	T, h, m, Q	2	4*2=8
	Other		**Number of var.**	
	Cp_w_23		1	
Other	**Var. specified**		**Number of comp. var.**	
	Qeva, Qeva(hs, cs, max), Eff_eva		5	

Total number of variables: 4+8+1+5=18

2. Equation

	Eqn. specified	Eqn. number
Property	T24=f(h24, Q24) (2) h23=f(T23, Q23) (2) Cp_w_23=f(T23, Q23) CALL: 11e (4)	9
Mass balance	m10=m11 m23=m24	2
NH3 balance	X10=x11	1
Energy balance	m11*h11=m10*h10+Qeva Qeva=m23*(h23-h24)	2
Heat transfer	Qeva,hs=m23* Cp_w_23*(T23-T10) Qeva,cs=m10*(h11e-h10) Qeva,max=min(Qeva,hs, Qeva,cs) Qeva=Eff_eva*Qeva,max	4

Total number of equations: 9+2+1+2+4=18

3. Assumption

Total assumptions: 0

4. Input

Design model
T23, T24, m23
Performance model
T23, m23, Eff_eva

Design: 3
Performance: 3

Absorber

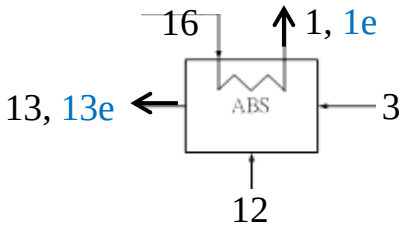

1. Variable

State point	**Var. per state point**	**Var. specified**	**# of SPs**	**Total SP var. #**
	8	m, T, P, x, h, Q, v, s	1	8*1=8
	4	h, Q, v, s	2	4*2=8
	Other		**Number of var.**	
			0	
Other	**Var. specified**		**Number of comp. var.**	
	Qabs, Qabs(hs, cs, max), Eff_abs		5	

Total number of variables: 8+8+5=21

2. Equation

	Eqn. specified	**Eqn. number**
Property	PL=P13 CALL: 13, 1e, 13e (12)	13
Mass balance	m1=m16 m12+m3=m13	2
NH3 balance	m12*x12+m3*x3=m13a*x13a x1=x16	2
Energy balance	m16*h16+Qabs=m1*h1 m12*h12+m3*h3=Qabs+m13*h13	2
Heat transfer	Qabs, hs=m3*h3+m12*h12-m13*h13e Qabs,cs=m16*(h1e-h16) Qabs,max=Qabs,cs Qabs=Eff_abs*Qabs,max	4

Total number of equations: 13+2+2+2+4=23

3. Assumption

Total assumptions: 0

4. Input

Design model
Performance model
Eff_abs

Design: 0
Performance: 1

HX

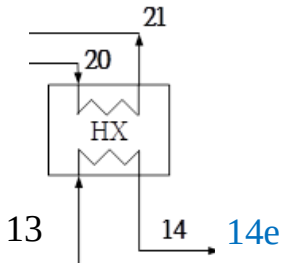

1. Variable

	Var. per state point	Var. specified	# of SPs	Total SP var. #
State point	8	m, T, P, x, h, Q, v, s	1	8*1=8
	4	h, Q, v, s	1	4*1=4
	4	T, h, m, Q	2	4*2=8
	Other		**Number of var.**	
	Cp_w_20		1	
Other	**Var. specified**		**Number of comp. var.**	
	Qhx, Qhx(hs, cs, max), Eff_hx		5	

Total number of variables: 8+4+8+1+5=26

2. Equation

	Eqn. specified	Eqn. number
Property	PL=P14 h21=f(T21, Q21) (2) h22=f(T22, Q22) (2) Cp_w_20=f(T20, Q20) CALL: 14, 14e (8)	14
Mass balance	m13=m14 m20=m21	2
NH3 balance	x13=x14	1
Energy balance	m13*h13=m14*h14+Qhx Qhx=m20*(h21-h20)	2
Heat transfer	Qhx,hs=m13*(h13-h14e) Qhx,cs=m20*Cp_w_20*(T13-T20) Qhx,max=min(Qhx,hs ,Qhx,cs) Qhx=Eff_hx*Qhx,max	4

Total number of equations: 14+2+1+2+4=23

3. Assumption

Q14=0; Total assumptions: 1

4. Input

Design model
~~T20, m20(HW)~~
Performance model
Eff_hx

Design: ~~2~~, 0
Performance: 1

Hot water

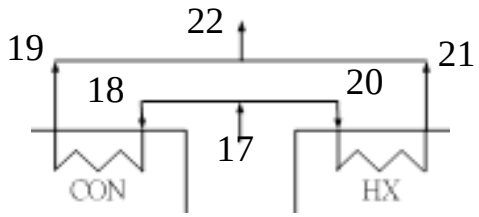

1. Variable

State point	**Var. per state point**	**Var. specified**	**# of SPs**	**Total SP var. #**
	4	T, h, m, Q	2	4*2=8
	Other		**Number of var.**	
Other	**Var. specified**		**Number of comp. var.**	

Total number of variables: 8

2. Equation

	Eqn. specified	**Eqn. number**
Property	T17=T18 T17=T20 T22=f(h22, Q22) (2) h17=f(T17, Q17) (2)	6
Mass balance	m17=m18+m20 m22=m19+m21	2
NH3 balance		
Energy balance	m19*h19+m21*h21=m22*h22	1
Heat transfer		

Total number of equations: 6+2+1=9

3. Assumption

Total assumptions: 0

4. Input

Design & Performance models
T17, m17

Design & performance: 2

Pump

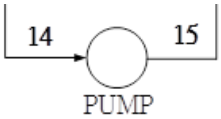

1. Variable

State point	Var. per state point	Var. specified	# of SPs	Total SP var. #
	Other		Number of var.	
	Swp, Wp		2	
Other	Var. specified		Number of comp. var.	
			0	

Total number of variables: 2

2. Equation

	Eqn. specified	Eqn. number
Property		
Mass balance		
NH3 balance		
Energy balance	Swp=v14*(P15-P14) h15=h14+Swp m14*h14+Wp=m15*h15	3
Heat transfer		0

Total number of equations: 3

3. Assumption

Total assumptions: 0

4. Input

Design & Performance models

Design & performance: 0

Appendix B The VC model

Please refer to Figure 5.8 for the schematic diagram for the VC model.

Compressor

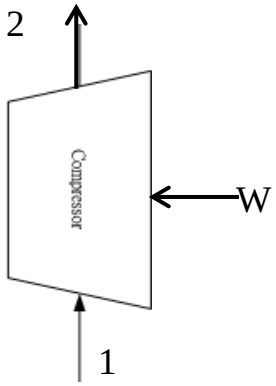

1. Variable

State point	Var. per state point	Var. specified	# of SPs	Total SP var. #
	5	T, P, h, s, m	2	5*2=10
Other	**Var. specified**		**Number of comp. var.**	
	s_2, h_2, W, eta_is		4	

Total number of variables: 10+4=14

2. Equation

	Eqn. specified	Eqn. number
Property	h1=f(T1, P1), s1=f(T1, P1) h2=f(T2, P2), s2=f(T2, P2) s_2=s1, h_2=f(s_2, P2)	6
Mass balance	m1=m2	1
Energy balance		0
Heat transfer		0
Other	W=f(P1, P2), m1=f(P1, P2), eta_is=f(P1, P2), eta_is=(h_2-h1)/(h2-h1)	4

Total number of equations: 6+1+4=11

3. Assumption

Total assumptions: 0

4. Input

Performance model

Performance: 0

Condenser

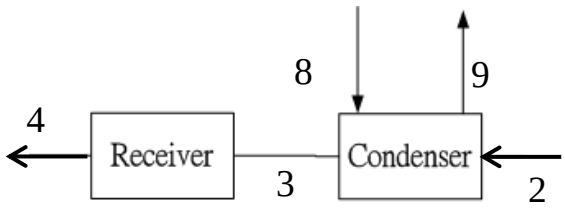

1. Variable

	Var. per state point	Var. specified	# of SPs	Total SP var. #
State point	6	T, P, h, s, m, x	2	2*6=12
	5	T, h, s, m, x	2	2*5=10
Other	**Var. specified**		**Number of comp. var.**	
	Qc, Qc_max, UA_c, NTU_c, Eff_c		5	

Total number of variables: 12+10+5=27

2. Equation

	Eqn. specified	Eqn. number
Property	P3=P2, P4=0.979*P3 T3, h3, s3=f() (3) T4, h4,s4=f() (3) h8, s8=f() (2) T9, s9=f() (2)	12
Mass balance	m2=m3 m3=m4 m8=m9	3
Energy balance	Qc=m2*(h2-h4) Qc=m8*(h9-h8)	2
Heat transfer	Qc=Eff_c*Qc_max Qc_max=m8*(T3-T8)*4.18 NTU_c=UA_c/m8*4.18 Eff_c=1-exp(-NTU_c)	4

Total number of equations: 12+3+2+4=21

3. Assumption

x3=1, x4=0, x8=0, x9=0

Total assumptions: 4

4. Input

Performance model
UA_c, T8, m8

Performance: 3

Expansion valve

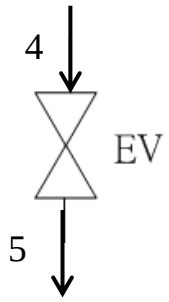

1. Variable

State point	Var. per state point	Var. specified	# of SPs	Total SP var. #
	5	T, P, s, h, m	1	5
Other	**Var. specified**		**Number of comp. var.**	

Total number of variables: 5

2. Equation

	Eqn. specified	Eqn. number
Property	P5*0.91=P1 T5, s5=f() (2)	3
Mass balance	m5=m4	1
Energy balance	h5=h4	1
Heat transfer		

Total number of equations: 3+1+1=5

3. Assumption

Total assumptions: 0

4. Input

Performance model

Performance: 0

Evaporator

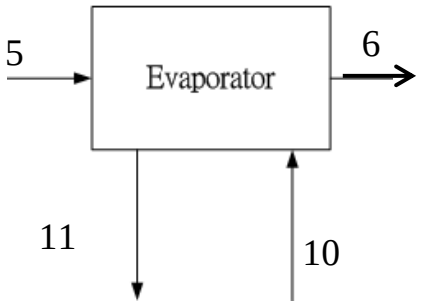

1. Variable

	Var. per state point	Var. specified	# of SPs	Total SP var. #
State point	6	T, P, h, s, m, x	1	6
	5	T, h, s, m, x	2	2*5=10
Other	**Var. specified**		**Number of comp. var.**	
	Qe, Qe_max, UA_e, NTU_e, Eff_e		5	

Total number of variables: 6+10+5=21

2. Equation

	Eqn. specified	Eqn. number
Property	P6=P1 T6, h6, s6=f() (3) h10, s10=f() (2) T11, s11=f() (2)	8
Mass balance	m6=m5 m10=m11	2
Energy balance	Qe=m5*(h1-h5) Qe=m10*(h10-h11)	2
Heat transfer	Qe=Eff_e*Qe_max Qe_max=m10*(T10-T5)*4.18 NTU_e=UA_e/m8*4.18 Eff_e=1-exp(-NTU_e)	4

Total number of equations: 8+2+2+4=16

3. Assumption

X6=1, x10=0, x11=0, T1=T6+12.9

Total assumptions: 4

4. Input

Performance model
UA_e, T10, m10

Performance: 3

VITA

VITA

Yi-Shu Kung
Civil Engineering School, Purdue University

Education
B.S., Civil Engineering, 2006, National Taiwan University, Taiwan
M.S., Civil Engineering, 2008, National Taiwan University, Taiwan
Ph.D., Civil Engineering, 2015, Purdue University, West Lafayette, Indiana

Research Interests
HVAC system
Absorption chiller and heat pump
Building energy system modeling and simulation